United States
Environmental Protection
Agency

Office of Research and
Development
Washington DC 20460

EPA/600/R-98/022
March 1998

EPA

Evaluating the Relation Between Ozone, NO_x and Hydrocarbons: The Method of Photochemical Indicators

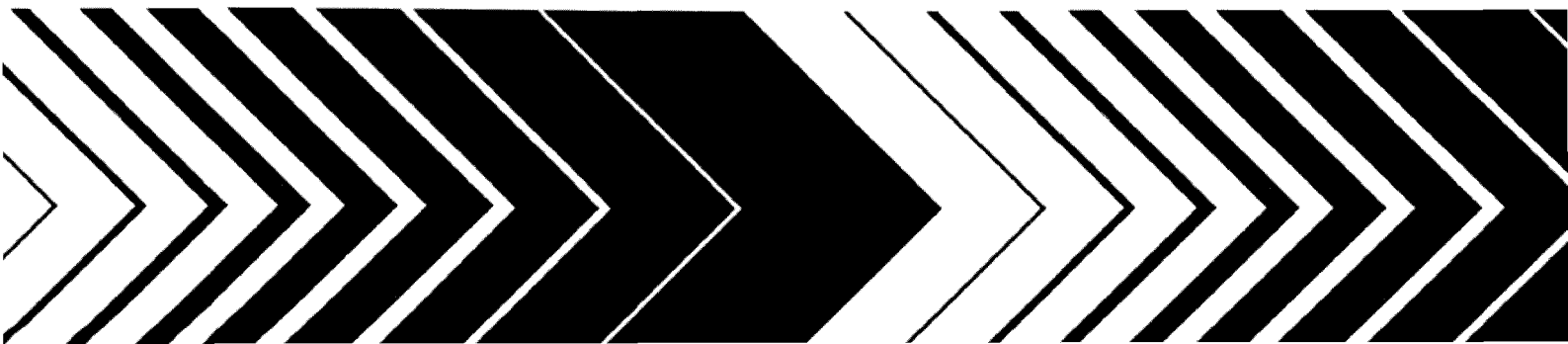

EVALUATING THE RELATION BETWEEN OZONE, NO_X AND HYDROCARBONS: THE METHOD OF PHOTOCHEMICAL INDICATORS

by

Sanford Sillman
Department of Atmospheric, Oceanic and Space Sciences
University of Michigan
Ann Arbor, Michigan 48109-2143

Cooperative Agreement No. CR822083-01

Project Officer

James M. Godowitch
Atmospheric Modeling Division
National Exposure Research Laboratory
Research Triangle Park, NC 27711

NATIONAL EXPOSURE RESEARCH LABORATORY
OFFICE OF RESEARCH AND DEVELOPMENT
U.S. ENVIRONMENTAL PROTECTION AGENCY
RESEARCH TRIANGLE PARK, NC 27711

NOTICE

The information in this document has been funded wholly or in part by the United States Environmental Protection Agency under Cooperative Agreement No. CR822083-01 to the University of Michigan. It has been subjected to the Agency's peer and administrative review, and it has been approved for publication as an EPA document. Mention of trade names or commercial products does not constitute an endorcement or recommendation for use.

ACKNOWLEDGMENTS

The work represented here was funded by Cooperative Agreement No. CR822083-01 with the U. S. Environmental Protection Agency. Results for the UAM simulations for New York and Los Angeles were provided by Jim Godowitch and Neil Wheeler, each of whom made many helpful suggestions. I also wish to thank Neil Wheeler and the California Air Resources Board for providing me with measurments in the Los Angeles basin, Bob Imhoff and his colleagues in the Southern Oxidant Study for providing me with measurements from Atlanta, and Pete Daum and his colleagues for sharing their NARE results with me. Discussions with Jana Milford and Tom Ryerson were also especially helpful.

ABSTRACT

The method of photochemical indicators is a way to evaluate the sensitivity of O3 to its two main precursors, nitrogen oxides (NO_X) and reactive organic gases (ROG), directly from ambient measurements. The method is based on identifying measureable species or species ratios that are closely associated with O3-NO_X-ROG predictions in photochemical models. Several species of this type have been identified: O3/NO_Y (where NO_Y is total reactive nitrogen), O3/NO_Z (where NO_Z=NO_Y-NO_X), O3/HNO3, H_2O_2/HNO3, H_2O_2/NO_Z, and H_2O_2/NO_Y. In each case, high values of the proposed indicator are associated with NO_X-sensitive chemistry in models and low values are associated with ROG-sensitive chemistry. This report presents a summary of O3-NO_X-ROG sensitivity in models and the chemistry that motivate the choice of species as photochemical indicators. It shows the correlation between model NO_X-ROG predictions and indicator values for a variety of models, including simulations for Lake Michigan, the northeast corridor, Atlanta and Los Angeles. The indicator-NO_X-ROG correlation remains consistent in model scenarios with radically different assumptions about anthropogenic and biogenic emission rates and meteorology and in models with different chemical mechanisms. The report shows correlations between O3, NO_Z and H_2O_2 in models and in ambient measurements, which provide a basis for evaluating the accuracy of critical assumptions associated with the indicator method. Case studies are described for Atlanta and Los Angeles in which measured values of indicator ratios were used as a basis for evaluating model scenarios. It is shown in which model scenarios with different NO_X-ROG predictions often give similar values for peak O3 but different values for indicator ratios. The case studies illustrate how comparisons between model results and measured indicator values can be used as a basis for model evaluation. Uncertainties associated with the indicator method (including measurement uncertainties, dry deposition and surface effects) are discussed.

CONTENTS

FIGURES

TABLES

SECTION 1
OVERVIEW

For many years there has been uncertainty about the relation between low-level ozone and its two major anthropogenic precursors: reactive organic gases (ROG) and nitrogen oxides (NO_X). It is generally known that for some conditions ozone concentrations increase with increasing NOx emissions and are largely independent of ROG, while for other conditions ozone increases with ROG and does not increase (or may even decrease) with NO_X. However, it is difficult to determine whether individual air pollution events are dominated by NO_X-sensitive or ROG-sensitive chemistry.

The uncertain relationship between ozone, ROG and NO_X has made it especially difficult to develop effective control policies for ozone. Ozone as an air pollutant is responsible for widespread violations of air quality standards, affecting most major metropolitan areas in the U.S. A large effort has been made to reduce emission of ozone precursors, but it is unclear whether these efforts have been effective in controling ozone levels (NRC, 1991). Because of the complex relationship between ozone and its precursors, there is far greater uncertainty about the effectiveness of control strategies for ozone than for other pollutants associated with air quality violations. A control strategy that relies on reductions in emissions of ROG will not be effective in a region where ozone concentrations are driven by NO_X-sensitive chemistry. Similarly, a control strategy that relies on NOx reductions will not be effective during air pollution events with ROG-sensitive chemistry.

The task of analyzing the ozone-NO_X-ROG relationship is commonly based on predictions from photochemical models. These models use estimates for emission rates of ozone precursors in combination with meteorological information (wind speeds, vertical diffusion, temperatures, etc.) and a representation of ozone chemistry in order to simulate the ozone formation process for a specific air pollution event. Predictions for the effectiveness of ROG vs. NO_X controls are derived by repeating the simulations with reduced emission rates for ROG or NO_X. The accuracy of these control strategy predictions has frequently been called into question, largely because of uncertainties

associated with emission inventories. Inventories for anthropogenic ROG emissions may be underestimated by up to a factor of two (Fujita et al., 1992), while recent research has shown that the emission rate for isoprene, the most important biogenic ROG, is approximately four times higher than previous estimates (Geron et al., 1994, 1995). Both of these uncertainties have a large impact on model predictions of the effectiveness of ROG vs. NO_X controls. It is frequently possible to generate model scenarios with either NO_X- and ROG-sensitive chemistry while remaining within the bounds of uncertainty associated with emissions and other model input.

A more fundamental problem with the model-based approach for O_3-NO_X-ROG sensitivity is the difficulty in evaluating model predictions against real-world measurements. There is no direct way to evaluate a control strategy prediction, because it is never possible to repeat an air pollution event with reduced ROG or NO_X emissions and compare its outcome with model results. Model evaluations can only be done by comparing predictions from the model base case with ambient measurements. The problem with most model evaluations is that the accuracy of model predictions for the base case does not guarantee that model predictions for control strategies are also accurate. In particular, the most common test of model performance - comparison with ambient ozone - gives no basis for confidence in model predictions for control strategies. This is because different model scenarios often give similar values for ozone in the base case, while giving very different predictions for the response of ozone to reductions in ROG or NO_X.

This report presents a new approach to the problem of evaluating O_3-NO_X-ROG sensitivity: the *method of photochemical indicators*. The goal of the method is to identify measureable species or species ratios that are closely linked to model control strategy predictions, so that NO_X-sensitive or ROG-sensitive chemistry can be associated with specific values of these species ratios. If successful, the method of photochemical indicators would provide a way to evaluate NO_X-ROG sensitivity based solely on ambient measurements, without using models. A more modest application of the method would be to evaluate the performance of model scenarios. The nature of the indicator ratios associated with this method is that they will always assume different values in models with NO_X-sensitive chemistry as opposed to models with ROG-sensitive chemistry. Thus, the indicator ratios (unlike ozone) provide a basis for choosing between NO_X-sensitive and ROG-sensitive model scenarios.

The method of photochemical indicators is part of a broader attempt to develop observation-based methods (OBMs) that seek to analyze O_3-NO_X-ROG chemistry based on extensive field measurements rather than model predictions (e.g. Cardelino et al., 1995).

The method of photochemical indicators was developed based on a series of photochemical model applications designed to represent a wide range of physical conditions and situations. These have included simulations for four metropolitan regions: the Lake Michigan airshed, the New York-Boston urban corridor, Atlanta and Los Angeles. They have included simulations with anthropogenic ROG emissions doubled from inventory estimates, reflecting uncertainty in inventories identified by Fujita et al. (1992). They have included scenarios with anthropogenic ROG emissions reduced by half from inventory estimates, reflecting conditions that may occur in Europe today or in the U.S. following the application of an effective ROG control program. They have included scenarios with biogenic ROG emissions based on the current BEIS2 inventory (Geron et al., 1994) and also on the older BEIS1 inventory with much lower emission rates (Pierce et al., 1990), and scenarios with zero biogenic emissions. They have included simulations with changed wind speeds and vertical mixing rates in order to represent conditions that might be either more or less stagnant than the events used as test cases. They have included results from two very different model types: a regional-scale model developed by Sillman et al. at the University of Michigan (Sillman et al., 1993) and the Urban Airshed Model (UAM-IV)(Morris and Myers, 1990), familiar to air pollution researchers. These two models include different representations of photochemistry: a mechanism based on Lurmann et al. (1986) (similar to the more familiar SAPRC mechanism) with various updates and isoprene chemistry based on work by Paulson and Seinfeld (1992) in the Michigan model; and the Carbon Bond IV mechanism (Gery et al., 1989) in UAM-IV.

Species and species ratios that can be used as indicators for NO_X-ROG sensitivity were sought based on an analysis of model results. In order to be useful as a photochemical indicator a species or species ratio must satisfy the following four criteria:

(i) The indicator must involve measureable species.

(ii) The indicator must consistently show different values in model scenarios with NO_X-sensitive chemistry as opposed to model scenarios with ROG-sensitive chemistry. The difference between NO_X-sensitive and ROG-sensitive indicator values must also be large enough so that the NO_X-ROG indication is less likely to be obscured by uncertainties in measurement techniques.

(iii) The correlation between indicator values and NO_X-ROG sensitivity must remain reasonably constant in models with widely different assumptions. The purpose of the method would be undermined if the indicator correlation were limited to models with a fixed range of assumptions, e.g. about biogenic ROG.

(iv) The indicator should be closely linked with the chemical factors that govern NO_X-ROG sensitivity. It should not just represent an empirical curve-fitting exercise or be an artifact of an individual model.

Two classes of species have been identified that appear to meet these criteria. These species are as follows.

A. *Ratios involving ozone and total reactive nitrogen*: $\frac{O3}{NO_y}$, where NO_y represents total reactive nitrogen (NO_X, PAN, HNO_3, alkyl nitrates and other nitrogen-containing species produced from NO_X); $\frac{O3}{NO_Z}$, where NO_Z represents NO_X reaction products, NO_y-NO_X; and $\frac{O3}{HNO3}$.

B. *Ratios involving hydrogen peroxide and total reactive nitrogen*: \f(H_2O_2,HNO_3), $\frac{H2O2}{NO_Z}$, and $\frac{H2O2}{NO_y}$.

In each case, a high value for the indicator ratio corresponds to a situation in which the ozone concentration is primarily sensitive to NO_X, while a low value corresponds to a situation in which O_3 is primarily sensitive to ROG. This interpretation applies only for indicator values during the afternoon (concurrent with peak O_3) and only for NO_X-ROG sensitivity at the same location as the indicator value.

Among these alternatives, the ratios involving hydrogen peroxide (especially $\frac{H2O2}{HNO3}$) provide more consistent results in photochemical models and are more closely linked to the photochemical processes that drive NO_X-ROG chemistry, but these are also more difficult to measure. Among the ratios involving ozone, $\frac{O3}{NO_Z}$ has a stronger link with NO_X-ROG chemistry than $\frac{O3}{NO_y}$, but the latter has certain advantages associated with situations involving power plants.

An important component of the indicator method concerns the need to evaluate the accuracy of the indicator predictions. The correlation between NO_X-ROG sensitivity and the indicator ratios is based entirely on the results of photochemical models. As such, the indicator method faces the same type of challenge as the conventional photochemical models: how can the predicted NO_X-ROG sensitivity be proven?

Model results have suggested an important test for the validity of the method. The chemistry associated with NO_X-ROG sensitivity and the indicator ratios also suggests that a linear correlation should be found between O_3 and the sum: $NO_Z+2H_2O_2$, evaluated during the afternoon following a period of photochemical activity. This linear correlation is predicted in three-dimensional models that include both chemistry and transport, and is

shown in Section 4. The correlation is closely associated with the role of O_3, NO_Z and H_2O_2 as indicators for NO_X-ROG sensitivity. It is well-known that O_3 increases with NO_Z but that the rate of increase (dO_3/dNO_Z) decreases at higher NO_Z and is lower in some urban areas (e.g. Los Angeles) relative to rural sites (Trainer et al., 1993). The indicator method provides an additional interpretation: high O_3/NO_Z ratios in rural areas represent NO_X-sensitive chemistry while low O_3/NO_Z ratios in central Los Angeles represent ROG-sensitive chemistry. If this interpretation is valid, then the correlation between O_3 and the sum $NO_Z+2H_2O_2$ will remain linear, even while the O_3-NO_Z slope varies. Thus, an examination of measured O_3, NO_Z and H_2O_2 provides both a general evaluation of the indicator method and a test for problems (e.g. measurement errors or erroneous model assumptions) in each individual application of the method.

In summary, the indicator method provides several advantages over conventional methods of analysis of O_3-NO_X-ROG sensitivity. Unlike conventional photochemical models, the indicator predictions are not sensitive to assumptions about emission rates for anthropogenic or biogenic ROG. When used in combination with photochemical models the indicator method provides a meaningful evaluation of the accuracy of model NO_X-ROG predictions. Finally, the indicator method includes a diagnostic test for its own accuracy, based on the predicted linear correlation between O_3, NO_Z and H_2O_2. The indicator method can be applied based on measurements for just three species, O_3, NO_X and NO_y, although the inclusion of measurements of H_2O_2, HNO_3 and CO would improve the reliability of the method.

The indicator method, like any new approach, involves problems and uncertainties that are not present in other methods. The following is a list of caveats for researchers who seek to use the indicator method.

(1) The indicator method provides information about NO_X-ROG sensitivity only at the time and place of the measurements. It is well known that NO_X-ROG sensitivity varies with location within a metropolitan area, with ROG-sensitive chemistry more likely in the urban center and NO_X-sensitive chemistry more likely downwind (Milford et al., 1989). Thus, it is inaccurate to infer NO_X-ROG sensitivity for an entire metropolitan area from measurements at a small number of locations. NO_X-ROG sensitivity can also vary from event to event and changes with time of day. Illustrations of this will be shown in the report below.

(2) The indicator method as presented here is designed to estimate NO_X-ROG sensitivity associated with ozone concentrations, not the instantaneous rate of ozone production. The NO_X-ROG sensitivity of ozone concentrations depends on photochemistry over an extended time period (typically 1-2 days) and transport from a significant distance upwind.

This impact of upwind transport and photochemistry is included in the models that were used to derive the indicator correlations.

(3) The indicator method is critically dependent on the accuracy of measurements, especially NO_y. Luke and Dickerson (1987) have warned that certain types of measurement systems characteristically underestimate NO_y, because HNO_3 (a major NO_y component) is deposited on the inlet tube. This type of measurement error would invalidate the use of NO_y as a NO_x-ROG indicator.

Model results suggest that values for O_3/NO_y and O_3/NO_z associated with NO_x- and ROG-sensitive chemistry differ by a factor of two, and values for H_2O_2/HNO_3 and other ratios with peroxides show an even larger difference between NO_x- and ROG-sensitive locations. Errors in measurements are likely to be important only if they are significant in comparison with this range of variation, i.e. 25% or higher. However errors in measurements are especially troublesome if they might lead to a systematic overestimate or underestimate in measured indicator ratios, since these would cause bias in the indicator NO_x-ROG interpretation.

Because of potential problems with NO_y measurements it is important to carefully evaluate measurement accuracy. One possible method for evaluating the accuracy of measured NO_y is to include simultaneous measurements of CO and SO_2 and examine correlations of these species with NO_y. Previous studies have identified a correlation between these species, reflecting their common anthropogenic origin (Parrish et al., 1991, Buhr et al., 1995). A deviation from the expected correlation between these species might be used to identify erroneous measurements.

Because these three species have a common anthropogenic origin, it should be possible to identify a consistent correlation between them, which could then be used to evaluate the accuracy of individual NO_y measurements.

(4) Species ratios that use NO_x, PAN or NO_x+PAN in place of NO_y, NO_z or HNO_3 do not correlate well with NO_x-ROG sensitivity and should not be used as photochemical indicators. This is a problem because NOy measurements that rely on older techniques have been found to represent the sum NO_x+PAN rather than true NO_x or NO_y (Logan, 1989). Recent reports have also erroneously used the ratio O_3/NO_2 as a NO_x-ROG indicator (LADCO, 1994). Also, species ratios must be based on simultaneous measurements (rather than O_3 in the afternoon versus NO_y in the morning or at a different location).

(5) Many of the species associated with the indicator method (NO_y, NO_z, H_2O_2 and HNO_3) can be rapidly removed from the atmosphere (and removed at varying rates) by surface deposition or deposition on aerosols. This may represent a major uncertainty for

the method. Correlations between NO_X-ROG senstivity and indicator values may change significantly if changes are made to model surface deposition rates. In addition, surface-level measurements at night cannot be used as NO_X-ROG indicators because the indicator concentrations at night are dominated by surface deposition processes.
(6) The indicator method was derived from models that did not include aerosol nitrates (NO_3^-) which are formed from gas-phase HNO3. It is therefore appropriate to include aerosol nitrate (converted to gas-phase equivalent units) in the sum for NOz, and interpret HNO3 in the indicator ratios as representing the sum of HNO3 and NO3-. Failure to include aqueous chemistry represents an additional source of uncertainty in the method.
(7) Surface measurements of NO_y are sometimes dominated by NO_X sources close to the measurement site. This would interfere with the direct use of NO_y in indicator ratios (e.g. O_3/NO_y or H_2O_2/NO_y). This problem can be avoided by using NO_Z (based on simultaneous measurement of NO_X and NO_y) instead of (or in addition to) NO_y.

This report presents a summary of research on the indicator method to date. Section 2 provides background information on the chemistry of O_3, NO_X and ROG that serves as a motivating factor for the selection of the various indicator ratios. This section also presents a concise summary of the current understanding of O_3-NO_X-ROG sensitivity that has emerged in recent years. The state of science associated with O_3-NO_X-ROG chemistry has seen great changes in the past ten years. The summary in Section 2 may serve both as an introduction to the field and a review for experienced researchers and regulators.

Section 3 presents the correlation between O_3-NO_X-ROG predictions and the various indicator ratios in photochemical models. It includes a description of the models used, general results for O_3-NO_X-ROG sensitivity, the extent of variation of the indicator-NO_X-ROG correlation in different model scenarios, and methods for quantitatively identifying the indicator values corresponding to the transition between NO_X- and ROG-sensitive chemistry. It also shows results for alternative choices (NO_y, AIRTRAK, O_3/NO_X, ROG/NO_X) which do not perform as well as the recommended indicator ratios. A complete presentation of model results is also included in the Appendix.

Section 4 examines the correlation between O_3, NO_Z and H_2O_2 as predicted by photochemical models and as observed during field measurement campaigns. As described above, this correlation represents a critical test for the accuracy of the indicator method. Section 5 shows results from applications of the indicator method for specific events in Atlanta and Los Angeles. These results include comparisons between predicted indicator values from a series of model scenarios, each designed to give different predictions for NO_X-ROG chemistry. These predictions are compared with measured indicator species

and ratios, which are used as a basis for accepting the results of some model scenarios and rejecting others. The comparison between model and measured values of photochemical indicators associated with predicted and observed (non-paired) peak O3 is proposed as a criterion for evaluating model performance. This criterion provides a much stronger basis for model evaluation then criteria based solely on model vs. measured O3. It is hoped that these case studies can be used as examples for future applications.

The contents of this report are based models and measurements for the northeast corridor and Lake Michigan (Sillman, 1995a), Atlanta (Sillman et al., 1995b, 1997a), New York and Los Angeles (1997a). More recent results from the Middle Tennesee Ozone Study (Sillman et al., 1997b) have been included only in summary form.

SECTION 2
CHEMISTRY OF O_3, NO_X AND ROG

This section includes two parts. The first part provides a summary of the various factors that can affect O_3-NO_X-ROG sensitivity, based on results from photochemical models. The original understanding that NO_X-ROG sensitivity is determined by ROG/NO_X ratios has been greatly modified in recent years. Additional factors include the impact of biogenic ROG, the geographical variation in NO_X-ROG chemistry as an air mass ages and moves downwind from an urban center, and the influence of meteorological stagnation in causing day-to-day variations in NO_X-ROG chemistry. An understanding of these factors can be of great help to researchers and to regulators who need to interpret the results of models or other NO_X-ROG analyses.

The second part analyses the specific chemical reactions and reaction sequences that create the division into NO_X-sensitive and ROG-sensitive regimes. This section also provides the theoretical basis for the link between NO_X-ROG sensitivity and the identified indicator ratios. As discussed below, O_3-NO_X-ROG chemistry is derived from reaction cycles involving odd hydrogen radicals (OH, HO_2 and RO_2, where R represents a carbon-hydrogen chain). NO_X-sensitive chemistry occurs when radical-radical reactions (HO_2+HO_2 and HO_2+RO_2, making peroxides) are the dominant sink for odd hydrogen, while ROG-sensitive chemistry occurs when nitrate-forming reactions (OH+NO_2, making nitric acid) are the dominant sink. From these chemical reaction sequences it is possible to derive a theoretical relationship between NO_X-ROG sensitivity and the species ratios that have been identified as photochemical indicators: O_3/NO_Z and H_2O_2/HNO_3. Section 3 will show how the correlation between NO_X-ROG sensitivity and photochemical indicators also appears in more complete photochemical simulations.

A more complete review of the state of science associated with O_3, NO_X and ROG is given in Sillman (1997c).

2.1. Factors affecting O_3-NO_X-ROG sensitivity in urban locations

For purposes of this study the terms "NO_X-sensitive" and "ROG-sensitive" will be defined based on the predicted response of ozone concentrations to a moderate (usually 35%) reduction in anthropogenic emissions of NO_X or ROG. Locations will be defined as NO_X-sensitive if the model results with reduced NO_X show a greater decrease of O_3 than the same percent reduction of ROG. However it should be recognized that the NO_X-sensitive and ROG-sensitive labels also depend on the size of the reductions. In general, NO_X reductions are more likely to result in reduced O_3 if a large percent reduction is applied. Roselle et al. (1995) have reported cases where a 25% reduction in ROG is predicted to result in lower O_3 than a 25% reduction in NO_X, but where a 75% reduction in NO_X results in lower O_3 than a 75% reduction in ROG.

The following discussion describes individual factors that have a large impact on NO_X-ROG predictions in models. The discussion refers to the the impact of each individual factor in isolation; i.e. all other things being equal, a change in the individual factor will tend to shift model responses in the direction of NO_X-sensitive or ROG-sensitive chemistry. These should not be used to infer NO_X-ROG sensitivity for individual locations, which result from the combination of many factors.

ROG/NO_X ratios: It is well known that the division between NO_X-sensitive and ROG-sensitive ozone photochemistry is closely associated with ROG/NO_X ratios (e.g. NRC, 1991). The O_3-NO_X-ROG relationship is conveiently summarized by isopleth plots, a form of which is shown in Figure 2-1. These plots show that the rate of ozone formation as a function of NO_X and ROG is highly nonlinear. When ROG/NO_X ratios are high the rate of ozone production increases with increasing NO_X but shows little sensitivity to ROG (NO_X-sensitive regime). When ROG/NO_X ratios are low the rate of ozone formation increases with increasing ROG and decreases with increasing NO_X (ROG-sensitive regime). Early analyses suggested that ROG-sensitive chemistry could be associated with ROG/NO_X ratio lower than 10 in an urban center during the morning hours while NO_X-sensitive chemistry could be associated with ROG/NO_X ratios greater than 20 (Blanchard et al., 1991).

The view that morning (6-9 a.m.) ROG/NO_X ratios can be used to determine NO_X-ROG sensitivity has been largely discredited (NRC, 1991, and references below). The problems with ROG/NO_X concentration ratios as a NO_X-ROG indicator include the following:

(i) It fails to account for the impact of biogenic ROG, which are mainly emitted during the midday and afternoon hours rather than at 6-9 a.m. and which are also disproportionately reactive (Chameides et al., 1988, 1992).
(ii) It fails to account for variations in ROG reactivity, which may occur either due to variations between urban areas or to changes in estimates of the speciation of emitted ROG (Chameides et al., 1992, Carter et al., 1994, 1995)
(iii) It fails to account for the geographic variation of NO_X-ROG sensitivity within a metropolitan area (Milford et al., 1989).
(iv) It fails to explain the fact that NO_X-ROG sensitivity can vary from event to event, even for the same metropolitan area. Event-by-event variations in NO_X-ROG sensitivity have been found in photochemical models, even though the ROG/NO_X emission ratios and morning concentrations do not vary (Milford et al., 1994, Roselle et al., 1995).
(v) It fails to account for the impact of multiday transport, which usually has greater sensitivity to NO_X than single-day events (Sillman et al., 1990a).

Despite these flaws, the morning ROG/NO_X ratio continues to be used, inappropriately, to analyze ROG-NO_X sensitivity (Hanna et al., 1996). Because of its repeated misuse, it is important to understand both the rationale for its use (i.e. the isopleth diagram) and its flaws.

Biogenic ROG and ROG reactivity: Chameides et al. (1988) showed that biogenic ROG, especially isoprene, have a significant impact on ozone chemistry in urban areas. More recently, results from the Ozone Transport and Assessment Group (OTAG) demonstrated that a switch from the older BEIS1 emission inventory to the newer BEIS2 inventory (with four times higher emission rates for isoprene) causes a shift from ROG-sensitive chemistry to NO_X-sensitive chemistry in models for several urban areas (OTAG, 1996). Similar results from Sillman et al. (1995b) for Atlanta, are included in this report.

Two aspects of biogenic ROG are especially important to understand. First, emission rates for isoprene, the most important biogenic ROG, are zero at night and very low during the morning. The maximum emission rate occurs during early afternoon (Geron et al., 1994, 1995). Consequently, analyses based on measured ROG during the morning hours would seriously underestimate the impact of biogenics. Second, isoprene and other biogenic ROG are extremely reactive, and their impact on photochemistry is therefore larger than would be suggested by their atmospheric concentration in comparison with anthropogenic ROG. When speciated ROG measurements are weighted according to reactivity or ozone-forming potential (Chameides et al., 1992, Carter et al., 1994, 1995) the impact of biogenic ROG always appears much larger than it would without reactivity-weighting.

Geographical variation and photochemical aging: A central feature of NO_X-ROG chemistry is the tendency for air parcels to change from ROG-sensitive chemistry to NO_X-sensitive chemistry as they age. Thus, an air parcel frequently has ROG-sensitive chemistry while it is close to its emission sources and increasingly NO_X-sensitive chemistry as it moves downwind.

Milford et al. (1989) demonstrated the resulting geographical variation in NO_X-ROG chemistry in a model for Los Angeles. As shown in Figure 2-2, model-derived isopleth plots show strongly ROG-sensitive chemistry for locations near downtown and NO_X-sensitive chemistry at downwind sites. This split between ROG-sensitive downtown and NO_X-sensitive downwind has appeared repeatedly in model applications and is a central feature of O_3-NO_X-ROG chemistry.

A similar, better-known pattern appears for power plant plumes. Power plants typically cause a decrease in O_3 in the fresh plume immediately downwind of the power plant, followed by an increase in O_3 relative to the background concentration as the plume moves further downwind (White et al., 1983). Although the decrease in O_3 in the fresh plume is due to NO titration (via the reaction $NO+O_3 \rightarrow NO_2$) rather than NO_X-ROG chemistry, the fresh plume also exhibits ROG-sensitive chemistry with respect to ozone formation, while the downwind plume with enhanced O_3 has NO_X-sensitive chemistry.

The evolution towards NO_X-sensitive chemistry as air moves downwind is due largely to the removal of NO_X as the air mass ages. NO_X has a relatively short photochemical lifetime (3-6 hours) while many ROG species have lifetimes of 1 day or longer. Consequently, ROG/NO_X ratios always increase as an air mass ages. The addition of biogenic ROG as the air mass moves downwind also contributes to the conversion from ROG-sensitive to NO_X-sensitive chemistry. The increase in ROG/NO_X ratios with age is illustrated in Figure 2-1, which shows calculated ROG and NO_X concentrations in simulated air parcels, superimposed on isopleths that give the ozone production rate as a function of ROG and NO_X. In these model calculations, air parcels were initialized with an ROG-NO_X mix that would initially exhibit ROG-sensitive chemistry, but they evolve towards a higher ROG/NO_X ratio and NO_X-sensitive chemistry over the simulated 8-hour period.

It is generally accepted that rural locations are characterized by NO_X-sensitive chemistry, except in locations that are directly impacted by urban or power plant plumes (e.g. Sillman et al., 1990a, McKeen et al., 1991, Roselle et al., 1995). Rural air masses are typically far downwind from emission sources (except for biogenics) and show the chemical characteristics of aged air (Trainer et al., 1993), which includes NO_X-sensitive chemistry. Because these air masses frequently have 80-100 ppb ozone they can be

associated with regional transport and can have a significant impact on NO_X-ROG chemistry even in downwind urban areas (Sillman et al., 1990a). Similarly, events involving transport for periods of longer than one day are more likely to be NO_X-sensitive. ROG-sensitive chemistry is more likely in events dominated by local photochemical production rather than transport.

Meterological stagnation and density of emissions: A little-known feature of ozone photochemistry is the tendency for extremely stagnant episodes (i.e. with light winds and low mixing heights) in locations with high emission rates to exhibit ROG-sensitive chemistry, while episodes with greater meteorological dispersion or lower emission rates show NO_X-sensitive chemistry. This feature needs to be distinguished from the effects of chemical composition (i.e. ROG/NOx ratios and biogenic ROG) or transport vs. local photochemistry.

Milford et al. (1994 , see also Sillman et al., 1993) demonstrated the tendency for model calculations with high ROG and NO_X concentrations to exhibit ROG-sensitive chemistry while events with lower ROG and NO_X concentrations but with the same initial ROG/NO_X ratio would show NO_X-sensitive chemistry. This is also illustrated in the air parcel calculations in Figure 2-1. The series of air parcels shown here initially had the same ROG/NO_X ratio but different concentrations. Following an 8-hour simulation the air parcels with higher initial concentrations (corresponding to stagnant meteorology) still had ROG-sensitive chemistry while the parcels with lower initial concentrations (corresponding to greater meteorological dispersion) had NO_X-sensitive chemistry. Milford et al. also found that ROG- and NO_X-sensitive chemistry in models is correlated with high and low values of NO_Y respectively (see Figure 2-3). The higher NO_Y corresponded to stagnant meteorology while lower NO_Y corresponded to locations with greater dispersion.

Similar results were found in the ROM simulation by Roselle et al. (1995). Roselle et al. showed that events with the highest O3 concentrations were more likely to exhibit ROG-sensitive behavior, while events with lower O3 (corresponding to the 99th and 95th percentile of O3 in the simulation) were more likely to show NO_X-sensitive behavior. The difference between the higher and lower O3 in these simulations corresponded to stagnant events in contrast to events with greater dispersion.

The difference in NO_X-ROG chemistry between stagnant events and events with dispersion explains the tendency for models to predict different NO_X-ROG chemistry in the same location for different events. It also explains the tendency for ROG-sensitive chemistry to be associated with the largest cities while NO_X-sensitive chemistry is more often associated with smaller cities (e.g. Roselle and Schere., 1995).

The connection between NO_X-ROG chemistry and meteorological stagnation adds an additional dimension of uncertainty to the NO_X-ROG predictions of photochemical models, especially when model accuracy is evaluated solely in terms of ozone concentrations. Dispersion rates are especially difficult to estimate when winds are light and variable, and simulated peak ozone increases sharply as wind speed is decreased. This dependency of ozone on wind speed increases as wind speeds get lower. Models can simulate correct ozone through a series of compensating errors, e.g. overly stagnant meteorology in combination with underestimated biogenic ROG or underestimated regional transport; or vice versus. These types of compensating errors would cause changes in model predictions for NO_X-ROG sensitivity.

The association between ROG-sensitive chemistry, large cities and stagnant meteorology is due in part to the influence of biogenic ROG. Stagnant events tend to have higher concentrations of anthropogenic NO_X and ROG, whose sources are concentrated near urban centers, but not biogenic ROG which have a more ubiquitous source. However, there is also a factor directly related to photochemistry. Events with higher NO_X tend to have slower, less efficient chemistry (on the basis of ozone production per NO_X) (Liu et al., 1987, Lin et al., 1988) and consequently have a slower rate of evolution towards NO_X-sensitive chemistry.

Summary: The above description creates an image of the type of situations that are more likely to be associated with ROG-sensitive chemistry as opposed to NOx-sensitive chemistry. ROG-sensitive chemistry is associated with: low ROG/NO_X ratios; relatively low impact of biogenic hydrocarbons; locations close to emission sources as opposed to downwind; situations dominated by short-term local photochemistry as opposed to multiday transport; and large cities with stagnant meteorology. NO_X-sensitive chemistry is associated with the opposite. However, <u>these characterizations should be used as a general basis for understanding the behavior of photochemical models and not as predictions for specific locations</u>. NO_X-ROG predictions are subject to a great deal of uncertainty and need to be examined individually for each location. The description given here is only useful as a basis for understanding the impact of individual factors in isolation and for understanding differences in NO_X-ROG predictions between various model scenarios. Subsequent sections (Section 3 and the Appendix) will show NO_X-ROG predictions from individual model scenarios with varying ROG/NO_X emission ratios, biogenic ROG, location, vertical mixing rates and wind speeds. The differences between scenarios are consistent with the general description given here.

2.2 Chemistry of O_3, NO_X and ROG and its relation to photochemical indicators.

The chemistry of O_3, NO_X and ROG and its division into NO_X-sensitive and ROG-sensitive regimes can be derived directly from the reaction sequences that produce ozone. The analysis of NO_X-ROG chemistry in terms of reaction sequences, presented here, is important only in terms of theory. However it provides a rationale for the selection of specific species ratios as NO_X-ROG indicators. While the justification for NO_X-ROG indicators comes from results of more complete photochemical simulations, it is useful to show that the identified species are linked to NO_X-ROG chemistry in a more general sense than can be shown just from model results.

The chemistry of ozone formation can be understood from the following simplified reaction sequence.

$$RH + \text{[illegible]}O_2 + H_2O \qquad \text{R1}$$

$$RO_2 + NO \text{ [illegible]} + HO_2 + NO_2 \qquad \text{R2}$$

$$HO_2 + NO \xrightarrow{[O_2]} OH + NO_2 \qquad \text{R3}$$

$$CO + OH \xrightarrow{[O_2]} HO_2 + CO_2 \qquad \text{R4}$$

RH represents a generic hydrocarbon chain, and RO_2 represents an organic peroxy radical. Most hydrocarbon reaction sequences follow this format. The sequence is initiated by a reaction between a primary hydrocarbon and the OH radical, creating an RO_2 chain, and followed by a rapid reaction of the RO_2 with nitric oxide. The RO_2+NO reaction leads to the production of HO_2, which also reacts with NO to return the original OH radical. The RO_2+NO reaction also leads to the production of intermediate ROG species (represented here as R'CHO), which continue to react via a similar sequence until it is oxidized to CO or CO_2* .

---

* For example, here is the reaction sequence for propane (C_3H_8):

$$C_3H_8 + OH \xrightarrow{[O_2]} C_3H_7O_2 + H_2O \qquad \text{R1'}$$

$$C_3H_7O_2 + NO \xrightarrow{[O_2]} C_2H_5CHO + HO_2 + NO_2 \qquad \text{R2'}$$

Reactions R2 and R3 are the ozone-producing reactions, because the conversion from NO to NO_2 is followed by photolysis of NO_2 ($NO_2+hn \rightarrow NO+O$, $O+O_2+M \rightarrow O_3+M$). In this simplified version, the rate of ozone production can be associated with the rate of reaction R1, or with the summed rates of R2 and R3.

It is obvious that the rate of the above reaction sequence is controlled by the availability of odd hydrogen (or odd-H) radicals (OH, HO_2 and RO_2). The sum of odd-H radicals ($OH+HO_2+\sum RO_2$) is conserved in each of the above reactions. The behavior of the reaction system can be understood in terms of the following reactions that act as odd-H sinks or sources (Kleinman et al., 1986, Sillman et al., 1990a, 1995a):

$$HO_2 + HO_2 \rightarrow H_2O_2 + O_2 \qquad \text{R5}$$

$$RO_2 + HO_2 \rightarrow ROOH + O_2 \qquad \text{R6}$$

$$OH + NO_2 \rightarrow HNO_3 \qquad \text{R7}$$

$$O_3 + h\nu \xrightarrow{[H_2O]} 2\,OH \qquad \text{R8}$$

Photolysis of ozone (R8) is often the largest source of odd-H radicals. Photolysis of intermediate hydrocarbons (chiefly formaldehyde, HCHO, and other aldehydes) also provides a significant radical source and may exceed R8 in urban locations. The two major sinks for radicals are the formation of peroxides (R5 and R6) and the formation of nitric acid (R7). Net formation of PAN can also be a significant radical sink (Sillman et al., 1995c). The PAN reactions are included here for completeness:

$$RO_2 + NO_2 \rightarrow PAN \qquad \text{R9}$$

$$PAN \rightarrow RO_2 + NO_2 \qquad \text{R10}$$

Because the odd hydrogen radicals are short-lived, reactions R5-R8 form a steady state in which the radical source reaction (R8) is balanced by the radical sinks (R5, R6 and R7, along with net production of PAN). The resulting equation for odd-H radicals is:

$$S_H = P_{HNO3} + 2P_{H2O2} + 2P_{ROOH} + P_{PAN} \qquad (2\text{-}1)$$

where S_H represents the odd-H source (equal to $j_8[O3]$ with photolysis rate j_8 for reaction R8), P_{HNO3} represents the production rate for HNO_3 (equal to $k_7[OH][NO_2]$ with rate constant k_7 for reaction R7), P_{H2O2} and P_{ROOH} represents the production rate for peroxides (equal to $k_5[HO_2]^2$ and $k_6[HO_2][RO_2]$, respectively) and P_{PAN} represents net production of PAN and other PAN-like species.

The split into NO_X-sensitive and ROG-sensitive regimes for ozone can be derived directly from the above analysis of odd-H radicals. When peroxides represent the dominant sink for radicals, then equation (1) reduces to:

$$S_H = P_{ROOH} = 2k_5[HO_2]^2 + 2k_6[HO_2][RO_2] \quad (2\text{-}2)$$

In this situation the sum $[HO_2]+[RO_2]$ will be largely unaffected by ROG and NO_X, being determined entirely by the size of the radical source (S_H, dependent on sunlight, H_2O and O_3). The rate of ozone production, equal to the summed rates of reactions R2 (=RO_2+NO) and R3 (=HO_2+NO), will increase in direct proportion with NO_X and will show little dependence on ROG. ROG contributes to ozone production only to the extent that it increases the radical source (S_H), and even this impact is reduced by the quadratic term for HO_2. This corresponds to the NO_X-sensitive regime for ozone.

When nitric acid represents the dominant sink for radicals the situation is very different:

$$S_H = P_{HNO3} = k_7[OH][NO_2] \quad (2\text{-}3)$$

Here the concentration of the OH radical decreases with increasing NO_X. OH may also increase slightly with increasing ROG because ROG adds to the radical source (S_H). Since the rate of ozone production is approximately equal to the rate of reaction R1 (=RH+OH), ozone production will decrease with increasing NO_X. Ozone production will also increase with increasing ROG, possibly in a more-than-linear fashion. This corresponds to the ROG-sensitive regime.

A complete solution for the above nine-reaction system (Sillman, 1995a) showed that the split between the ROG-sensitive and NO_X-sensitive regimes occurs when the radical sinks through the formation of peroxides (R5 and R6) and the radical sink through the formation of nitric acid (R7) are exactly equal. Since each peroxide represents a sink for two odd-H radicals the transition from ROG- to NO_X-sensitive chemistry corresponds to

$$P_{HNO3} = 2(P_{H2O2} + P_{ROOH}) \quad (2\text{-}4)$$

The instantaneous rate of production of O_3 will be NO_X-sensitive whenever the instantaneous rate of production of peroxides ($P_{H2O2} + P_{ROOH}$) is greater than the instantaneous rate of production of nitric acid (P_{HNO3}) multiplied by 0.5, and that the rate of production of O_3 will be ROG-sensitive whenever the rate of production of nitric acid multiplied by 0.5 is greater than the rate of production of peroxides. This result suggests that the NOx-ROG sensitivity of ozone concentrations (as opposed to the instantaneous production rate) might be correlated with the ratio $\frac{H_2O_2}{HNO_3}$, using measured H_2O_2 and HNO_3 concentrations rather than production rates. Both of these species are relatively long-lived (1-2 days in the convective mixed layer, assuming dry deposition velocities of 1.0 cm/sec for H_2O_2 and 2.5 cm/sec for HNO_3). Deposition represents the largest sink for both species. The 1-2 day lifetime suggests that $\frac{H_2O_2}{HNO_3}$ will represent photochemical conditions representative of ozone formation over a 1-2 day period, which is appropriate for a diagnosis of NO_X-ROG sensitivity for ozone concentrations. The validity of $\frac{H_2O_2}{HNO_3}$ as an indicator for NO_X-ROG chemistry will be examined in Section 3.

The theoretical basis for O_3/NO_Z and O_3/HNO_3 as NO_X-ROG indicators can also be derived from the steady-state equation for odd-H radicals. Assuming that the radical source (S_H) is due to ozone photolysis, R8, the radical equation (2-1) can be rewritten as

$$j_8[O_3] = P_{HNO3} + 2P_{H2O2} + 2P_{ROOH} + P_{PAN} \qquad (2\text{-}1a)$$

Since the transition between the NO_X- and ROG-sensitive regimes occurs when the radical sink terms for peroxides and nitric acid are equal to each other (equation 2-4), the NO_X-ROG transition also corresponds to:

$$j_8[O_3] = 2P_{HNO3} + P_{PAN} \qquad (2\text{-}5a)$$

or

$$\frac{[O_3]}{2P_{HNO3} + P_{PAN}} = \frac{1}{j_8} \qquad (2\text{-}5b)$$

This result suggests the use of either O_3/NO_Z or O_3/HNO_3 as a NO_X-ROG indicator. A low value for O_3/NO_Z or O_3/HNO_3 suggests that the ratio $\frac{[O_3]}{2P_{HNO3} + P_{PAN}}$ was low for much of the air mass history, corresponding to ROG-sensitive chemistry, while a high value for O_3/NO_Z or O_3/HNO_3 suggests that the ratio $\frac{[O_3]}{2P_{HNO3} + P_{PAN}}$ was high for much of the air mass history, corresponding to NO_X-sensitive chemistry As was the case

for $\frac{H_2O_2}{HNO_3}$, the indicator ratios O_3/NO_Z and O_3/HNO_3 both involves species with a 1-2 day lifetime and therefore reflect the chemistry associated with a cumulative period of ozone production. Unlike $\frac{H_2O_2}{HNO_3}$, the equation for $\frac{O_3}{NO_Z}$ suggests that the NO_X-ROG transition may vary with cloud cover or with water vapor, both of which affect the reaction rate parameter, j8.

The linear correlation between O_3 and the sum $2H_2O_2+NO_Z$, proposed as an evaluation for the indicator method, is also based on the theoretical analysis of the steady-state radical equation (2-1). The radical equation suggests that there should be a linear correlation between O_3 and $(2H_2O_2+NO_Z)$ because the former represents the odd-H radical source and the latter represents the sum of radical sinks. Since the indicator method is linked in theory to the role of these species as radical sources and sinks, it is important that the measured correlation between these species show reasonable correspondence with model results. The slope between O_3 and $(2H_2O_2+NO_Z)$ is expected to vary with water vapor concentration because the rate of the photolysis reaction R8 includes dependence on water vapor. The slope should also vary from day to day based on cloud cover (which also affects the photolysis reaction) and rainfall (which removes H_2O_2 and HNO_3). However it should show relatively little variaion between rural and urban locations during the same time period. This predicted linear correlation should contrast with the relation between O_3 and NO_Z, which often shows a decreasing O_3-NO_Z slope as NOz increases (Daum et al., 1996). The slope between O_3 and $(2H_2O_2+NO_Z)$ might be expected to increase slightly in urban locations due to the added radical source associated with hydrocarbons.

The above analysis has identified correlations between NO_X-ROG sensitivity and indicator ratios based solely on an analysis of ozone production. It has not included the impact of NO_X titration, i.e. removal of ozone through the reaction O_3+NO which is commonly associated with power plants and other large NO_X emission sources. Subsequent results are based on models with a more complete representation of photochemistry and include this effect. However the indicator-NOx-ROG correlations (for both O_3/NO_Z and $\frac{H_2O_2}{HNO_3}$) show a characteristic failure in locations where O_3-NO_Z-ROG chemistry is dominated by ozone destruction via the O_3+NO reaction rather than by photochemical production of ozone. Since NO_X-ROG chemistry is primarily of interest in situations dominated by ozone production this problem should not limit its use. The indicator correlations shown in the next section appear to function correctly in models that include large area NO_X sources (i.e. large cities). However care must be taken when

indicator measurements are made in the immediate vicinity of a large NO_X point source, e.g. a power plant.

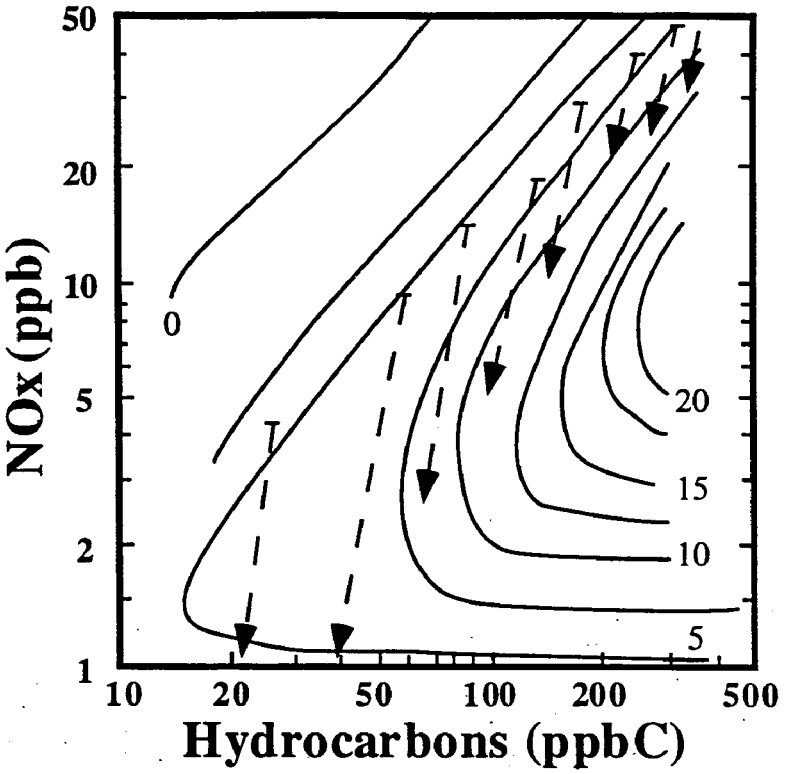

Figure 2-1. Isopleths showing net rates of ozone production in ppb/hour, averaged over an 8-hour daytime period, as a function of NO_X and ROG concentrations. Isopleths range from 0 to 20 ppb/hour in intervals of 2.5 ppb/hr. The dashed lines represent calculated evolution of NO_X and ROG concentrations over an eight-hour period for air parcels with an initial ROG/NO_X ratio of 5:1, adapted from Milford et al. (1994).

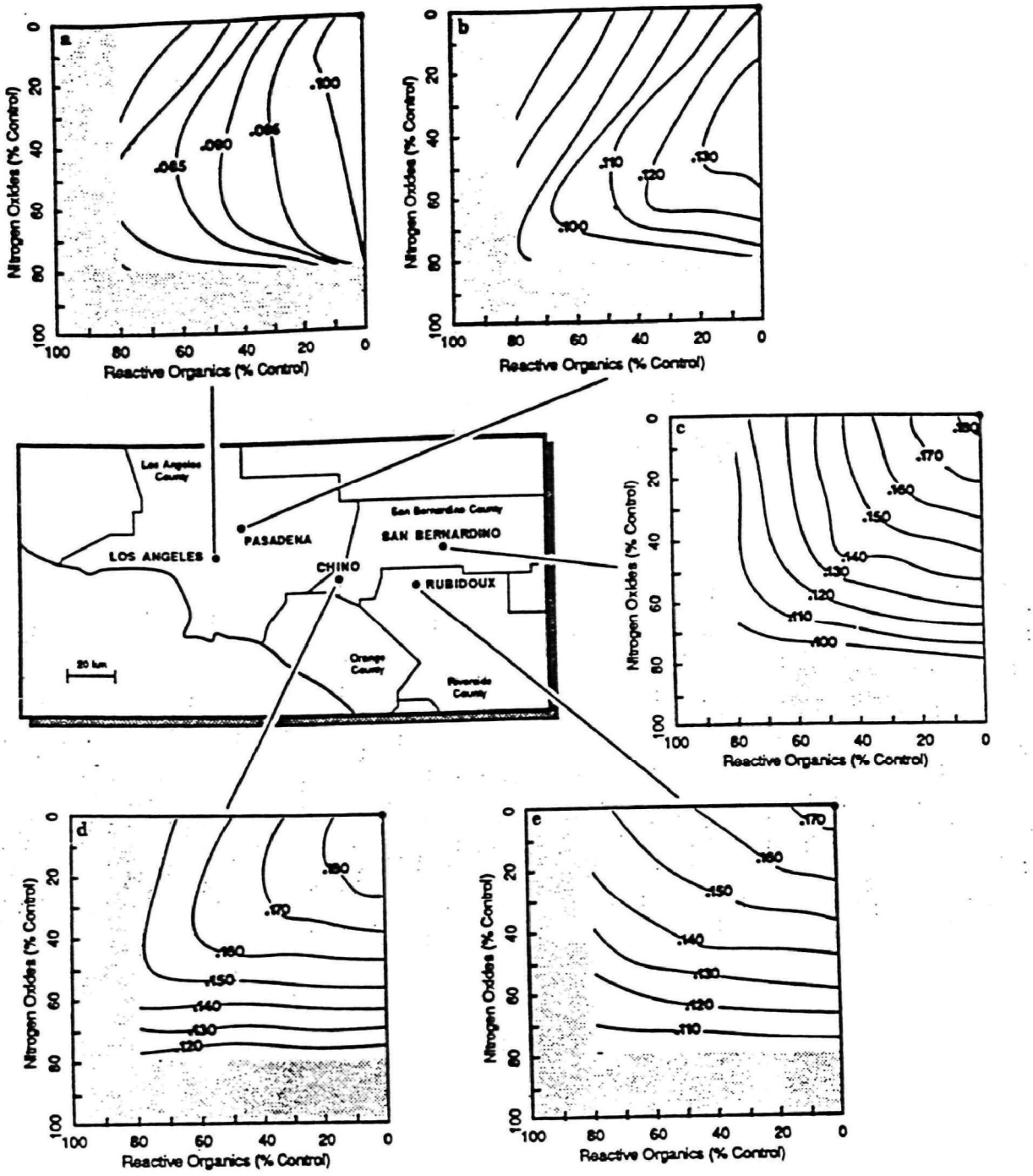

Figure 2-2. Predicted response of peak ozone concentrations (ppm) at locations across the Los Angeles basin, to spatially uniform NO_X and ROG emissions reductions. The upper right-hand corner of each response diagram corresponds to the base case. (a) Downtown Los Angeles; (b) Pasadena; (c) San Bernadino; (d) Chino; (e) Roubidoux. From Milford et al., 1989.

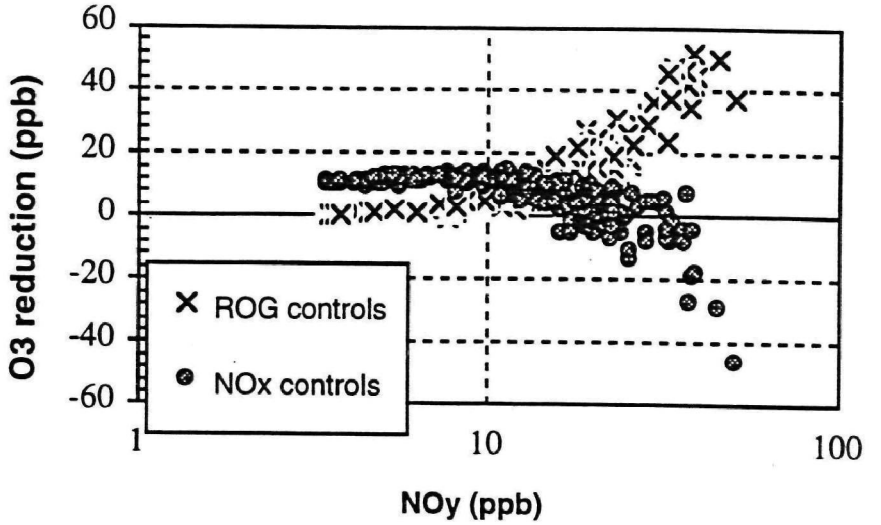

(a) Lake Michigan regional simulation - base case

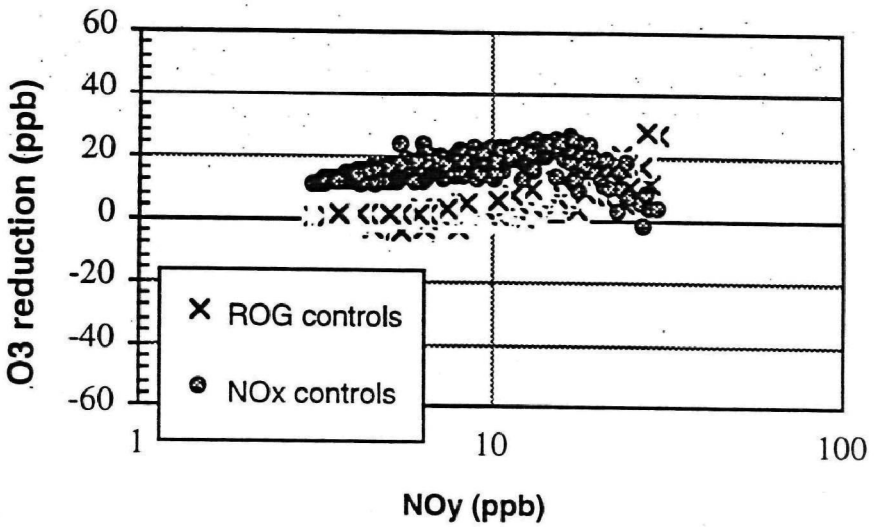

(b) Northeast corridor regional simulation - base case

Figure 2-3. Predicted reduction in peak O_3 (in ppb) resulting from a 35% reduction in the emission rate for anthropogenic ROG (crosses) and from a 35% reduction in the emission rate for NO_X (circles) plotted against NO_Y (ppb) coincident with the ozone peak. Simulations are described in Section 3.1. From Sillman (1995a) based on Milford et al. (1994) and Sillman (1993).

SECTION 3
RESULTS FROM PHOTOCHEMICAL SIMULATIONS

This section will present results for O_3-NO_X-ROG sensitivity from a series of photochemical simulations and analyze the correlation between NO_X-ROG sensitivity and the various photochemical indicators as predicted by the models.

Results will be based on groups of three simulations: an initial scenario, a simulation with anthropogenic ROG emissions reduced by a fixed percentage (usually 35%) relative to the initial scenario, and a simulation with anthropogenic NO_X emissions reduced by the same percentage relative to the initial scenario. Results will be shown for a specific hour (usually in the afternoon, and corresponding to the time of peak O_3 occurring in the initial model scenario). ROG-sensitivity will be reported as the difference between O_3 in the initial scenario and O_3 in the simulation with reduced ROG at the same time and location. NO_X-sensitivity will be similarly reported as the difference between O_3 in the initial scenario and O_3 in the simulation with reduced NO_X. These results for model ROG- and NO_X-sensitivity will be presented in comparison with values for photochemical indicators at the same time and location in the initial model scenario. Results will typically be reported for every location in the model domain or sub-region of interest.

Complete graphical results will be shown for two indicator ratios: $\frac{O_3}{NO_Z}$ and $\frac{H_2O_2}{HNO_3}$. Results for the other indicator ratios are visually very similar to these two, and will be presented in abbreviated form. In addition, a concise method for tabulating results of the NO_X-ROG-indicator correlation will be developed, based on a statistically defined transition between indicator values associated with ROG-sensitive chemistry and indicator values associated with NO_X-sensitive chemistry. This statistically defined transition point will be used to summarize results from all model scenarios and for each indicator ratio. Graphical results will also be shown for indicator ratios that did not correlate well with NO_X-ROG sensitivity: $\frac{O_3}{NO_X}$ and the ratio of reactivity-weighted hydrocarbons to NO_y.

The simulation results shown here should not be interpreted as recommendations for specific ozone abatement strategies or as statements about NO_X-ROG sensitivity in specific locations. Many of the simulations use outdated inventories for anthropogenic emissions. Most of the simulations use the BEIS1 inventory for biogenics, which underestimates isoprene by a factor of three or more (Geron et al., 1994) and consequently causes model results to be biased in favor of ROG controls. In addition, the selection of model scenarios for the NO_X-ROG analysis deliberately favored ROG-sensitive scenarios, especially for Atlanta. A meaningful evaluation of NO_X-ROG indicators is only possible in model scenarios that include both NO_X-sensitive and ROG-sensitive subregions, which did not occur in some of the NO_X-sensitive scenarios. Despite these caveats, the model NO_X-ROG results are offered as meaningful indications of NO_X-ROG sensitivity in relation to each other; i.e., the differences in NO_X-ROG sensitivity between model scenarios represent tendencies that are likely to be reproduced in other NO_X-ROG models.

3.1 Description of photochemical simulations

Results are based on five separate model applications: a regional-scale simulation for the Lake Michigan airshed, a regional-scale simulation for the northeast corridor, an urban-scale (UAM-IV) simulation for New York, an urban-scale (UAM-IV) simulation for Atlanta, and an urban-scale (UAM-IV) simulation for Los Angeles. Preliminary results are also shown for the Middle Tennesee Ozone Study in Nashville. A detailed description of each simulation is given here.

(a) Lake Michigan regional simulations:

Event: August 1-2, 1988.

Model: Regional-scale model developed at the University of Michigan.

Chemistry: Lurman et al. (1986) with various updates, including reaction rates from DeMore et al. (1992), added RO_2+HO_2 reactions from Jacob and Wofsy (1988), isoprene chemistry from Paulson and Seinfeld (1992), photolysis rates from Madronich (1987), column ozone equal to 325 DU, aerosol optical depth 0.68, representing moderately polluted conditions, clear skies. Dry deposition velocities over land were: O_3 and NO_2, 0.6 cm s^{-1}; NO, 0.1 cm s^{-1}; HNO_3, 2.5 cm s^{-1}; PAN, 0.25 cm s^{-1}; and H_2O_2, 1.0 cm s^{-1}. Deposition velocities over water were reduced to 0.05 cm s^{-1} for all these species, reflecting a probable surface inversion over cold water during the simulated events.

Grid resolution and domain size: 20x20 km horizontal resolution, 3 vertical layers. The vertical structure accounts for stable conditions over Lake Michigan during the daytime and generates a confined sub-layer for urban emissions from Chicago, with typical heights 200-500 meters. The vertically confined Chicago plume is consistent with recent aircraft measurements by Hillery (1995). The domain extends from south of Chicago to the northern end of Lake Michigan, 220x380 km. This was combined with a coarse-resolution model for regional transport that included most of the eastern U.S. (Sillman et al., 1990b). NO_X-ROG sensitivity was based on reduced emissions throughout both model domains.

Horizontal advection: Smolarkiewicz (1983) for the local domain, Prather (1986) for regional transport.

Meteorology: Winds were interpolated from measurements at sites in the Lake Michigan region and from regional measurements from the National Weather Service. Some modifications were made in wind speeds to improve model performance vs. measured ozone. Mixing heights were based on measured vertical temperature profiles at land-based sites, along with the assumption that growth of the mixed layer ceases as air travels over Lake Michigan.

Emissions: Anthropogenic emissions are from the NAPAP 1980 inventory (EPA, 1986). Biogenic emissions are derived from data by Lamb et al. ((1985) in combination with land use data by Matthews (1983), similar to BEIS1.

Alternate scenarios: Modified scenarios include doubled anthropogenic ROG emissions and anthropogenic emissions reduced by half. NO_X-ROG results are reported for 6 pm, which corresponded to peak or near-peak O_3 in all scenarios.

Reference: Sillman et al., 1993.

(b) Northeast corridor regional simulations:

Event: June 14-15, 1988.

Model: Regional-scale model developed at the University of Michigan.

Chemistry: Lurman et al. (1986) with various updates, including reaction rates from DeMore et al. (1992), added RO_2+HO_2 reactions from Jacob and Wofsy (1988), isoprene chemistry from Paulson and Seinfeld (1992), photolysis rates from Madronich (1987), column ozone equal to 325 DU, aerosol optical depth 0.68, representing moderately polluted conditions, clear skies. Dry deposition velocities over land were: O_3 and NO_2, 0.6 cm s^{-1}; NO, 0.1 cm s^{-1}; HNO_3, 2.5 cm s^{-1}; PAN, 0.25 cm s^{-1}; and H_2O_2, 1.0 cm s^{-1}. Deposition velocities over water were reduced to 0.05 cm s^{-1}

for all these species, reflecting a probable surface inversion over cold water during the simulated events.

Grid resolution and domain size: 20x20 km horizontal resolution, 3 vertical layers. The vertical structure accounts for stable conditions over the Atlantic Ocean during the daytime and generates a confined sub-layer for land-based emissions. The domain extends from south of Chicago to the northern end of Lake Michigan, 480x560 km. This was combined with a coarse-resolution model for regional transport that included most of the eastern U.S. (Sillman et al., 1990b). NO_X-ROG sensitivity was based on reduced emissions throughout both model domains.

Horizontal advection: Smolarkiewicz (1983) in the local domain, Prather (1986) for regional transport.

Meteorology: Winds were interpolated from measurements at sites along coastal New England and from regional measurements from the National Weather Service. Some modifications were made in wind speeds to improve model performance vs. measured ozone. Mixing heights were based on measured vertical temperature profiles at land-based sites, along with the assumption that growth of the mixed layer ceases as air travels over the Atlantic Ocean.

Emissions: Anthropogenic emissions are from the NAPAP 1980 inventory (1986). Biogenic emissions are derived from data by Lamb et al. ((1985) in combination with land use data by Matthews (1983), similar to BEIS1.

Alternate scenarios: Modified scenarios include the following: a scenario with zero biogenic emissions; a scenario with doubled isoprene emissions and mixed layer heights reduced by half; a scenario with wind speeds reduced by half; a scenario with increased deposition velocities (4 cm s^{-1} for H_2O_2 and HNO_3 over land) and wind speeds reduced by half. NO_X-ROG results are reported for 6 pm, which corresponded to peak or near-peak O_3 in all scenarios.

Reference: Sillman et al., 1993.

(c) New York urban simulations:

Event: July 21, 1980.

Model: Urban Airshed Model (UAM-IV).

Chemistry: Carbon Bond IV.

Grid resolution and domain size: 8x8 km horizontal grid cell resolution, 5 or 7 vertical layers. The domain extends from central New Jersey to eastern Connecticut and Long Island (248x200 km). Upwind conditions were derived from the Regional

Oxidant Model, with nominal 20x20 km horizontal grid resolution and domain covering the eastern half of the U.S.

Horizontal advection: Different scenarios use either Smolarkiewicz (1983) or Bott (1989).

Meteorology: Two scenarios were included with different meteorology. One used the UAM-IV diagnostic wind processor in combination with measured vertical profiles of temperature and wind speeds from the National Weather Service. The other scenario used results from a dynamic mesoscale meteorological model (MMM) by Ulrickson and Hass (1990), including four-dimensional data assimilation.

Emissions: Anthropogenic emissions are from the Rao and Sistla (1993). Biogenic emissions are from BEIS1 (Pierce et al., 1990).

Alternate scenarios: Two scenarios were included: a scenario with five model vertical layers and meteorology from the UAM diagnostic wind processor ("DWM-5") and a scenario with seven model vertical layers and meteorology from the mesoscale meteorological model ("MMM-7"). The latter scenario had lower wind speeds and resulted in higher ozone. NO_X-ROG results are reported for 5 pm. Peak O_3 occured at 3 pm.

(d) Atlanta urban simulations:

Event: August 9-11, 1992.

Model: Urban Airshed Model (UAM-IV).

Chemistry: Carbon Bond IV.

Grid resolution and domain size: 4x4 km horizontal resolution, 5 or 7 vertical layers in different scenarios. The domain includes metropolitan Atlanta (108x140 km) but does not include regional-scale chemistry and transport. Upwind conditions had O_3=55 ppb, based on measurements upwind of Atlanta, and NO_X=1 ppb. In addition, the scenarios included here have upwind H_2O_2 (=1 ppb), HNO_3 (=2 ppb) and PAN (=0.75 ppb). These modified upwind concentrations were derived from correlations between O_3 and NO_Z (Trainer et al., 1993) and O_3 and PAN (Roberts et al., 1995) at rural sites in eastern North America.

Horizontal advection: Smolarkiewicz (1983).

Meteorology: UAM-IV diagnostic wind processor in combination with measured vertical profiles of temperature and wind speeds. Mixing heights based on measured vertical profiles and methods described by Marsik et al. (1995).

Emissions: Anthropogenic emissions are from Cardelino et al. (1994). Biogenic emissions are from BEIS1 (Pierce et al., 1990).

Alternate scenarios: The scenarios shown here all had mixing heights reduced by 20% relative to the base case, in order to enhance model sensitivity to ROG. They include a scenario with BEIS1 biogenics and a scenario with tripled emission rates for isoprene, approximately equal to the BEIS2 inventory (Geron et al., 1995). NO_X-ROG results are reported for 5 pm.

Reference: Sillman et al., 1995b, 1997a.

(e) Los Angeles urban simulations:

Event: August 26-29, 1987.

Model: Urban Airshed Model (UAM-IV).

Chemistry: Carbon Bond IV.

Grid resolution and domain size: 5x5 km horizontal grid cell size, 5 vertical layers. The domain includes metropolitan Los Angeles (180x325 km). Boundary conditions were 30 ppb O_3.

Horizontal advection: Different scenarios use either Smolarkiewicz (1983) or Bott (1989).

Meteorology: UAM-IV diagnostic wind processor in combination with measured vertical profiles of temperature and wind speeds.

Emissions: Anthropogenic emissions are from the Southern California Air Quality Study (SCAQS) (Lawson et al., 1990, Wheeler et al., 1992). Biogenic emissions are from BEIS1 (Pierce et al., 1990).

Alternate scenarios: The scenario by Godowitch and Vukovich (1994) uses a version of UAM-IV with horizontal advection based on Bott (1989). Scenarios by Wagner et al. (1992) use the standard UAM-IV with horizontal advection based on Smolarkiewicz (1983). The scenarios by Wagner et al. include a base case, a case with doubled anthropogenic ROG and a case with tripled anthropogenic ROG. Simulated control strategies are based on 25% reductions relative to the initial scenarios, rather than 35% in the other case studies. NO_X-ROG results are reported for 3 pm.

Note: Recent, more detailed photochemical models for Los Angeles have been developed by Harley et al. (1993), Kumar et al. (1994) and Lu and Turco (1995).

Reference: Godowitch and Vukovich (1994), Wagner et al. (1992).

(f) Nashville simulations (preliminary):

Event: July 11-13, 1995.

Model: Nested urban and regional-scale model developed at the University of Michigan.

Chemistry: Lurman et al. (1986) with various updates, including reaction rates from DeMore et al. (1992), added RO_2+HO_2 reactions from Jacob and Wofsy (1988), isoprene chemistry from Paulson and Seinfeld (1992), photolysis rates from Madronich (1987), column ozone equal to 325 DU, aerosol optical depth 0.68, representing moderately polluted conditions, clear skies. The chemistry for this simulation also includes modified RO_2-RO_2 reactions and rates recommended by Kirchner and Stockwell (1996), which were not included in previous cases with this model. Dry deposition velocities over land were: O_3 and NO_2, 0.6 cm s^{-1}; NO, 0.1 cm s^{-1}; HNO_3, 2.5 cm s^{-1}; PAN, 0.25 cm s^{-1}; and H_2O_2, 2.5 cm s^{-1}. Deposition velocities for H_2O_2 were increased in comparison with (a) and (b) above, based on recent work by Hall et al. (1997).

Grid resolution and domain size: 5x5 km horizontal resolution, 3 vertical layers. The domain is 180x180 km, centered on downtown Nashville. This was combined with a coarse-resolution model for regional transport that included most of the eastern U.S. (Sillman et al., 1990b). NO_X-ROG sensitivity was based on reduced emissions throughout both model domains.

Horizontal advection: Smolarkiewicz (1983) for the local domain, Prather (1986) for regional transport.

Meteorology: Winds and mixing heights were derived from the Rapid Update Cycle (RUC) prognostic model (Benjamin, 1994), with modifications based on on-site measurements in the Nashville area.

Emissions: Anthropogenic emissions are from the NAPAP 1990 inventory (EPA, 1993) for the regional background. Emissions for the Nashville urban domain are from an indentory developed as part of the 1988 State Implementation Plan (SIP) for Nashville, developed by W. Davis (University of Tennesee, Knoxville) and used with permission from J. Walton (Tennesee Department of Environmental Quality). Biogenic emissions are from BEIS2 (Geron et al., 1994).

Alternate scenarios: Modified scenarios include cases with dry deposition of H2O2 and HNO3 increased to 4 cm s^{-1}, cases without the RO_2-RO_2 reactions recommended by Kirchner and Stockwell, cases with changed wind speeds and with reduced emission of biogenic hydrocarbons. NO_X-ROG results are reported for 4 pm, July 13, which corresponded to peak or near-peak O_3 in all scenarios.

Reference: Sillman et al., 1997b. This publication has been recently submitted for publication and has not yet been through peer review. Only preliminary results are included here.

3.2 Results

(a) $\frac{O3}{NO_Z}$, $\frac{O3}{NO_y}$ and $\frac{O3}{HNO3}$:

Figure 3-1 shows the correlation between model NO_X-ROG sensitivity and $\frac{O3}{NO_Z}$ for six model scenarios. The figure shows the reduction in O3 associated with a particular percentage reduction in anthropogenic ROG or NO_X emissions (usually 35%), defined as the difference between O3 in the initial scenario and O3 in the scenario with reduced ROG or NO_X at the same time and location. Negative values represent locations in which reduced anthropogenic emissions results in an increase in O3. The simulated NO_X-ROG reductions are plotted for all locations in the model domain, in comparison with $\frac{O3}{NO_Z}$ in the initial model scenario at the same time and location.

Each simulation shows a similar pattern. Locations with larger ozone reductions in response to reduced ROG rather than reduced NO_X (i.e. locations with ROG-sensitive chemistry) also have low $\frac{O3}{NO_Z}$ (<8) in the initial simulation, while locations with larger ozone reductions in response to reduced NO_X (i.e. locations with NO_X-sensitive chemistry) also have high $\frac{O3}{NO_Z}$ (>10). There is also a well-defined value for $\frac{O3}{NO_Z}$ that defines the transition between NO_X-sensitive and ROG-sensitive regions. This transition value remains the same in simulations for different metropolitan areas and for different model scenarios.

Figure 3-1 also shows that the correlation between NO_X-ROG sensitivity and the indicator ratio $\frac{O3}{NO_Z}$ remains consistent in model scenarios with very different overall NO_X-ROG results. For example: the Lake Michigan base case (Figure 3-1a) has primarily ROG-sensitive chemistry, especially in the locations with highest ozone in the plume from Chicago. When the Lake Michigan simulation is repeated with initial doubled ROG emissions (Figure 3-1b) the predicted NO_X-ROG sensitivity changes and the locations with highest ozone show approximately equal sensitivity to reductions in NO_X and ROG. A comparison of these two scenarios shows that $\frac{O3}{NO_Z}$ also changes from low values in the ROG-sensitive scenario to higher values in the more NO_X-sensitive scenario. The change

in $\frac{O3}{NO_Z}$ between the two scenarios is consistent with the overall correlation between NO_X-ROG chemistry and $\frac{O3}{NO_Z}$, and suggests that measured $\frac{O3}{NO_Z}$ might be used as a basis for choosing between the NO_X-ROG predictions of these two model scenarios.

Results from the two simulations for New York (Figures 3-1c and 3-1d) illustrate the impact of meteorology on NO_X-ROG predictions. The northeast corridor base case (Figure 3-1c) is characterized by relatively strong winds and vigorous vertical mixing, and results in a largely NO_X-sensitive simulation. The New York UAM scenario (with MMM-7 meteorology) has lighter winds and results in a largely ROG-sensitive simulation. The ROG-sensitive simulation also shows low $\frac{O3}{NO_Z}$ while the NO_X-sensitive simulation shows high $\frac{O3}{NO_Z}$. As with the Lake Michigan case, the change in $\frac{O3}{NO_Z}$ between these two scenarios is consistent with the overall correlation between $\frac{O3}{NO_Z}$ and NO_X-ROG sensitivity. Although these two results were produced with different photochemical models the difference between NO_X-ROG predictions appears to be due to the difference in meteorology between the two events rather than to differences between the models. When the northeast corridor simulation is repeated with lower wind speeds it shows ROG-sensitive chemistry, and when the New York UAM scenario is repeated with stronger wind speeds it shows NO_X-sensitive chemistry. (Results for these scenarios are shown in Appendix B). The correlation between $\frac{O3}{NO_Z}$ and NO_X-ROG sensitivity appears consistent between the two models.

Lastly, the contrast between simulations for Atlanta and Los Angeles (Figures 3-1e and 3-1f) illustrates the differences between cities with characteristics that favor NO_X-sensitive chemistry as opposed to ROG-sensitive chemistry. Los Angeles as an urban area has several characteristics that favor ROG-sensitive chemistry based on the description in Section 2: a large city with high density ofemissions; limited vertical dilution; relatively low emission rates of biogenic ROG in comparison with anthropogenic ROG; and domination by local chemistry rather than regional transport. By contrast, Atlanta is a relatively smaller city with lower emission density; higher ventillation rates than Los Angeles, and high rates of biogenic emissions. The simulation results in Figures 3-1e and 3-1f reflect these differences, showing extensive NO_X-sensitive chemistry in Atlanta and extensive ROG-sensitive chemistry in Los Angeles. The simulations show a similar difference between high $\frac{O3}{NO_Z}$ in Atlanta in association with NO_X-sensitive chemistry and low $\frac{O3}{NO_Z}$ in Los Angeles in association with ROG-sensitive chemistry. This difference in

$\frac{O3}{NO_Z}$ between Atlanta and Los Angeles, predicted by photochemical models, is also consistent with ambient measurements (see Section 5).

Although the correlation between $\frac{O3}{NO_Z}$ and NO_X-ROG sensitivity appears consistently in all six simulations, there are a few locations in the Los Angeles simulation (Figure 3f) that violate the general pattern. These locations are characterized by high $\frac{O3}{NO_Z}$ (>12) and ROG-sensitive chemistry. These locations are all characterized by a large negative response to reduced NO_X, i.e. reduced NO_X causes a significant increase in simulated O3 at these locations. These exceptional points occur in locations where NO_X-ROG sensitivity results are dominated by titration of O3 by direct emissions from a local NO_X source. As explained in Section 2, the association between $\frac{O3}{NO_Z}$ and NO_X-ROG sensitivity is derived in theory from the chemistry of ozone production and does not include NO_X titration. The same type of exception appears in results with most of the other indicator ratios (e.g. see Figure 3-4f). The exceptions do not appear in results for $\frac{O3}{NO_y}$, ilustrated in Figure 3-2, because locations dominated by NO_X titration all have characteristically high NO_y and low $\frac{O3}{NO_y}$.

Results from other simulations for the indicator ratios $\frac{O3}{NO_Z}$, $\frac{O3}{NO_y}$ and $\frac{O3}{HNO3}$ are all visually similar to the results in Figures 3-1 and 3-2. Complete results are shown in the Appendix. Summary transition values for NO_X- vs ROG-sensititive chemistry are: 8-10 for $\frac{O3}{NO_Z}$; 6-7.5 for $\frac{O3}{NO_y}$; and 10-15 for $\frac{O3}{HNO3}$.

A useful way to describe the correlation between NO_X-ROG sensitivity and indicator ratios is to compare the statistical distribution of indicator values associated with NO_X-sensitive chemistry with the distribution of indicator values associated with ROG-sensitive chemistry in individual photochemical simulations. The distribution of $\frac{O3}{NO_Z}$ for NO_X-sensitive and ROG-sensitive locations in the simulation for Los Angeles is shown in Figure 3-3. The following definition is used for this analysis: a location is defined as *NO_X-sensitive* if O3 in the simulation with reduced NO_X emissions is lower than O3 in both the initial simulation and the simulation with reduced ROG by at least 5 ppb. Similarly, a location is *ROG-sensitive* if O3 in the simulation with reduced ROG emissions is lower than O3 in both the initial simulation and the simulation with reduced NO_X by at least 5 ppb. Results of this analysis (Figure 3-3) show that a large majority of ROG-sensitive locations have much lower $\frac{O3}{NO_Z}$ than the NO_X-sensitive locations and there is

relatively little overlap between the range of $\frac{O3}{NO_Z}$ for ROG-sensitive locations and the range of \f(O3,NO_Z) for NO_X-sensitive locations. The 92nd percentile of the distribution of $\frac{O3}{NO_Z}$ for ROG-sensitive locations (8.25) is almost identical with the 8th percentile of the distribution of $\frac{O3}{NO_Z}$ for NO_X-sensitive locations (8.16). In other words, 92% of the ROG-sensitive locations have $\frac{O3}{NO_Z}$ below this value while 92% of the NO_X-sensitive locations have $\frac{O3}{NO_Z}$ above this value.

The presentation of model results in terms of percentile distributions of NO_X- and ROG-sensitive indicator values also provides a concise way of tablulating the indicator-NO_X-ROG correlation from individual simulations. Table 3-1 shows the 95th percentile indicator values for ROG-sensitive locations and the 5th-percentile indicator values for NO_X-sensitive locations for each model scenario. A comparison between the 95th and 5th percentile values provides an estimate for the extent of overlap between ROG-sensitive and NO_X-sensitive indicator values; i.e. when the 95th percentile ROG-sensitive value is equal to or lower than the 5th percentile NO_X-sensitive value there is little overlap between NO_X-sensitive and ROG-sensitive indicator values. The 95th and 5th percentile values also define the transition point between NO_X-sensitive and ROG-sensitive indicator values in each scenario and provide a convenient basis for comparison between indicator transition points in each simulation. This information is also presented graphically in Figure 3-4. The information in Figure 3-4 can be easily understood if it is kept in mind that 95% of the locations with ROG-sensitive chemistry in each simulation have indicator values below the solid line in the figure, while 95% of location with NO_X-sensitive chemistry have indicator values above the dashed line.

As shown in Table 3-1 and Figure 3-4 the correlation between NO_X-ROG sensitivity and the indicator ratios $\frac{O3}{NO_Z}$, $\frac{O3}{NO_y}$ and $\frac{O3}{HNO3}$ remains consistent for a wide range of simulations, including scenarios for different cities, different meteorology, widely varying anthropogenic emission rates, ROG/NO_X ratios and biogenic emission rates. The transition point between NO_X- and ROG-sensitive chemistry shows relatively little variation among the model scenarios. The values for the NO_X-ROG transition for each indicator, cited above, also appear clearly in Figure 3-4. The subsequent notes focus results that represent exceptions to this generally consistent pattern. The first three issues below (multiday transport, deposition rates and particulate nitrate) relate to uncertainties in science. The others (Smolarkiewicz advection and upwind boundary conditions) relate to model artifacts.

(1) The simulation for the northeast corridor with zero isoprene also shows NO_X-ROG transition values that are significantly higher than the other scenarios. The apparent reason for this discrepancy is that the urban plume from the New York metropolitan area still has ROG-sensitive chemistry even after 24 hours of downwind transport. Conseqnently the NO_X-ROG transition is affected by nighttime chemistry. In the other scenarios, plumes that are more than 24 hours downwind from emission sources are either all NO_X-sensitive (due to photochemical aging and loss of NO_X at night) or else have exited from the model domain. The NO_X-ROG transition in a 2-day-old plume may occur at a higher indicator ratio due to more rapid removal of HNO_3 relative to O_3 as the plume ages.

(2) The simulation for the northeast corridor with increased dry deposition rates for HNO_3 and H_2O_2 has a higher NO_X-ROG transition point than the other scenarios. This may represent a significant scientific uncertainty. The uncertain removal rate for HNO_3 is also related to uncertainties in the interpretation of particulate nitrate measurements, discussed below. In a sensitivity test shown here, increased deposition causes the NOx-ROG transition to increase by only 10%, but the change in deposition was relatively small (4 cm/s for HNO_3 vs 2.5 cm/s in the base case). Preliminary results for Nashville, included in Table 3-1, also has higher NO_X-ROG transition points in a scenario with high deposition.

(3) None of the simulations shown here include particulate nitrate. It is unclear whether particulate nitrate should be included implicitly in HNO_3, NO_Z or NO_y. To the extent that particulate nitrate is formed directly from HNO_3 and is ultimately derived from NO_X emissions, it should be either represented as a loss term for HNO_3 in model calculations or else included implicitly in model gas-phase HNO_3. But if particulate nitrate is emitted directly into the atmosphere, this directly emitted nitrate should not be included in the indicator ratios. Parrish et al. (1993) found that particulate nitrate was small compared to HNO_3 and other components of NO_Z at rural sites in eastern North America, but Tuazon et al (1980, 1981) found that NH_4NO_3 aerosols accounted for a significant fraction of total reactive nitrogen (assumed to include NO_3^- but not NH_3 or NH_4^+) at one site (but not all sites) in Los Angeles. Interpretation of particulate nitrate represents a significant uncertainty.

(4) The UAM-IV simulations for Los Angeles from Wheeler et al. (1992) generated much greater overlap between ROG-sensitive and NO_X-sensitive indicator values than any of the other simulations. The degree of overlap in the Wheeler et al. simulations might be due to the Smolarkiewicz advection calculation in combination with the extremely sharp gradients in O_3 and reactive nitrogen in the simulations. These simulations included gradients in ozone concentrations of 50 ppb or higher between adjacent 5x5 km horizontal

grid cells, with corresponding gradients in reactive nitrogen and H_2O_2. In the Smolarkiewicz advection calculation the presence of steep concentration gradients can cause results for individual locations to be affected by the concentrations of neighboring grid cells. This may be the cause of the imprecise NO_X-ROG-indicator correlation in the simulations by Wheeler et al. The simulation by Godowitch et al. represents the same event and uses similar meteorology and the same photochemical model, but advection is calculated based on Bott (1989) instead of Smolarkiewicz. The resulting simulation shows much less overlap between NO_X-sensitive and ROG-sensitive indicator values. Imprecision associated with the Smolarkiewicz advection calculation has been cited elsewhere (Chock, 1991).

Results tend to be somewhat better for $\frac{O_3}{NO_y}$ than $\frac{O_3}{NO_z}$, especially for the Los Angeles simulations by Wagner et al. Despite this, it is recommended that $\frac{O_3}{NO_z}$ be used as in indicator rather than (or in addition to) $\frac{O_3}{NO_y}$ whenever possible. This recommendation is partly based on the fact that a useful correlation has been found in measurements between O_3 and NO_Z (see the Los Angeles case study in Section 5, also Figures 4-3 and 4-4 and results in Trainer et al., 1993). In addition, measured $\frac{O_3}{NO_y}$ at surface sites may be dominated by on-site NO_X emissions.

In situations where only NO and NO_y measurements are available a useful approximation for NO_X and NO_Z might be made by using the steady-state relation between O_3, NO and NO_2:

$$\frac{NO}{NO_2} \leq \frac{j11}{k12 O_3} \qquad (3\text{-}1)$$

where j11 and k12 are the reaction rates for NO_2+hv->NO and NO+O3->NO_2, respectively. Chameides et al. (1990), Ridley et al. (1992) and others have found that the above equation underestimates $\frac{NO}{NO_2}$ in rural locations by ~30% due to the ozone-producing reactions (HO_2+NO->OH+NO_2). The underestimate is lower in urban centers. A plausible approximation for NO_X as a function of NO would be:

$$NO_X = NO(1+0.05\ O_3) \qquad (3\text{-}2)$$

where the coefficient 0.05 represents the ratio $j11/k12$ during full sunlight. This approximation tends to underestimate NO_X. This type of approximation has never been used as a basis for analyzing data sets in the absence of NO_2 and therefore must be

regarded as speculative. However it might provide a basis for evaluating the accuracy of measured NO_y and for identifying cases where measured NO_y may be dominated by on-site NO_x emissions.

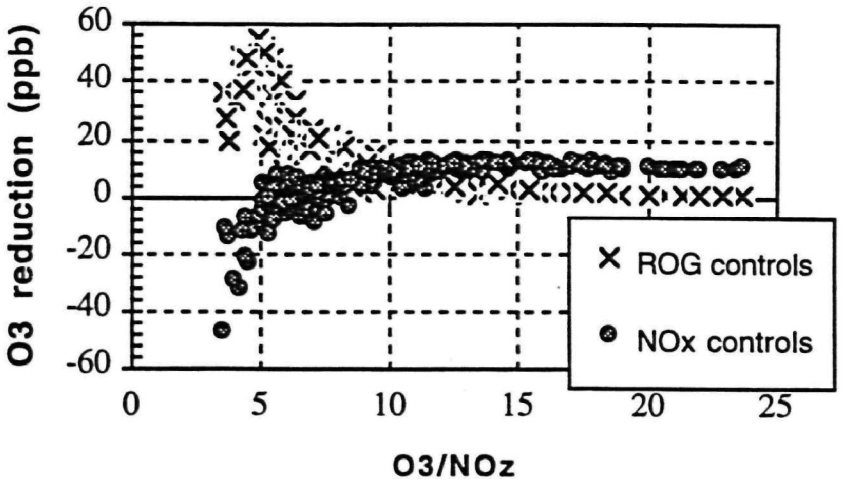

(a) Lake Michigan regional simulation - base case (6 pm)

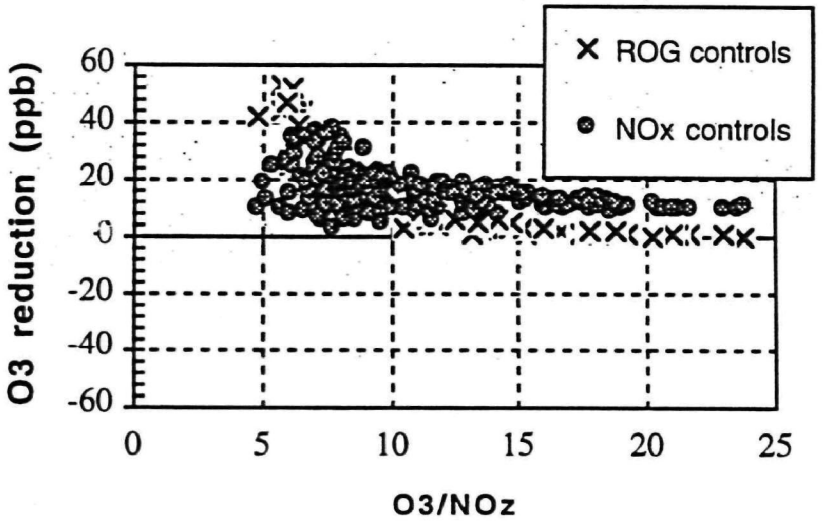

(b) Lake Michigan regional simulation - doubled ROG (6 pm)

Figure 3-1. Predicted reduction in afternoon O_3 (in ppb) resulting from a 35% reduction in the emission rate for anthropogenic ROG (crosses) and from a 35% reduction in the emission rate for NO_X (circles) plotted against O_3/NO_Z at the same time and location. Simulations are described in Section 3.1. From Sillman (1995a, 1997a).

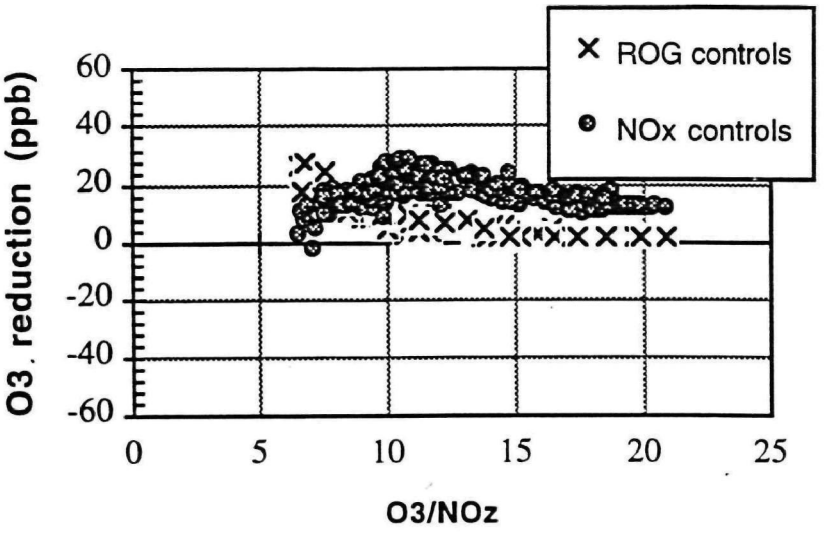

(c) Northeast corridor regional simulation - base case (6 pm)

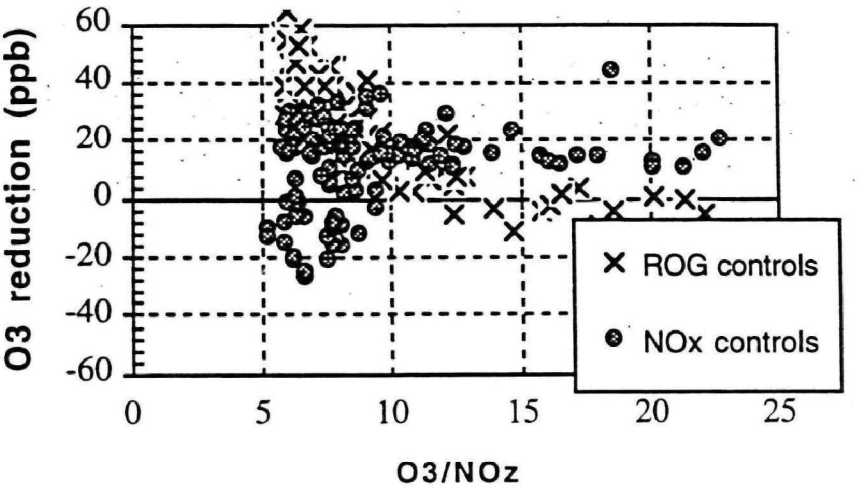

(d) New York urban simulation - "MMM-7" meteorology (5 pm)

Figure 3-1 (continued): Predicted reduction in afternoon O_3 (in ppb) resulting from a 35% reduction in the emission rate for anthropogenic ROG (crosses) and from a 35% reduction in the emission rate for NO_X (circles) plotted against O_3/NO_Z at the same time and location. Simulations are described in Section 3.1. From Sillman (1995a, 1997a).

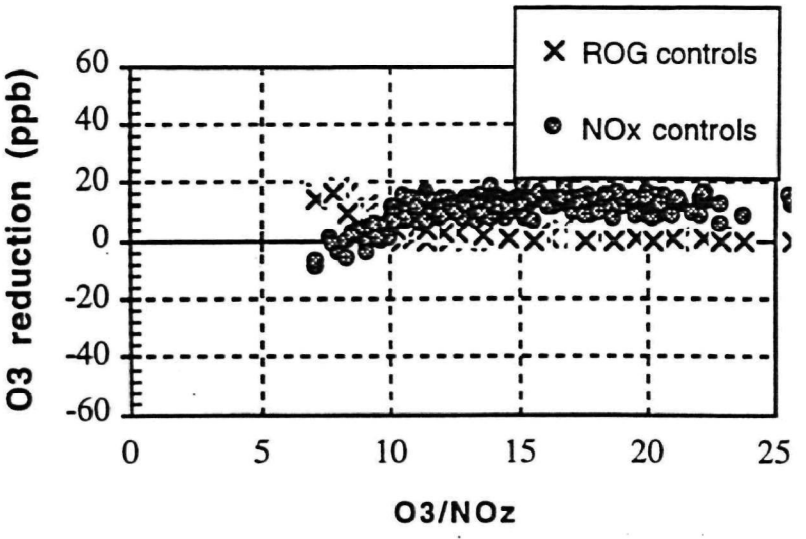

(e) Atlanta urban simulation - BEIS1 and low mixing height (5 pm)

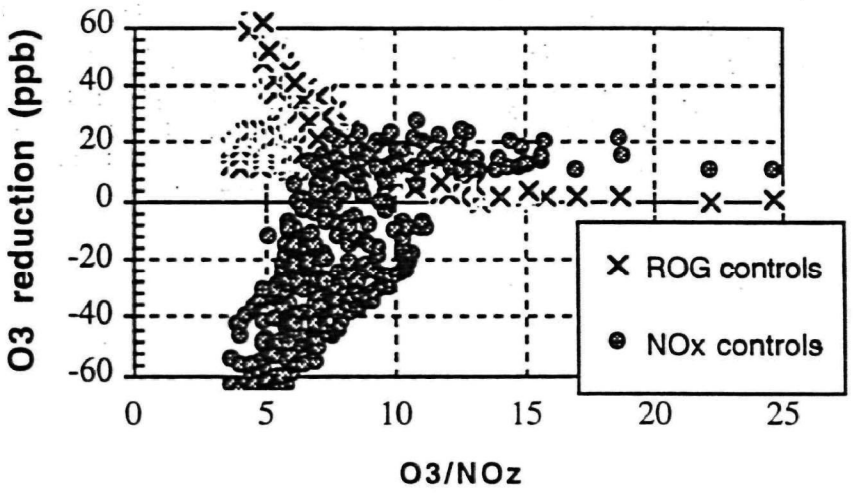

(f) Los Angeles urban simulation - Godowitch and Vukovich(1994) base case (3 pm)

Figure 3-1 (continued): Predicted reduction in afternoon O_3 (in ppb) resulting from a 35% reduction in the emission rate for anthropogenic ROG (crosses) and from a 35% reduction in the emission rate for NO_X (circles) plotted against O_3/NO_Z at the same time and location. Simulations are described in Section 3.1. From Sillman (1995a, 1997a).

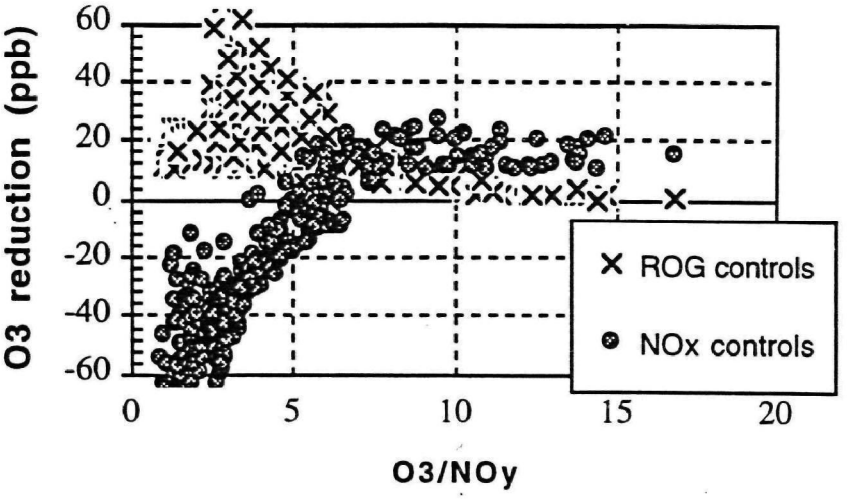

Figure 3-2 : Predicted reduction in afternoon O_3 (in ppb) resulting from a 35% reduction in the emission rate for anthropogenic ROG (crosses) and from a 35% reduction in the emission rate for NO_X (circles) plotted against O_3/NO_Y at the same time and location. Results are for the Los Angeles urban simulation by Godowitch and Vukovich (1994). From Sillman et al. (1997a).

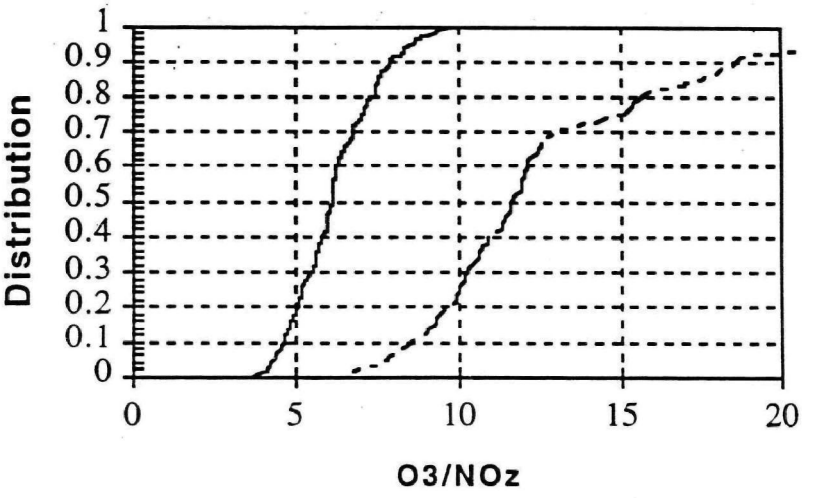

Figure 3-3 : Cumulative percentile distribution of O_3/NO_Z for locations with ROG-sensitive chemistry (solid line) and for locations with NO_X-sensitive chemistry (dashed line). Percentiles represent the fraction of the total array with O_3/NO_Z lower than the specified value. Results are for the Los Angeles urban simulation by Godowitch and Vukovich (1994) and based on analysis reported in Sillman et al. (1997a).

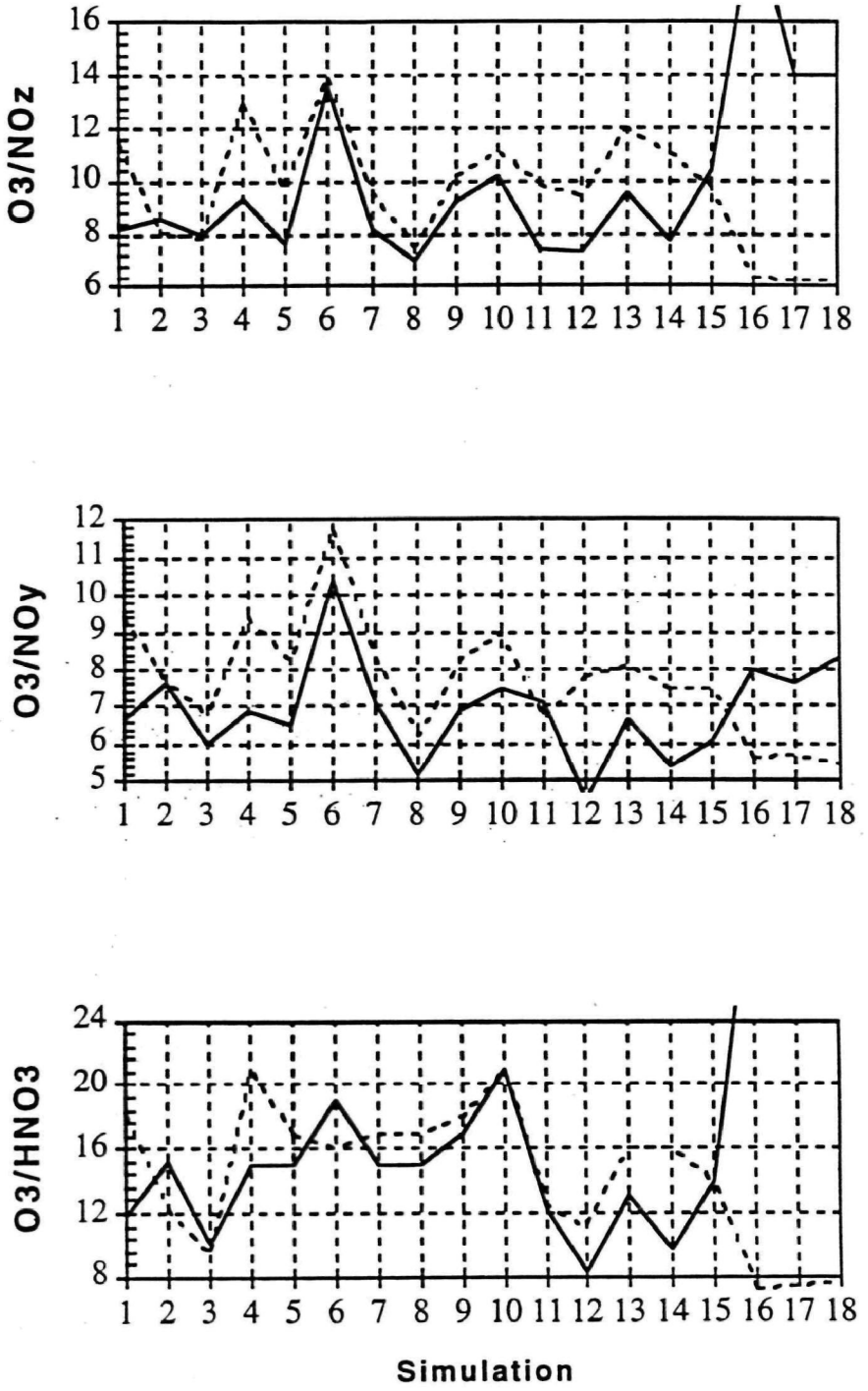

Figure 3-4: 95th-percentile indicator value for ROG-sensitive chemistry (solid line) and 5th percentile indicator value for NO_X-sensitive chemistry (dashed line) from 18 model scenarios identified in Table 3-1, for the indicator ratios O_3/NO_Z, O_3/NO_Y and O_3/HNO_3. In each simulation 95% of the locations with ROG sensitive chemistry have indicator ratios below the solid line, while 95% of the locations with NO_X-sensitive chemistry have indicator ratios above the dashed line.

Table 3-1

NO_X- and ROG-sensitive values for $\frac{O_3}{NO_y}$, $\frac{O_3}{NO_z}$ and $\frac{O_3}{HNO_3}$ as photochemical indicators

The table gives the 95th percentile value for the distribution of each indicator ratio over ROG-sensitive locations and the 5th percentile value for NO_X-sensitive locations for various model scenarios.

Model scenario	$\frac{O_3}{NO_z}$		$\frac{O_3}{NO_y}$		$\frac{O_3}{HNO_3}$	
	95th ROG	5th NO_X	95th ROG	5th NO_X	95th ROG	5th NO_X
Lake Michigan regional simulations:						
1. Base case	8.2	11.5	6.7	9.4	11.8	18.1
2. Doubled ROG	8.6	8.1	7.6	7.7	15.2	12.4
3. ROG reduced by half	7.9	7.8	6.0	6.8	10.1	9.4
4. Base case at 12:00 pm.	9.3	13.0	6.9	9.4	15	21
Northeast corridor regional simulations:						
5. Base case	7.6	9.7	6.5	8.2	15	17
6. Zero isoprene	13.6	14.0	10.4	11.8	19	16
7. Low mixing	8.2	9.6	7.1	8.4	15	17
8. Doubled isoprene and low mixing	7.0	7.5	5.2	6.2	15	17
9. Reduced wind speeds	9.2	10.2	6.9	8.2	17	18
10. Increased deposition, reduced winds	10.2	11.1	7.5	9.0	21	21
New York urban simulations:						
11. MMM-7 meteorology	7.4	9.9	7.1	6.7	12.1	12.6
12. DWM-5 meteorology	7.3	9.4	4.5	7.8	8.4	11.1
Atlanta urban simulations:						
13. BEIS1	9.6	12	6.7	8.1	13	16
14. Tripled isoprene	7.7	11	5.4	7.5	9.8	16
Los Angeles urban simulaions:						
15. Godowitch base case	10.4	9.8	6.1	7.5	14	14
16. Wagner base case	20	6.3	8.0	5.6	34	7.3
17. Wagner, doubled ROG	14	6.2	7.6	5.7	38	7.4
18. Wagner, tripled ROG	14	6.2	8.3	5.5	48	7.7
Nashville (preliminary)						
19. Base case	5.6	7.1	7.3	8.4	9.1	12
20. Older chemistry	5.8	7.0	7.4	8.1	9.5	12
21. Higher deposition (4 cm s^{-1})	6.4	8.4	8.6	10.2	11	15

(b) $\frac{H_2O_2}{HNO_3}$, $\frac{H_2O_2}{NO_z}$ and $\frac{H_2O_2}{NO_y}$:

The correlation between NO_X-ROG sensitivity and $\frac{H_2O_2}{HNO_3}$ is shown in Figure 3-5. Complete results are shown in the Appendix. The correlation for $\frac{H_2O_2}{NO_z}$ and $\frac{H_2O_2}{NO_y}$ is visually similar to $\frac{H_2O_2}{HNO_3}$ but with a different value for the transition between ROG-sensitive and NO_X-sensitive chemistry. The NO_X-ROG transition points are identified through the 95th percentile ROG-sensitive and 5th percentile NO_X-sensitive indicator values, which are shown in Figure 3-7 and Table 2. As was the case for $\frac{O_3}{NO_z}$, the ratio $\frac{H_2O_2}{HNO_3}$ is strongly correlated with NO_X-ROG sensitivity in model results, and the correlation remains consistent for different locations, model types and model scenarios. Changes in model assumptions that cause a shift in NO_X-ROG sensitivity also cause an equivalent change in the ratio $\frac{H_2O_2}{HNO_3}$. The same pattern is repeated for the other H_2O_2 ratios. As described in Section 2.1, the correlation between $\frac{H_2O_2}{HNO_3}$ and NO_X-ROG sensitivity is derived directly from the chemistry of ozone production and consequently has a strong theoretical justification. Model results show that $\frac{H_2O_2}{NO_z}$ and $\frac{H_2O_2}{NO_y}$ correlate with NO_X-ROG sensitivity equally well, although the theoretical justification is derived from $\frac{H_2O_2}{HNO_3}$.

The ratios involving H_2O_2 have two important advantages over $\frac{O_3}{NO_z}$ and its equivalents as an indicator for NO_X-ROG chemistry. First, the NO_X-ROG correlation is stronger for the indicators involving H_2O_2. A comparison of Figures 3-1 and 3-5 shows that the difference between NO_X- and ROG-sensitive values is much larger for the H_2O_2-based indicators than for the O_3-based indicators, making the possibility of error due to imprecise measurement less. The transition region between NO_X- and ROG-sensitive chemistry is also smaller in comparison to the difference between NO_X- and ROG-sensitive values for the H_2O_2-based indicators. The 95th percentile ROG and 5th percentile NO_X-sensitive values in Table 2 demonstrate the small exteent of overlap between NO_X-sensitive and ROG sensitive values for the H_2O_2-based indicators. Second, species correlations involving H_2O_2 provide an important diagnostic test for the validity of the indicator method, transition points and the accuracy of measurements. This is described below in

Section 4. The inclusion of tests for the accuracy of method rather than simply accepting the indicator NO_X-ROG correlation "on faith" is an important advantage for data sets that include H_2O_2. However H_2O_2 measurements are more difficult and less accurate than O_3, and the H_2O_2-based indicators and are more sensitive to model uncertainties, especially with regard to deposition rates (see below).

Most of the uncertainties described above in connection with the O_3-based indicators also apply to the H_2O_2-based indicators. As shown in Figure 3-4 for Los Angeles, an exception to the indicator NO_X-ROG correlation occurs for location where NO_X-ROG sensitivity is due to titration by direct NO_X emissions rather than by differing rates of ozone production. These exceptions do not appear in the NO_X-ROG correlation for the raio $\frac{H_2O_2}{NO_y}$ (Figure 3-5), although $\frac{H_2O_2}{HNO_3}$ has a stronger theoretical justification. The model results shown here do not include particulate nitrate, and it is uncertain whether particulate nitrate should be included in the indicator ratios. In addition, deposition rates for H_2O_2 and HNO_3 represent a greater uncertainty for the H_2O_2-based indicators than for the ratios involving O_3. Results from Hall and Claiborn (1997) show that the dry deposition rate for H_2O_2 should be equal to the rate for HNO_3 and may can have very high values (4 cm s^{-1} or more). Scenarios with increased deposition of H_2O_2 (including both the scenario for the northeast corridor with increased deposition and the Nashville base case) have NO_X-ROG transition values lower by 25%. The ratio $\frac{H_2O_2}{NO_y}$ is especially sensitive to changes in assumed deposition rates. H_2O_2 is also affected by wet deposition, not included here.

An additional uncertainty for the H_2O_2-based indicators is the interpretation given to H_2O_2 in models. Many photochemical mechanisms, including the CB-IV mechanism used in the UAM, do not include formation of organic peroxides. In these mechanisms H_2O_2 should be interpreted as representative of the sum of H_2O_2 and organic peroxides. Simulations with a more complete representation of organic peroxides (Sillman et al., 1995b, 1997b) have predicted that H_2O_2 will represent 50%-70% of total peroxides.

NO_X-ROG transition values for NO_X- vs ROG-sensititive chemistry based on the simulations used in this study are: 0.3-0.6 for $\frac{H_2O_2}{HNO_3}$; 0.2-0.35 for $\frac{H_2O_2}{NO_Z}$; and 0.2-0.3 for $\frac{H_2O_2}{NO_y}$. These transition values appear clearly in Figure 3-7. However preliminary results from Nashville (in simulations with updated photochemistry and higher dry deposition rates) have resulted in a lower estimate for NO_X-ROG transition values: 0.2-0.3 for $\frac{H_2O_2}{HNO_3}$; 0.15-0.20 for $\frac{H_2O_2}{NO_Z}$; and 0.13-0.17 for $\frac{H_2O_2}{NO_y}$. The difference

between the transition values for Nashville and the earlier estimates represents a major uncertainty and may lead to future modifications.

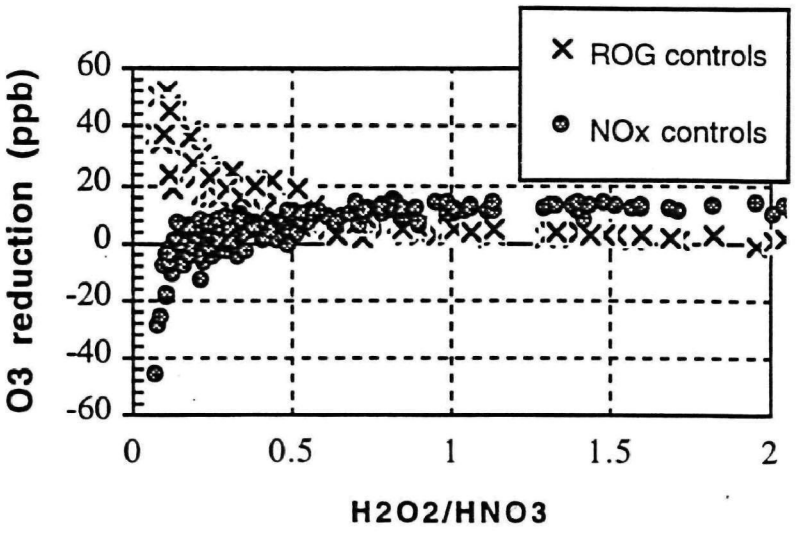

(a) Lake Michigan regional simulation - base case (6 pm)

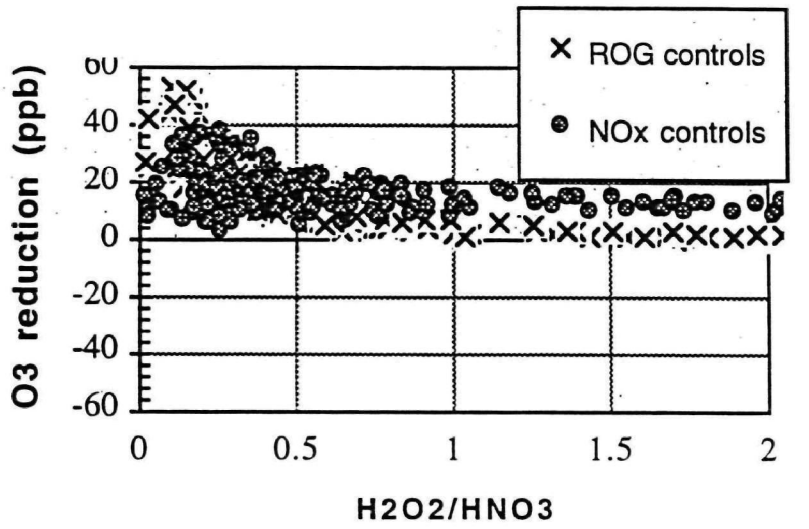

(b) Lake Michigan regional simulation - doubled ROG (6 pm)

Figure 3-5. Predicted reduction in afternoon O_3 (in ppb) resulting from a 35% reduction in the emission rate for anthropogenic ROG (crosses) and from a 35% reduction in the emission rate for NO_X (circles) plotted against H_2O_2/HNO_3 at the same time and location. Simulations are described in Section 3.1. From Sillman (1995a, 1997a).

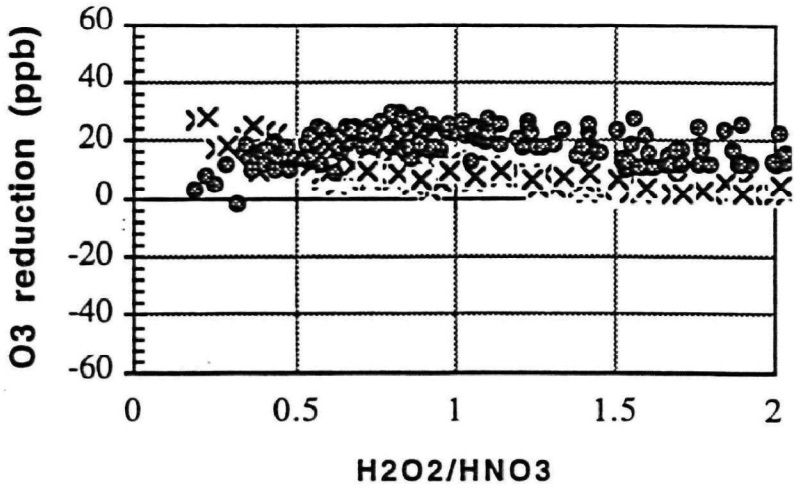

(c) Northeast corridor regional simulation - base case (6 pm)

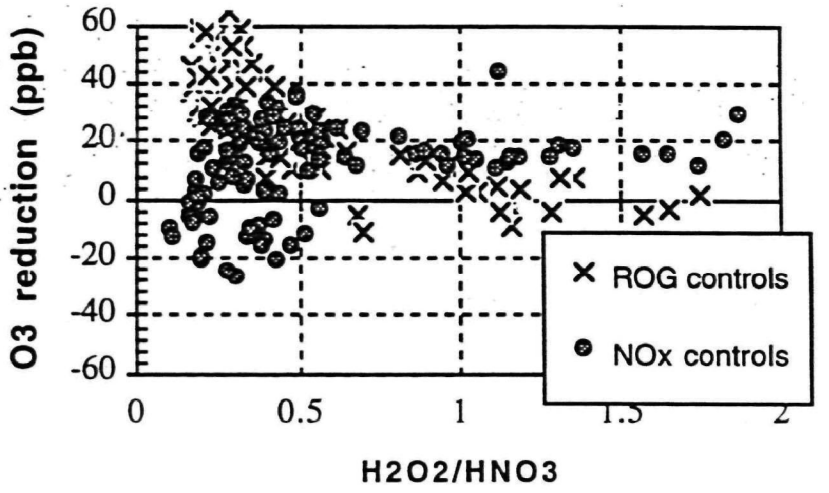

(d) New York urban simulation - "MMM-7" meteorology (5 pm)

Figure 3-5 (continued): Predicted reduction in afternoon O_3 (in ppb) resulting from a 35% reduction in the emission rate for anthropogenic ROG (crosses) and from a 35% reduction in the emission rate for NO_X (circles) plotted against H_2O_2/HNO_3 at the same time and location. Simulations are described in Section 3.1. From Sillman (1995a, 1997a).

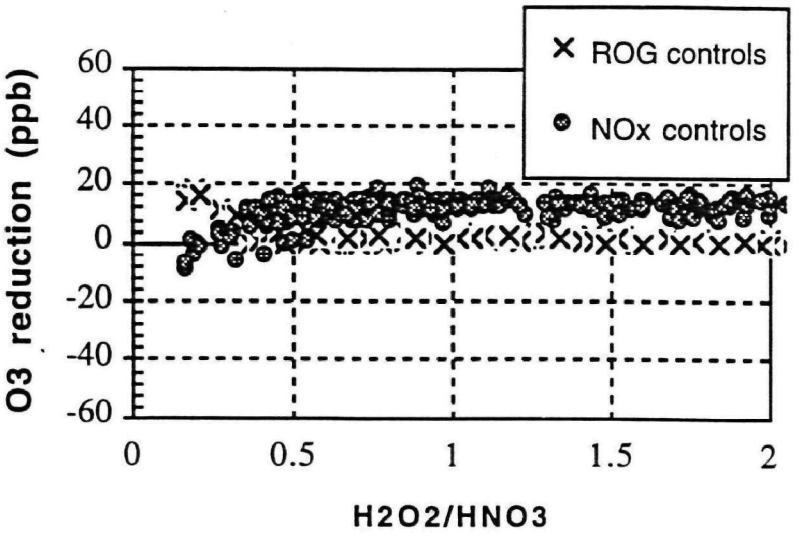

(e) Atlanta urban simulation - modified upwind conditions. (5 pm)

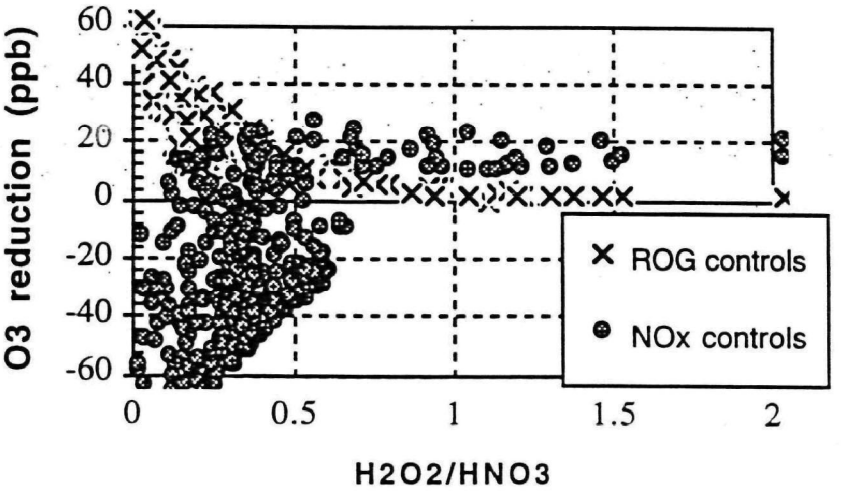

(f) Los Angeles urban simulation - Godowitch and Vukovich(1994) base case (3 pm)

Figure 3-5 (continued): Predicted reduction in afternoon O_3 (in ppb) resulting from a 35% reduction in the emission rate for anthropogenic ROG (crosses) and from a 35% reduction in the emission rate for NO_X (circles) plotted against H_2O_2/HNO_3 at the same time and location. Simulations are described in Section 3.1. From Sillman (1995a, 1997a).

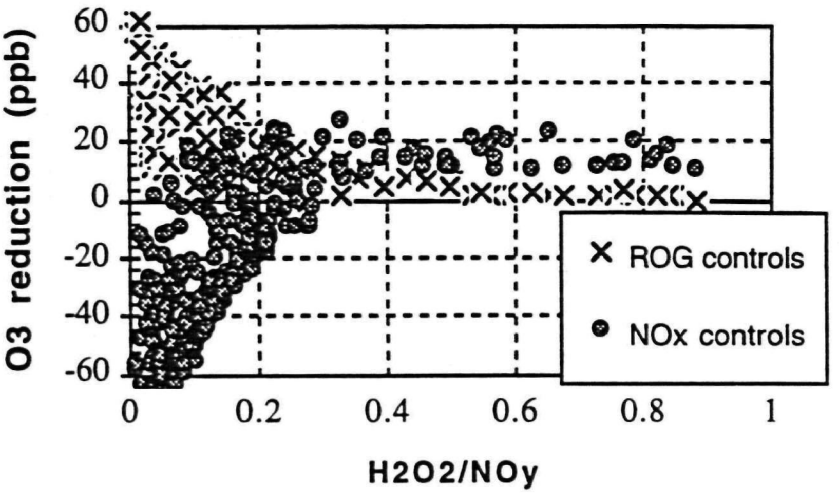

Figure 3-6 : Predicted reduction in afternoon O_3 (in ppb) resulting from a 35% reduction in the emission rate for anthropogenic ROG (crosses) and from a 35% reduction in the emission rate for NO_X (circles) plotted against H_2O_2/NO_Y at the same time and location. Results are for the Los Angeles urban simulation by Godowitch and Vukovich (1994). Based on the analysis reported in Sillman et al. (1997a).

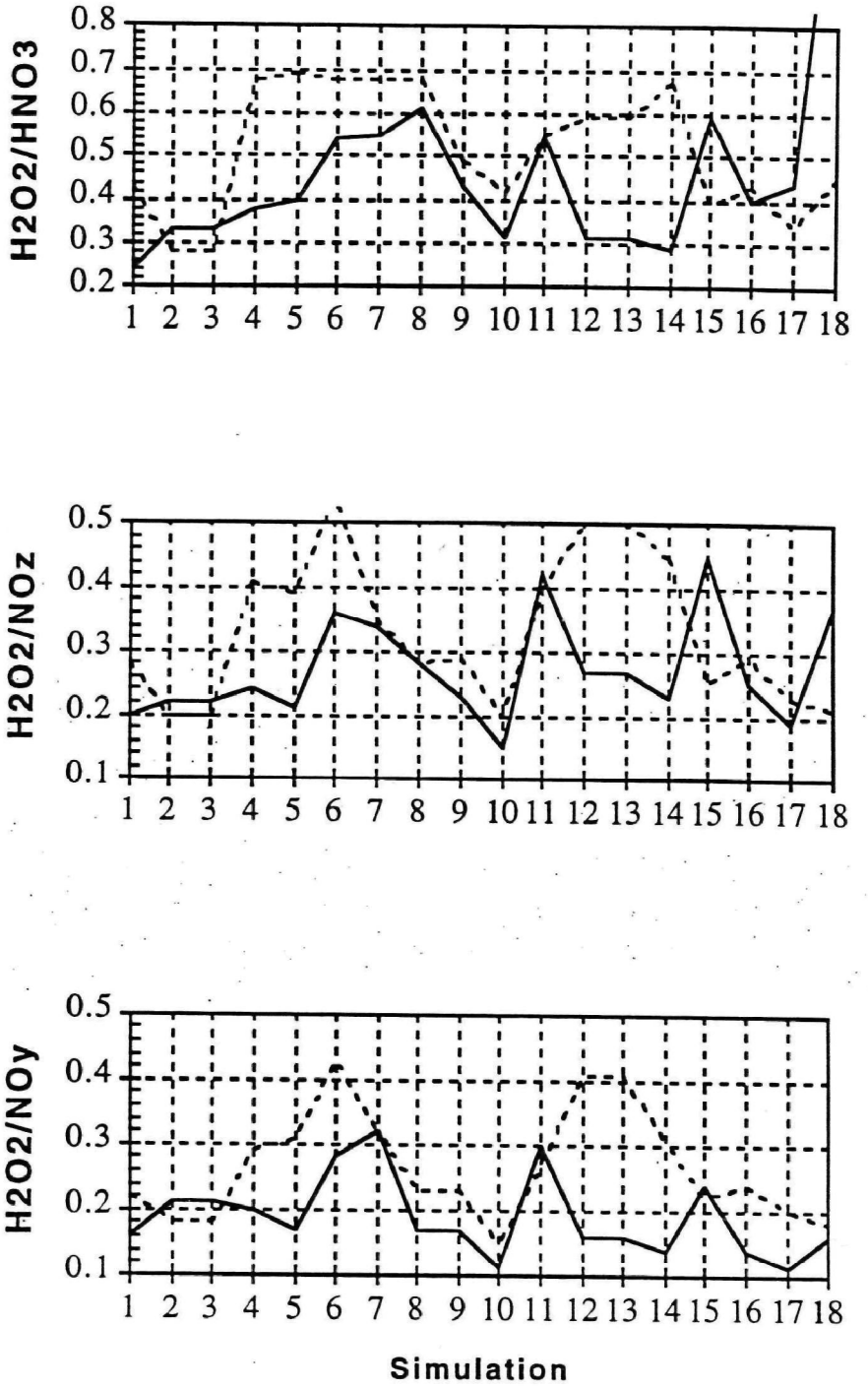

Figure 3-7: 95th-percentile indicator value for ROG-sensitive chemistry (solid line) and 5th percentile indicator value for NO_X-sensitive chemistry (dashed line) from 18 model scenarios identified in Table 3-2, for the indicator ratios H_2O_2/HNO_3, H_2O_2/NO_Z, H_2O_2/NOy. In each simulation 95% of the locations with ROG sensitive chemistry have indicator ratios below the solid line, while 95% of the locations with NO_X-sensitive chemistry have indicator ratios above the dashed line.

Table 3-2

NOx- and ROG-sensitive values for $\frac{H_2O_2}{HNO_3}$, $\frac{H_2O_2}{NO_z}$ and $\frac{H_2O_2}{NO_y}$ as photochemical indicators

The table gives the 95th percentile value for the distribution of each indicator ratio over ROG-sensitive locations and the 5th percentile value for NO_X-sensitive locations for various model scenarios.

Model scenario	$\frac{H_2O_2}{HNO_3}$		$\frac{H_2O_2}{NO_z}$		$\frac{H_2O_2}{NO_y}$	
	95th ROG	5th NO_X	95th ROG	5th NO_X	95th ROG	5th NO_X
Lake Michigan regional simulations:						
1. Base case	.24	.43	.20	.28	.16	.22
2. Doubled ROG	.33	.28	.22	.20	.21	.18
3. ROG reduced by half	.15	.27	.12	.22	.11	.20
4. Base case at 12:00 pm.	.38	.68	.24	.41	.20	.29
Northeast corridor regional simulations:						
5. Base case	.40	.69	.21	.39	.17	.31
6. Zero isoprene	.54	.68	.36	.54	.28	.43
7. Low mixing	.55	.68	.34	.35	.32	.32
8. Doubled isoprene, low mixing	.61	.68	.28	.28	.17	.23
9. Reduced wind speeds	.43	.49	.23	.29	.17	.23
10. Increased deposition, reduced winds	.31	.42	.15	.20	.11	.15
New York urban simulations:						
11. MMM-7 meteorology	.55	.55	.42	.40	.30	.27
12. DWM-5 meteorology	.31	.59	.27	.50	.16	.41
Atlanta urban simulations:						
13. BEIS1	.51	.56	.42	.43	.18	.29
14. Tripled isoprene	.29	.67	.23	.45	.14	.31
Los Angeles urban simulaions:						
15. Godowitch base case	.59	.39	.45	.25	.24	.22
16. Wagner base case	.40	.43	.25	.29	.14	.24
17. Wagner, doubled ROG	.44	.34	.19	.23	.11	.20
18. Wagner, tripled ROG	1.3	.45	.37	.21	.16	.18
Nashville (preliminary)						
19. Base case	.23	.30	.19	.21	.12	.17
20. Older chemistry	.24	.38	.19	.25	.14	.20
21. Higher deposition (4 cm s^{-1})	.23	.34	.18	.21	.11	.16

(c) Other indicators:

NO_y: Milford et al. (1994) recommended the use of NO_y as a NO_X-ROG indicator. As shown above in Figure 2-3, NO_X-sensitive chemistry is associated with low NO_y and ROG-sensitive chemistry is associated with high NO_y. The 95-th percentile NO_X-sensitive and 5th-percentile ROG-sensitive values for NO_y are shown in Table 3-3 and Figure 3-11 below. NO_y succeeds as a NO_X-ROG indicator because ROG-sensitive chemistry is associated with urban centers and large cities, which have characteristically high NO_y, while NO_X-sensitive chemistry is associated with smaller cities and downwind and rural locations that have low NO_y. However the NO_X-ROG transition for NO_y changes significantly in models when emission rates of anthropogenic and/or biogenic ROG are changed. The variation in the NO_X-ROG transition for NO_y is illustrated in Table 3-3 and Figure 3-11 below and in Sillman (1995a). This report recommends the use of $\frac{O_3}{NO_y}$ rather than NO_y as a NO_X-ROG indicator because the former shows less sensitivity to model assumptions.

$\frac{O_3-O_{3b}}{NO_y}$ and AIRTRAK: Graham Johnson (1984, 1990, see also Blanchard et al., 1993) developed a correlation between NO_X-ROG sensitivity and measured parameters based on a series of smog chamber experiments. In the Johnson formulation, NO_X-sensitive chemistry is expected when chemistry has run to completion, i.e. most of the initially emitted NO_X has been converted to NO_Z species. For NO_X-sensitive conditions the rate of ozone production per emitted NO_X is expected to reach a constant, maximum value (~4 in smog chamber experiments). For ROG-sensitive conditions the rate of ozone production per emitted NO_X is expected to be lower. More sophisticated model calculations by Liu et al. (1987) and Lin et al. (1988) suggest that the ozone production efficiency (defined as the rate of ozone production per NO_X removal, and associated with the slope of ozone vs. NO_Z) shows significant variation.

The AIRTRAK method can be evaluated by using the ratio $\frac{O_3-O_{3b}}{NO_y}$ as a NO_X-ROG indicator in the photochemical models described in this report. The parameter O_{3b} represents background ozone, i.e. upwind conditions in the simulations (usually 40 ppb). The exact formulation by Johnson is slightly different from $\frac{O_3-O_{3b}}{NO_y}$ because it includes modifications for production of particulate nitrate (assumed to be zero in the models used

here). The correlation between model NO_X- ROG sensitivity and $\frac{O_3-O_{3b}}{NO_y}$ is shown in Figures 3-8, Figure 3-11 and Table 3-3.

Results show that $\frac{O_3-O_{3b}}{NO_y}$ does correlate successfully with NO_X-ROG sensitivity. The NO_X-ROG transition point (3.5-5.5) is comparable with results from smog chambers (4.1). The NO_X-ROG correlation is less precise than the correlations for $\frac{O_3}{NO_y}$ shown above. There is also greater overlap between the NO_X-and ROG-sensitive values of \f(O3-O3b, NOy) .

$\frac{O_3}{NO_X}$ and $\frac{ROG}{NO_X}$ ratios: Results for these ratios show a poor correlation with model NO_X -ROG sensitivity. Results are shown in Figures 3-9 and 3-10.

The use of $\frac{O_3}{NO_X}$ as a NO_X-ROG indicator has never been formally suggested, but in recent years it has been used as a popular substitute for $\frac{O_3}{NO_y}$ when NO_y measurements are not available (LADCO, 1994). Results (Figure 3-9) show that $\frac{O_3}{NO_X}$ does not correlate well with NO_X-ROG sensitivity. The ratio (O_3, NO_X+PAN) also does not correlate well with NO_X-ROG sensitivity.

ROG/NO_X ratios have frequently been used to evaluate NO_X-ROG sensitivity, especially in regulatory applications (Blanchard et al., 1991). Correlations between NO_X-ROG sensitivity and various forms of the ROG/NO_X ratio, including ROG/NO_y and reactivity-weighted ROG (expressed as propene-equivalent carbon, defined by Chameides et al. (1992)) were tested in photochemical simulations. Results (Figure 3-10) show that ROG/NO_X ratios correlate poorly with model NO_X-ROG sensitivity. It has previously been shown that the ROG/NO_X ratio in the morning is a poor predictor of NO_X-ROG sensitivity at the time of maximum ozone (see Section 2.1). Figure 3-10 suggests that ROG/NO_X ratios during the afternoon also correlate poorly with concurrent NO_X-ROG sensitivity even when the reactivity of the ROG mix is taken into account. The poor correlation occurs because the various ROG/NO_X ratios are associated with instantaneous O_3-NO_X-ROG chemistry at the time and place of measurement but not with the process of ozone production over a full day. It is possible that future research will identify ways of using this ROG/NO_X ratios as indicators for NO_X-ROG dependence of instantaneous rates of ozone production (as opposed to NO_X-ROG sensitivity of ozone concentrations, which has been investigated here.)

Cardelino et al. (1995) developed an observation-based method for evaluating NO_X-ROG chemistry based on measured NO_X and ROG, which are readily available

through the PAMS network. Their method includes an extensive analysis of instantaneous NO_X-ROG chemistry (derived from NO_X and ROG measurements) to determine the cumulative NO_X-ROG sensitivity of ozone that is produced over a multi-hour period. The poor results for ROG/NO_X ratios as photochemical indicators in this study does not have any implications concerning the accuracy of the method of Cardelino et al. (1995). Measured ROG (especially speciated ROG and biogenics) and NO_X should also be an important part of model evaluations. However the conventional use of ROG/NO_X ratios as a "rule of thumb" for NO_X-ROG chemistry is inaccurate.

Sillman (1995a) used the ratio $\frac{HCHO}{NO_y}$ as a NO_X-ROG indicator. This gave better results than the other ROG/NO_X ratios because HCHO is related both to ROG reactivity and the chemistry over a period of several hours. Results have been included in Table 3-3 and Figure 3-11. The correlation between $\frac{HCHO}{NO_y}$ and NO_X-ROG sensitivity is plausible but not as strong as the other indicators.

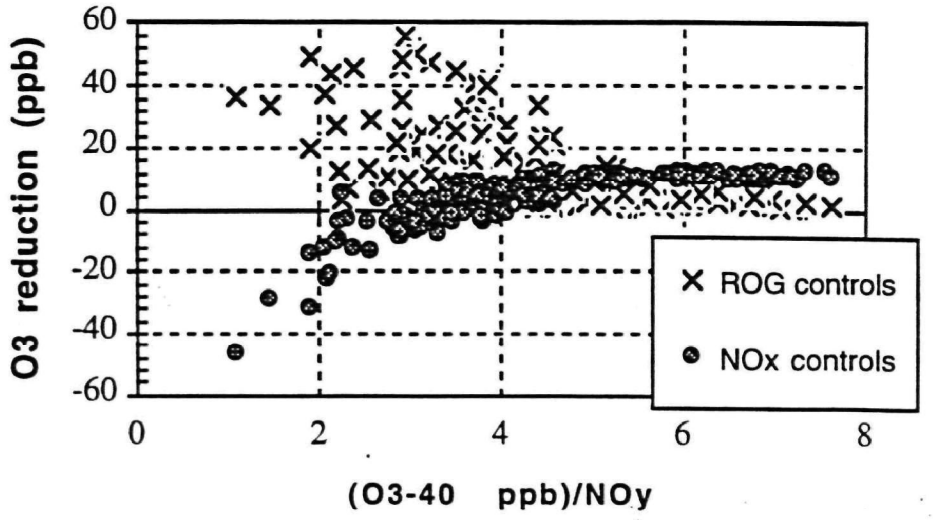

Figure 3-8 : Predicted reduction in afternoon O_3 (in ppb) resulting from a 35% reduction in the emission rate for anthropogenic ROG (crosses) and from a 35% reduction in the emission rate for NO_X (circles) plotted against $(O_3\text{-}40 \text{ ppb})/NO_Y$ at the same time and location. Results are for the Lake Michigan urban simulation. From Sillman (1995a).

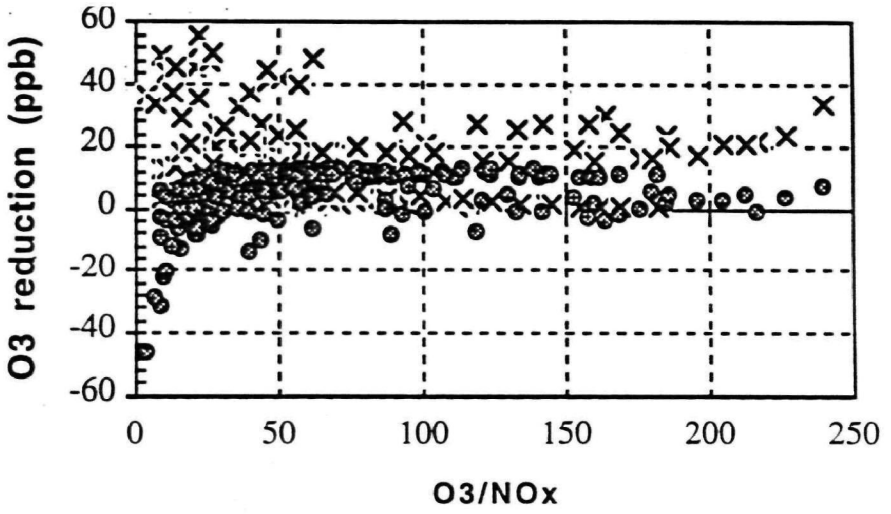

Figure 3-9 : Predicted reduction in afternoon O_3 (in ppb) resulting from a 35% reduction in the emission rate for anthropogenic ROG (crosses) and from a 35% reduction in the emission rate for NO_X (circles) plotted against O_3/NO_X at the same time and location. Results are for the Lake Michigan urban simulation.

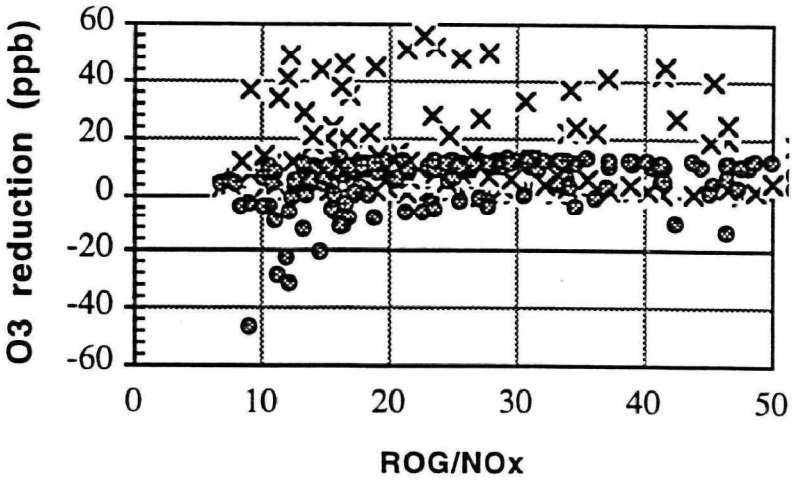

(a)

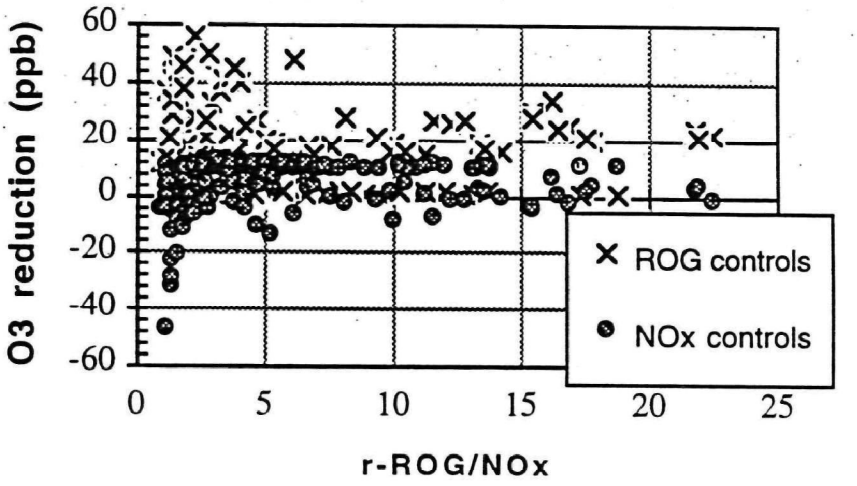

(b)

Figure 3-10 : Predicted reduction in afternoon O_3 (in ppb) resulting from a 35% reduction in the emission rate for anthropogenic ROG (crosses) and from a 35% reduction in the emission rate for NO_X (circles) plotted against (a) ROG/NO_X and (b) $rROG/NO_y$ at the same time and location, where rROG represents reactivity-weighted ROG as propene equivalent carbon (Chameides et al. (1992) in ppbC. Results are for the Lake Michigan urban simulation. Based on results in Sillman (1995a).

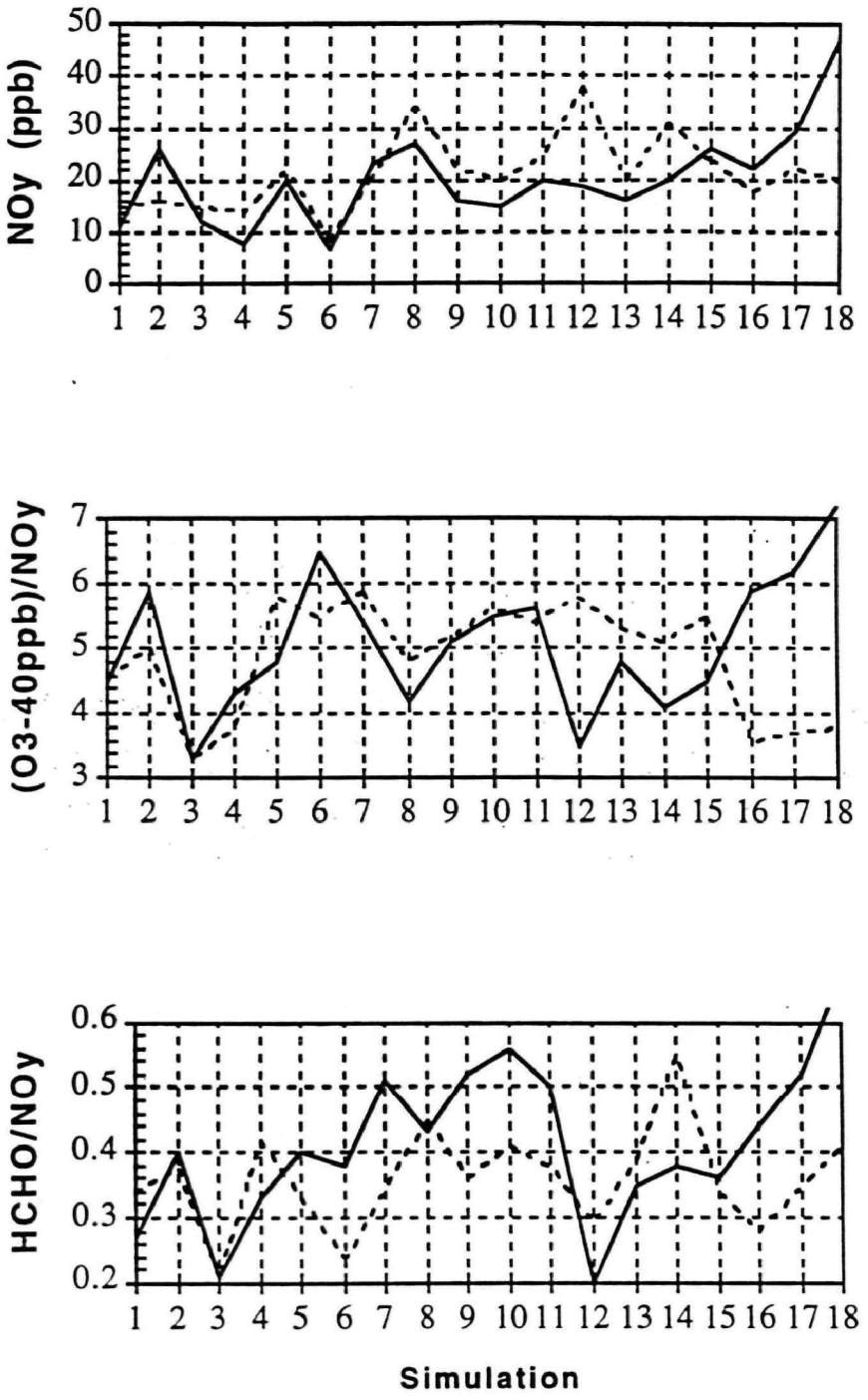

Figure 3-11: 95th-percentile indicator value for ROG-sensitive chemistry (solid line) and 5th percentile indicator value for NO_X-sensitive chemistry (dashed line) from 18 model scenarios identified in Table 3-3, for the indicators: NO_y, (O_3-40ppb)/NO_y, HCHO/NOy. Results for NOy show the 95th percentile value for NOx-sensitive chemistry (solid line) and 5th percentile for ROG-sensitive chemistry because ROG-sensitive chemistry is associated with higher values for this indicator.

Table 3-3

NOx- and ROG-sensitive values for other photochemical indicators.

The table gives the 95th percentile value for the distribution of each indicator ratio over ROG-sensitive locations and the 5th percentile value for NO_X-sensitive locations for various model scenarios. the indicator s shown here are not recommended for use.

Model scenario	NO_y*		$\frac{O_3\text{-}40\ ppb}{NO_Z}$		$\frac{HCHO}{NO_y}$	
	95th NO_X	5th ROG	95th ROG	5th NO_X	95th ROG	5th NO_X
Lake Michigan regional simulations:						
1. Base case	11	15	4.5	4.6	.27	.34
2. Doubled ROG	26	16	5.9	5.0	.40	.38
3, ROG reduced by half	12	15	3.3	3.3	.21	.21
4. Base case at 12:00 pm.	7.8	14	4.3	3.8	.33	.42
Northeast corridor regional simulations:						
5. Base case	20	22	4.8	5.8	.40	.33
6. Zero isoprene	6.9	8.6	6.5	5.5	.38	.24
7. Low mixing	23	21	5.4	5.9	.51	.35
8. Doubled isoprene, low mixing	27	34	4.2	4.8	.43	.45
9. Reduced wind speeds	16	22	5.1	5.2	.52	.36
10. Increased deposition, reduced winds	15	20	5.5	5.6	.56	.41
New York urban simulations:						
11. MMM-7 meteorology	20	25	5.6	5.4	.50	.38
12. DWM-5 meteorology	19	38	3.5	5.8	.20	.29
Atlanta urban simulations:						
13. BEIS1	16	20	4.8	5.3	.35	.39
14. Tripled isoprene	20	31	4.1	5.1	.38	.55
Los Angeles urban simulaions:						
15. Godowitch base case	26	24	4.5	5.5	.36	.34
16. Wagner base case	22	18	5.9	3.6	.44	.28
17. Wagner, doubled ROG	29	22	6.2	3.7	.52	.35
18. Wagner, tripled ROG	47	20	7.2	3.8	.67	.41

* Results for NO_y give the 95th percentile for NO_X-sensitive locations and the 5th percentile for ROG-sensitive locations because low NO_y corresponds to NO_X-sensitive chemistry.

SECTION 4
SPECIES CROSS-CORRELATIONS AS A BASIS FOR EVALUATING THE INDICATOR METHOD

Significant insights into the chemistry of ozone production can be gained by examining cross-correlations between various species associated with ozone chemistry. The use of species cross-correlations has been developed largely by Trainer et al. (1993) and Parrish et al. (1993) who analyzed correlations between ambient ozone, NO_y and NO_Z. In this section it will be shown that the method of photochemical indicators is closely related to a predicted correlation between three species: O_3, NO_Z and H_2O_2. This predicted correlation can be used to evaluate the viability of the indicator method in general, and can also be used as a diagnostic tool to evaluate the accuracy of individual field measurements.

Trainer et al. (1993) has shown that measured O_3 consistently increases with NO_Z in measurements of photochemically aged air (defined by $\frac{NOx}{NOy} < 0.4$) during the afternoon at rural sites in eastern North America. As shown in Figure 4-1, the slope of O_3 vs. NO_Z tends to be highest at low NO_Z (<5 ppb) and decreases at higher NO_Z, giving the O_3-NO_Z correlation a nonlinear or "bent-over" appearance. Trainer et al. speculated that the difference in the O_3-NO_Z slope at low and high NO_Z was related to the switch between NO_X-sensitive and ROG-sensitive chemistry. They also reported that O_3 increased with NO_Z in the Los Angeles basin with a slope that was significantly lower than the slope at rural eastern sites.

Results from this report and from Sillman (1995a) suggest that NO_X-ROG chemistry is correlated with the absolute value of the $\frac{O_3}{NO_Z}$ ratio rather than the slope between O_3 and NO_Z for an individual data set. As shown in Figure 4-2, model O_3-NO_Z correlations show an ambiguous pattern when compared with model NO_X-ROG sensitivity. The characteristic nonlinear "bend-over" in the O_3-NO_Z correlation can appear for both NO_X-sensitive and ROG-sensitive conditions, depending on the $\frac{O_3}{NO_Z}$ ratio. As shown in

Figures 4-1 and 4-2, there is a characteristic decrease in the slope between O_3 and NO_Z as NO_Z increases from 3 to 10 ppb, even though these represent likely NO_X-sensitive rural measurements (Figure 4-1, Trainer et al., 1993) and NO_X-sensitive simulation results. By contrast, O_3 increases at a near-constant rate as NO_Z increases from 15 to 30 ppb in Figure 4-2, even though this region represents ROG-sensitive simulation results. From Figure 4-2, it might be possible to associate NO_X-sensitive locations with a high slope between O_3 and NO_Z, ROG-sensitive locations with a lower slope, and the region of transition between NO_X- and ROG-sensitive chemistry with a change in slope. However a stronger correlation with NOx-ROG chemistry can be found by using the $\frac{O_3}{NO_Z}$ ratio rather than the slope as an indicator (see also Figures 3-1a and 3-8).

The theory associated with photochemical indicators suggests that O_3 should increase with NO_Z for both NO_X-sensitive and ROG-sensitive chemistry but that the rate of increase should be lower for ROG-sensitive chemistry. Under NO_X-sensitive conditions O_3 is expected to increase with NO_Z at a rate determined by the production efficiency for ozone (defined by Lin et al. (1988) as the rate of production of ozone divided by the rate of removal of NO_X, $\frac{P(O_3)}{L(NO_X)}$). But for ROG-sensitive conditions the correlation between O_3 and NO_Z is determined by the supply of odd-H radicals, where the source is proportional to O_3 and the NO_Z represents the accumulated sink. The sum of odd-H sinks, approximately equal to the sum $NO_Z+2H_2O_2$, should increase linearly with O_3. The predicted linear correlation between O_3 and the sum $NO_Z+2H_2O_2$ is a central feature of the indicator theory.

As shown in Figure 4-3, correlations between O_3 and NO_Z should show a range of variation between a maximum O_3-NO_Z slope, representing NO_X-sensitive chemistry, and a minimum O_3/NO_Z ratio that represents the ROG-sensitive limit. The correlation between O_3 and the sum $NO_Z+2H_2O_2$ shows a linear increase and represents the ROG-sensitive limit for the $\frac{O_3}{NO_Z}$ ratio (since for the ROG-sensitive limit $NO_Z>>H_2O_2$). The transition between NO_X-sensitive and ROG-sensitive chemistry occurs when \f(O_3,NO_Z) is greater than \f(O_3,$NO_Z+2H_2O_2$) by 50%, i.e. the NO_X-sensitive region is defined by:
$\frac{O_3}{NO_Z} > 1.5 \frac{O_3}{NO_Z+2H_2O_2}$.

In simulations with high deposition (4 cm/sec for both H_2O_2 and HNO3) the ratio $\frac{O_3}{NO_Z+2H_2O_2}$ was found to decrease by 25%. The NO_X-ROG transition point for $\frac{H_2O_2}{HNO_3}$ also decreased by 25% but the NOx-ROG transition point for $\frac{O_3}{NO_Z}$ decreased by only 10% (see Tables 3-1 and 3-2). It is not yet clear whether the criteria given above

($\frac{O3}{NO_Z} > 1.5 \frac{O3}{NO_Z+2H_2O_2}$) can be used to establish the NO_X-ROG transition but it represents an important test for the theory.

The predicted linear correlation between O3 and the sum $NO_Z+2H_2O_2$ provides the following tests for the indicator theory:

(1) The predicted linear correlation should be confirmed by ambient measurements. If confirmed, the linear correlation provides evidence that the interpretation of O3, NO_Z and H_2O_2 as NO_X-ROG indicators is consistent with the ambient behavior of these species.

(2) It provides independent confirmation of the NO_X-ROG transition point for $\frac{O3}{NO_Z}$. The NO_X-ROG transition points identified in Section 3.0 are sensitive to model assumptions about sunlight, water vapor and dry deposition rates. These can be evaluated for individual data sets by comparing the ratio $\frac{O3}{NO_Z+2H_2O_2}$ with ratios in photochemical models. The NO_X-ROG transition point for an individual data set can be established from the formula: $\frac{O3}{NO_Z} = 1.5 \frac{O3}{NO_Z+2H_2O_2}$. This can be compared to the transition points from the photochemical models in Section 3.

(3) It provides a diagnostic test for the accuracy of individual measurements. Deviation from the expected correlation between O3, NO_Z and H_2O_2 may provide evidence that an individual set of measurements is flawed. Similar diagnostic tests might be performed by comparing O3 - NO_Z correlations with previous ambient measurements by Trainer et al.

Recent aircraft measurements by Daum et al. (1996) provide important confirmation for the method. Daum et al. measured O3, NO_X, NO_Y and H_2O_2 over the Atlantic Ocean between Cape Cod and Nova Scotia, corresponding to air exported from the northeastern U.S. The resulting correlation for O3 vs. NO_Z (Figure 4-4) shows a nonlinear increase, comparable to the results from Trainer et al. (1993), with the slope for O3 vs. NO_Z decreasing at high NO_Z. The same series of measurements showed a linear correlation between O3 and the sum $NO_Z+2H_2O_2$ (Figure 4-5). The ratio $\frac{O3}{NO_Z+2H_2O_2}$ varies from 7 at low O3 to 5 at high O3 (110 ppb). These measurements show excellent agreement with the photochemical model from Sillman (1995a), shown in Figure 4-3 ($\frac{O3}{NO_Z+2H_2O_2} = 6$). Staffelbach et al. (1997a,b) also measured O3, NO_X, NO_Y and H_2O_2 during an air pollution event in Switzerland. They found a similar linear correlation between O3 and the sum $NO_Z+2H_2O_2$ but with a higher ratio ($\frac{O3}{NO_Z+2H_2O_2} = 10$). The higher ratio is attributed to higher deposition rates.

The recent field measurement campaign (1995) in Nashville, TN, associated with the Southern Oxidant Study, included extensive measurements of O_3, NO_x, NO_y H_2O_2 and other related species (PAN, HNO_3). Preliminary results (Sillman et al., 1997b) showed a linear correlation between O_3 and the sum $NO_z+2H_2O_2$, similar to the results reported by Daum et al. (1996) but with a slightly higher ratio ($\frac{O_3}{NO_z+2H_2O_2}$ =7). This pattern is consistent with model results for Nashville and with results shown here, though it supports the use of higher dry deposition estimates. A similar correlation and ratio was found in aircraft measurements on two separate days (July 11 and 13, 1995). Aircraft measurements during a third day (July 18) reported significantly higher ratio ($\frac{O_3}{NO_z+2H_2O_2}$ =9), possibly due to rainout of H_2O_2.

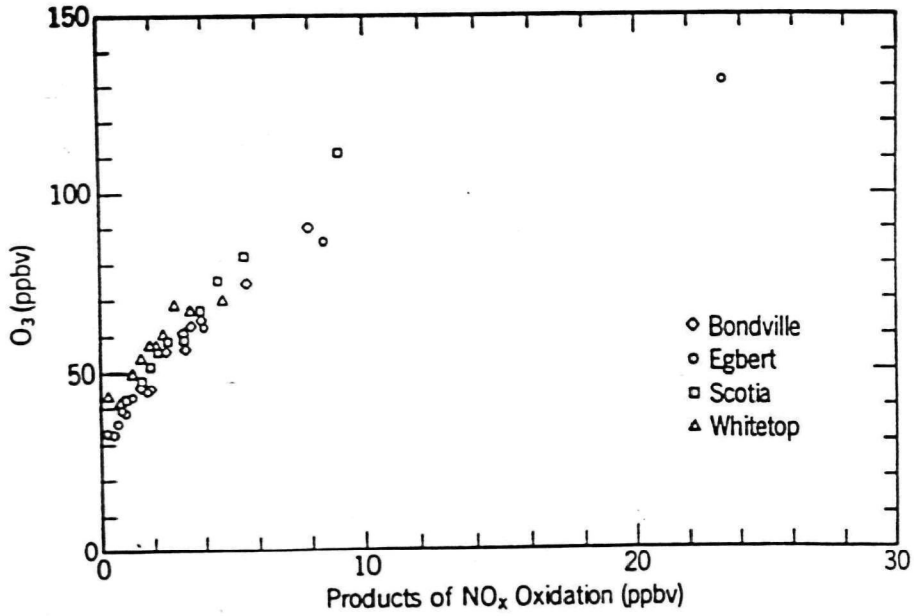

Figure 4-1 : Measured ozone as a function of NO_Z at four rural sites in eastern North America (Bondville, IL, Egbert, ON, Scotia, PA and Whitetop, NC). For Whitetop NO_Z is represented as the sum of measured PAN, HNO_3 and NO_3^-. For the other sites NO_Z is the difference between measured NO_y and NO_X. From Trainer et al. (1993).

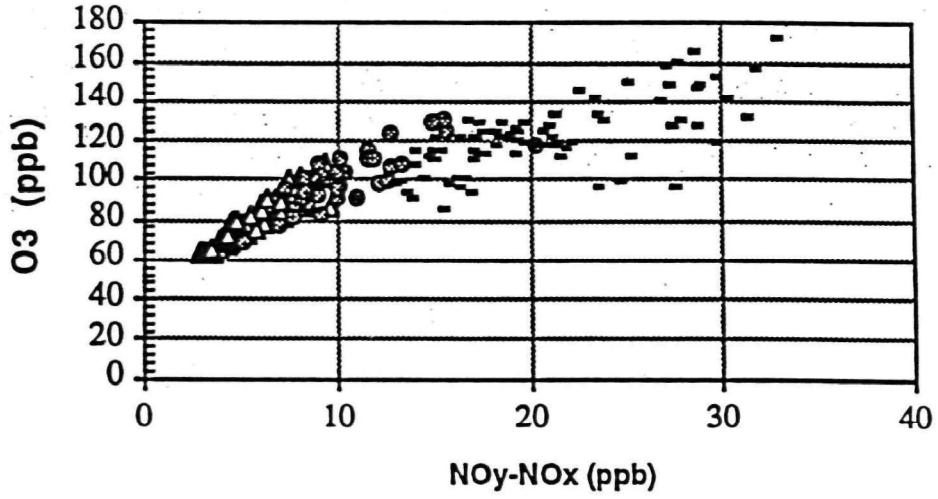

Figure 4-2 : Simulated afternoon concentrations of O_3 vs. NO_Z for locations with NO_X-sensitive chemistry (triangles), ROG-sensitive chemistry (points) and intermediate chemistry (circles) from the Lake Michigan regional simulation base case (Sillman et al., 1993).

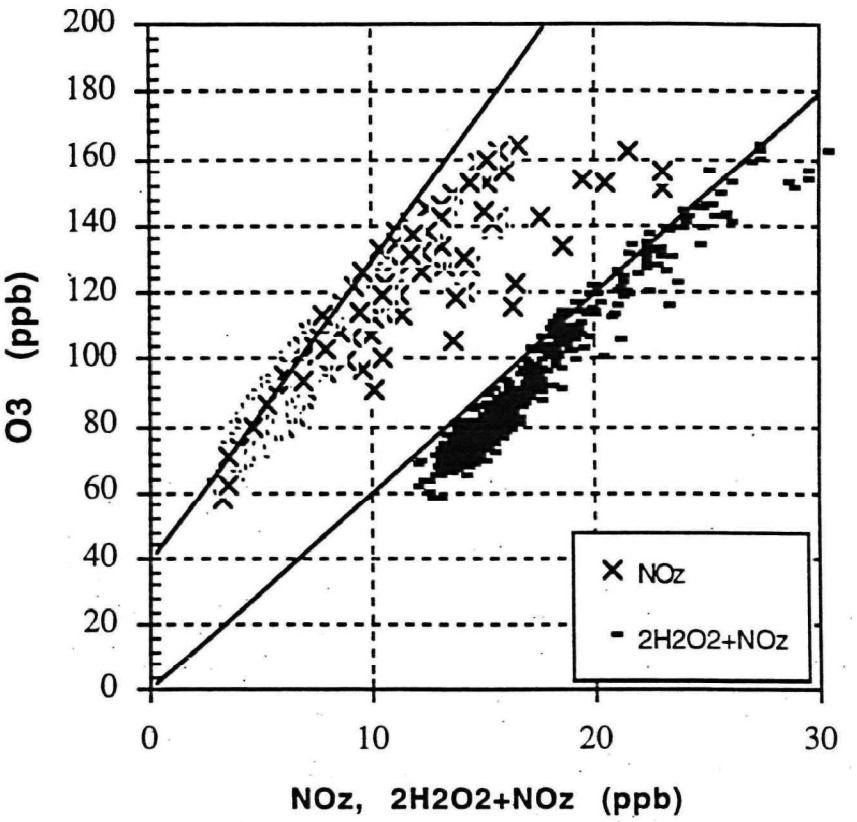

Figure 4-3. Correlation between O_3 and NO_Z (crosses) and O_3 and the sum $2H_2O_2+NO_Z$ (dashes), all in ppb, from the northeast corridor regional simulation base case. The lines correspond to an slope between O_3 and NO_Z of 9:1 and a ratio of 6:1, representing maximum and minimum values of O_3 vs. NO_Z in NO_X-sensitive and ROG-sensitive regions respectively.

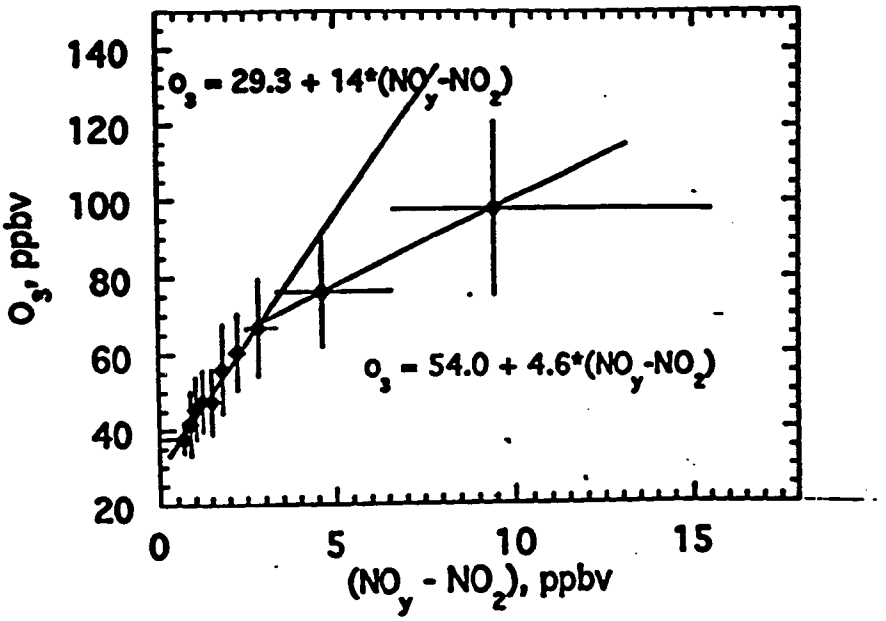

Figure 4-4 : O_3 concentration (ppb) vs (NO_y-NO_2) from aircraft measurements over the Atlantic Ocean. The data were collected at 10-second intervals, ordered by (NO_y-NO_2) concentrations and divided into 10 intervals. Each point on the plot represents the average NO_y-NO_2 corresponding to one of those intervals. Horizontal bars represent the range of NO_y-NO_2 included in each interval; vertical bars represent the standard deviation of the O_3 concentration measured over the interval. Slope and intercept were calculated from the individual data points. From Daum et al. (1996).

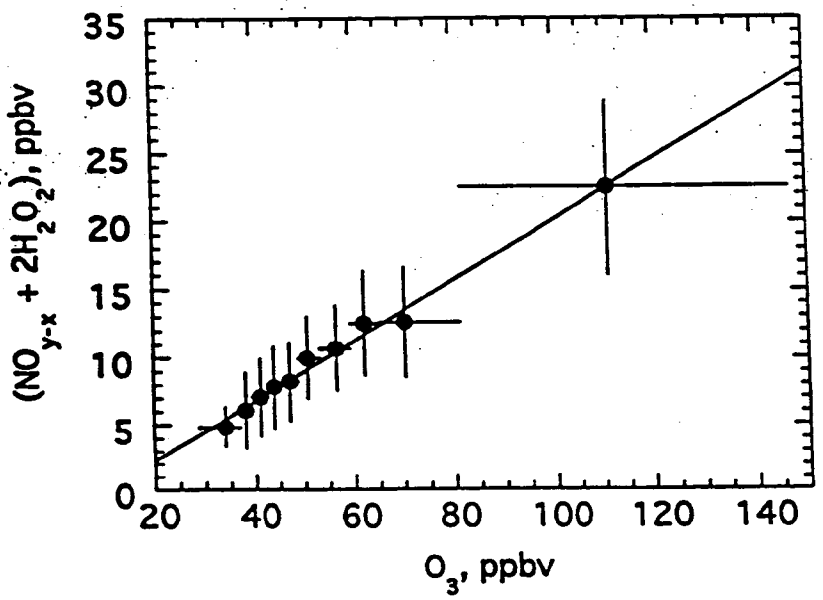

Figure 4-5 : The sum NO_z+$2H_2O_2$ vs. O_3 (ppb) from aircraft measurements over the Atlantic Ocean. Sixty second ordered by O_3 concentrations and divided into 10 intervals. Each point on the plot represents the average O_3 corresponding to one of those intervals. Horizontal bars represent the range of O_3 included in each interval; vertical bars represent the standard deviation of the NO_z+$2H_2O_2$ sums over the interval. Slope and intercept were calculated from the individual data points. From Daum et al. (1996).

SECTION 5
CASE STUDIES OF THE INDICATOR METHOD FOR ATLANTA AND LOS ANGELES

This section presents two case studies that illustrate the possible use of the method of photochemical indicators. The case studies are based on field measurement campaigns during specific air pollution events in Atlanta and Los Angeles. Measured O_3, NO_X and NO_Y have been used in combination with photochemical models to evaluate NO_X-ROG sensitivity in each city. It is hoped that these methods will serve as examples for similar studies elsewhere.

An important facet of the case studies shown here is the development of a series of model scenarios with different ROG-NO_X chemistry. In the case study for Atlanta a deliberate effort was made to generate plausible scenarios with both NO_X-sensitive and ROG-sensitive chemistry. This was achieved by varying the assumed rate of anthropogenic and biogenic emissions (including both the BEIS1 and BEIS2 inventories) and by varying wind speeds and mixed layer heights by 20%. In the case study for Los Angeles scenarios were generated with anthropogenic ROG emissions increased by up to a factor of three, resulting in a significant change in the predicted NO_X-ROG response. Each of these model scenarios generated different values for the indicator ratios $\frac{O_3}{NO_Y}$ and $\frac{O_3}{NO_Z}$ which can then be evaluated against ambient measurements. A central feature of the method is the development of model scenarios with different NO_X-ROG responses, rather than an attempt to "validate" a single model scenario or to only include scenarios with identical NO_X-ROG responses.

Results of this section also demonstrate that the measured indicator ratio $\frac{O_3}{NO_Y}$ has different values in a likely NO_X-sensitive environment (Atlanta) in comparison with a likely ROG-sensitive environment (Los Angeles). The difference in measured $\frac{O_3}{NO_Y}$ between Atlanta and Los Angeles corresponds closely to the difference between NO_X- and ROG-

sensitive environments predicted by the photochemical models in Section 3. However, the NO_X-ROG predictions are subject to a number of caveats: (1) NO_X-ROG sensitivity varies greatly from event to event, so that events in Atlanta with more stagnant meteorology might have ROG-sensitive chemistry. (2) NO_X-ROG sensitivity has been shown to vary with location in Los Angeles (Milford et al., 1989), and downwind locations in the Los Angeles basin are likely to have NO_X-sensitive chemistry. (3) The NO_X-ROG sensitivity results are critically dependent on the accuracy of measured NO_y.

The methods shown here would be strengthened if measured H_2O_2 were also included. This is because the indicator ratios with H_2O_2 show a stronger correlation with NO_X-ROG chemistry and are less dependent on model assumptions, and because measured H_2O_2 would allow the field measurements to be evaluated in terms of the O_3-NO_Z-H_2O_2 correlation. The Nashville field measurement campaign associated with the Southern Oxidant Study should provide an example of an analysis based on H_2O_2 (Sillman et al., 1997b). A case study based on H_2O_2 was also carried out by Jacob et al. (1995) in rural Virginia. They found that $\frac{H_2O_2}{NOy}$ shifts from values associated with NOx-sensitive chemistry in summer to values associated with ROG-sensitive chemistry in fall, possibly associated with a seasonal change in photochemistry.

5.1 Atlanta

Model scenarios were developed for the air pollution episode of August 9-11, 1992 in Atlanta. The simulations are based on the Urban Airshed Model (UAM-IV) and are described in detail in Section 3. Simulations were performed using two different inventories for anthropogenic emissions: an inventory developed by the Georgia Department of Natural Resources(1987) based on the NAPAP 1985 national inventory(R) and an updated inventory developed by Cardelino et al. (1994). Estimates for NO_X emissions from both point and area sources differ by a factor of two between the inventories, and similar differences are found for ROG/NO_X ratios. Smaller differences are found for individual ROG. Separate model scenarios were also generated with biogenic emissions from the BEIS1 inventory and with tripled isoprene emissions, comparable to the newer BEIS2 inventory (Geron et al., 1995). Additional scenarios were generated with the height of the daytime mixed layer reduced by 20% from the initial estimate. The 20% reduction was used to generate a plausible scenario with ROG-sensitive chemistry, and lies within the range of uncertainty for vertical mixing identified by Marsik et al. (1995). The resulting six scenarios are:

(A1) 1987 anthropogenic emission inventory, and BEIS1 biogenic inventory, equivalent to the base case in Sillman et al (1995b).

(A2) 1987 anthropogenic emission inventory with tripled isoprene.

(B1) 1994 anthropogenic emission inventory, BEIS1 biogenics.

(B2) 1994 anthropogenic emission inventory with tripled isoprene.

(C1) 1994 inventory with mixing heights reduced by 20%.

(C2) 1994 inventory with mixing heights reduced by 20% and tripled isoprene.

Aircraft-based measurements for O_3 and NO_y were made downwind of Atlanta between 4:15 and 5:15 pm on both August 10 and August 11 (Imhoff et al., 1995). NO_y was measured using a gold tube converter with CO injection (Bollinger et al., 1983) which was mounted external to the helicopter in the free air stream. The NO produced was drawn through ~6 m of Teflon tubing to a Thermo Electron Instruments Model 42 nitrogen oxides analyzer. Tests indicated that very little O_3 (<3 ppb) survived the gold-tube converter and therefore no adjustment was applied for the possible reduction of NO with O_3 in the tubing. Wind direction was from the north on August 10 and from the southwest on August 11, and the location of the measurements was correspondingly different. On both days the measurements covered a region extending from near downtown Atlanta to approximately 40 km downwind. The spatial pattern of measured O_3 and NO_y confirmed that the aircraft regularly intercepted a plume of polluted air, which was believed to be associated with Atlanta. The measurements were made at 500-600 m. altitude above ground.

Figure 5-1 shows measured values for O_3 vs. NO_y on August 10, 1992 in comparison with model results from each of the six model scenarios. The measured O_3-NO_y correlations show a broad region in which O_3 increases with NO_y, generally associated with NO_y between 5 and 15 ppb. This O_3-NO_y correlation is consistent with previous rural measurements (Trainer et al., 1993). The measurements also show a range of locations in which O_3 does not increase with NO_y, typically associated with higher NO_y. These uncorrelated points may represent locations close to emission sources where NO_x/NO_y is large, so that photochemical production of O_3 that would otherwise be associated with the observed NO_y has not yet occurred. The use of O_3/NO_y as a photochemical indicator suggests that the locations with high NO_y and low O_3/NO_y may also represent ROG-sensitive chemistry.

The model results in Figure 5-1 represent a subset of the model domain including downtown Atlanta and the downwind urban plume, at the same time (4-5 pm) and altitude (600 km) as the measurements but not necessarily at the same horizontal location. Results for all model scenarios show that O_3 increases with NO_y in a pattern broadly consistent

with the observed O_3-NO_y correlation. However, there are some differences between the simulated and observed O_3-NO_y correlation and differences between individual simulations. The models show a much smaller region with uncorrelated O_3 and NO_y, possibly because the model grid resolution (4x4 km) is too coarse to include NO_x plumes from individual emission sources. Model scenarios with the BEIS1 biogenic inventory all show a lower rate of increase of O_3 with NO_y, both in comparison with the model scenarios with increased isoprene and in comparison with measurements. Peak O_3 occurred further downwind in the model (40 km south of the Georgia Tech campus) than in measurements (20 km south of Georgia Tech), but the region with measured high O_3 (>140 ppb) extends south and overlaps with the location of the model peak.

The most important evaluation for the six model scenarios is an examination of measured O_3 and concurrent NO_y in the vicinity of the measured peak O_3, in comparison with peak O_3 and concurrent NO_z in each model scenario. This comparison is especially important because the model behavior in the vicinity of peak O_3 has a dominant impact on NO_x-ROG control strategies, and the difference in the NO_x-ROG responses of the six model scenarios is most obvious for the peak O_3 in each scenario. The near-continuous sampling of O_3 and NO_y in the aircraft-based measurements provides an excellent basis for characterizing the region of the Atlanta urban plume associated with peak O_3. Because photochemical models use 4 km grid resolution, we have used the range of measured O_3 and NO_y within 4 km of the measured peak O_3 as a basis for characterizing the peak-O_3 region. As shown in Figure 5-2, ozone within 4 km of the measured peak varies by 20 ppb (130-150 ppb) while NO_y varies between 7 and 15 ppb. This range of O_3 and NO_y is used as a basis for evaluating the performance of individual model scenarios, i.e. model peak O_3 and concurrent NO_y is expected to fall within the range of measured O_3, NO_y and O_3/NO_y ratios found within 4 km of the measured peak O_3.

Results (Figure 5-2) show that several model scenarios (B1, C1) generate peak ozone that is close to the observed peak, but with concurrent NO_y that is significantly higher than the observed value. The poor performance of these scenarios in comparison with measured O_3 and NO_y can also be seen in the complete data set (Figure 5-1), but is highlighted when the evaluation focuses on peak O_3 and concurrent NO_y. Other model scenarios (A1, A2) show good agreement with both peak O_3 and concurrent NO_y.

The indicator ratio $\frac{O_3}{NO_y}$ associated with peak O_3 shows great variation among the six model scenarios, reflecting the difference in model NO_x-ROG sensitivity. The NO_x-sensitive model scenarios (A1, A2 and B2) all show $\frac{O_3}{NO_y}$ greater than the NO_x-ROG transition ratio (7). The ratios for scenarios A1 and A2 (11-13) are significantly higher

than the transition ratio. By contrast the ROG-sensitive scenario (C1) has a $\frac{O3}{NOy}$ (=5.5) lower than the transition ratio. This correlation between $\frac{O3}{NOy}$ and NO_X-ROG sensitivity is consistent with the results of Section 3.

Measured $\frac{O3}{NOy}$ in the vicinity peak O3 shows a range of values (10-20) that is significantly higher than the NO_X-ROG transition. This high $\frac{O3}{NOy}$ is consistent with NO_X-sensitive chemistry. The measurements show good agreement with the strongly NO_X-sensitive model scenarios (A1 and A2) and show poor agreement with the ROG-sensitive scenario (C1). It is important to note that the ROG-sensitive scenario shows good agreement with measured peak O3. If model performance was evaluated solely in terms of measured peak O3, then scenarios A1, A2, B1 and C1 would all be acceptable even though they show different NO_X-ROG responses. The model-measurement comparison for the indicator ratio $\frac{O3}{NOy}$ in connection with peak O3 provides a stronger basis for evaluating model scenarios.

Results for both August 10 and August 11 are summarized in Table 2, are similar to August 10. The model results and measurements both suggest that August 11 is more likely to have NO_X-sensitive chemistry than August 10.

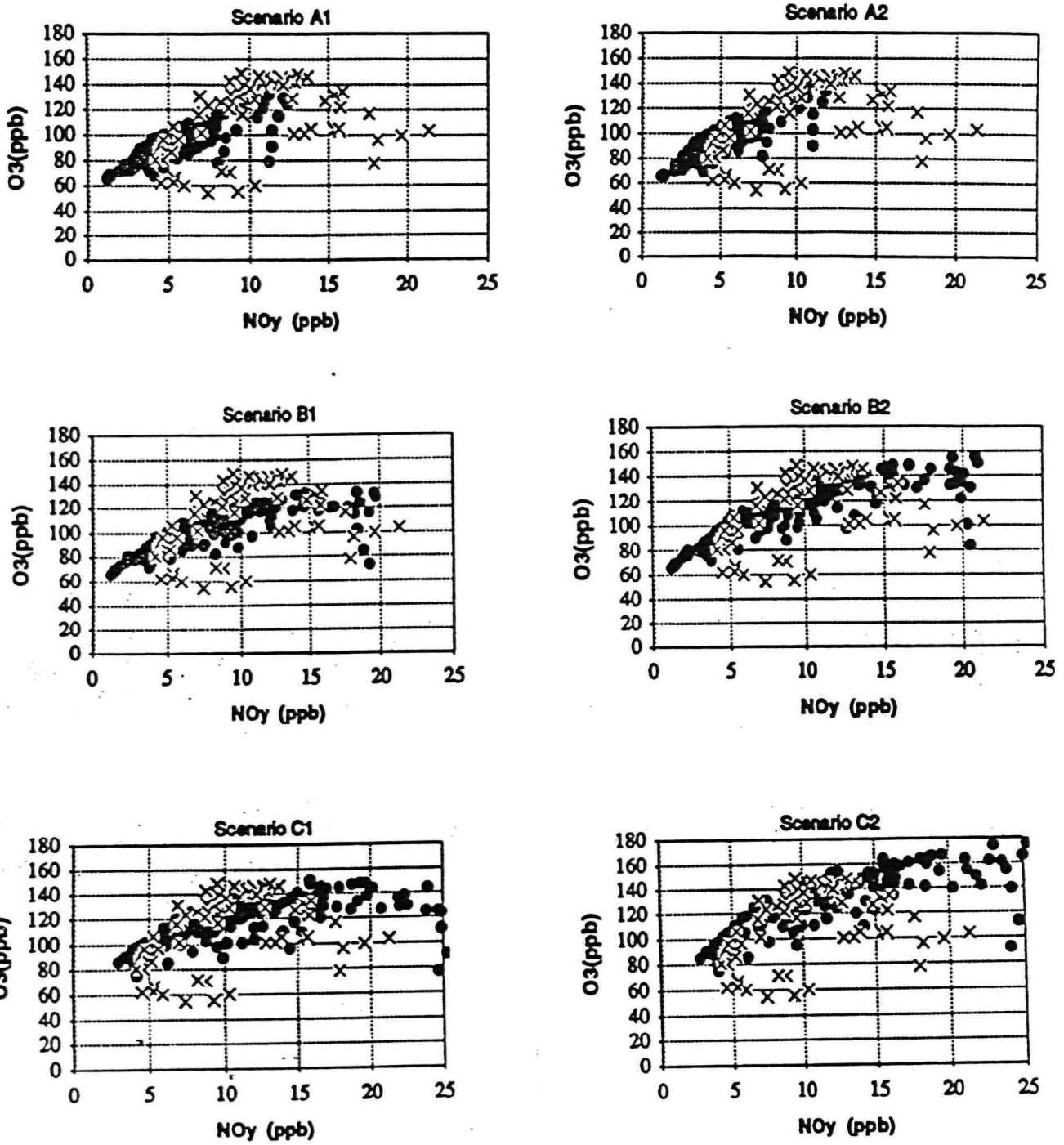

Figure 5-1. Correlation between O3 and NO_y (ppb) in the urban plume 10 to 40 km south of Atlanta, measured by aircraft 600 m. above ground at 4:00-5:20 pm, August 10, 1992 (crosses), compared with simulated O3 and NO_y (solid circles) from six model scenarios described in the text. From Sillman et al. (1997a) based on measurements by Imhoff et al. (1995).

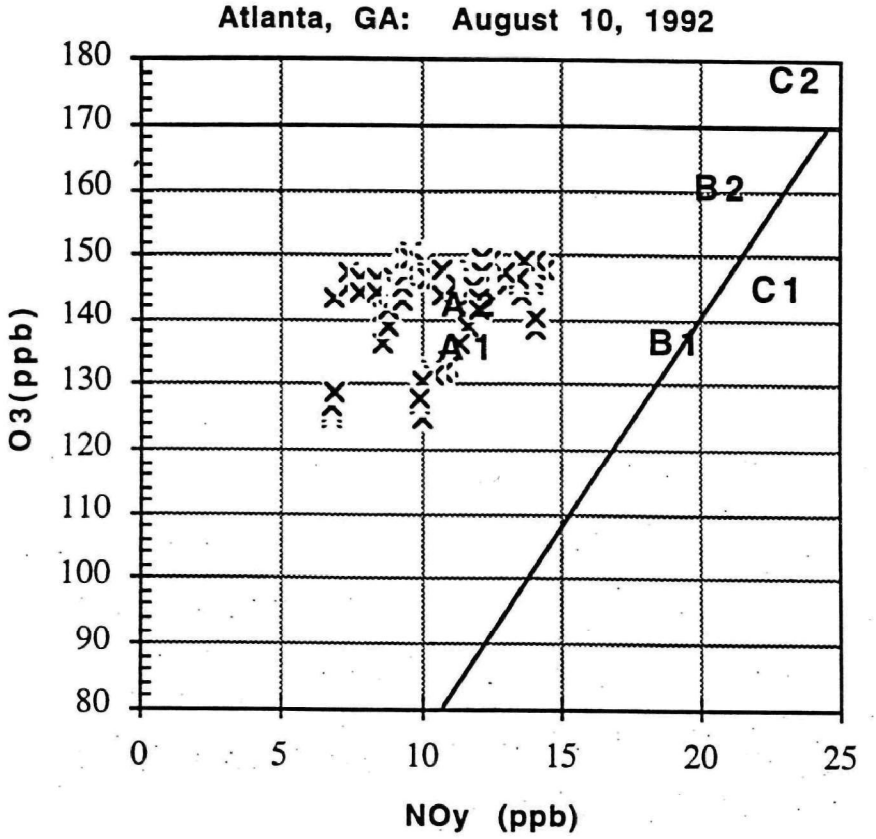

Figure 5-2. Peak O_3 and concurrent NO_y (ppb) in the Atlanta urban plume on 8-10-92. The crosses represent measurements at 600 m elevation, 4-5 pm, for locations within 4 km of the measured peak O_3. Bold letters represent domain-wide peak O_3 and concurrent NO_y at 600 m elevation, 4-5 pm for the model scenarios identified in the text. The line (O_3/NO_y=7) corresponds to the transition point between NO_x- and ROG-sensitive chemistry based on O_3/NO_y as a photochemical indicator.

Table 5-1

O_3, NO_y and NO_x-ROG sensitivity in simulations for Atlanta

The table gives simulated peak O_3, concurrent NO_y, peak O_3 in simulations with 35% reductions in anthropogenic ROG emissions and peak O_3 in simulations with 35% reductions in NOx emissions, for six model scenarios. Scenarios A1 and A2 use anthropogenic emissions from Georgia[9]; the other scenarios use Cardelino[11]. Scenarios C1 and C2 have daytime mixing heights reduced by 20% relative to the base case. Scenarios A1, B1 and C1 have biogenic emissions from (BEIS1[12]; scenarios A2, B2 and C2 have isoprene emissions increased by a factor of three. Observed values give the range of measured values within 4 km of observed peak O_3.

	August 10, 1992				August 11, 1992			
Scenario	peak O_3	NO_y	reduced ROG	reduced NO_x	peak O_3	NO_y	reduced ROG	reduced NO_x
A1	132	11	126	118	131	9	128	112
A2	141	11	137	122	136	9	132	113
B1	132	15-21	126	127	147	12	141	128
B2	157	22	150	144	166	17	163	145
C1	149	16-27	143	147	165	16	159	153
C2	177	25	167	164	184	19	180	160
Observed	130-150	7-15			123-148	8-12		

5.2 Los Angeles

Results for Los Angeles are based on simulations for the event of August 26-29, 1987 developed by Godowitch and Vukovich and by Wagner et al. (1992), described in Section 3. These models used an anthropogenic emission inventory for southern California developed in association with the Southern California Air Quality Study (SCAQS). In addition, Wagner et al. (1992) generated alternative scenarios with emissions of anthropogenic ROG increased by factors of two and three relative to the initial estimate. NO_X-ROG responses were tested relative to each of these cases.

Measurements of O_3, NO, NO_2, PAN, HNO_3 and aerosol nitrate were made at eight surface sites in the Los Angeles basin (Lawson et al., 1990). The measurement sites were: downtown Los Angeles, Hawthorne, Long Beach City College, Anaheim, Burbank, Azuza, Claremont and Rubidoux. HNO_3 and particulate nitrate were measured using a transition-flow reactor (Ellestad et al., 1989), and O_3, NO_2, NO_X and PAN were measured using a Luminox detector (R-30). In this report it is assumed that NO_y is equal to the sum of the five measured nitrogen-containing species. Parrish et al.(1993) found that these five species account for 90% of measured NO_y in the eastern U.S. Aerosol nitrate is not included in model photochemistry, but it is appropriate to assume that model HNO_3 is equal to the sum of measured HNO_3 and aerosol nitrate in model-measurement comparisons.

Figure 5-3 shows measured O_3 vs. NO_y and O_3 vs. NO_Z from all eight surface measurement sites in the Los Angeles basin during the hours of 1-5 pm, August 27, 1987. The combined results from all sites provide enough measurements to identify correlations among the species. Virtually no correlation appears between O_3 and NO_y, but there is a strong correlation between O_3 and NO_Z. A similar correlation between O_3 and NO_Z has appeared in previous measurements in Los Angeles (Tuazon et al., 1981, Trainer et al., 1993).

As reported by Trainer et al., the correlation between O_3 and NO_Z in Los Angeles is similar to the O_3-NO_Z correlations at rural sites in eastern North America. However $\frac{O_3}{NO_Z}$ in Los Angeles is much lower than either the measured ratios at rural eastern sites and also much lower than $\frac{O_3}{NO_y}$ reported above for Atlanta. The O_3 and NO_Z measurements for Los Angeles from Figure 5-3 have an average O_3/NO_Z ratio equal to 4, and $\frac{O_3}{NO_Z}$ associated

with peak O3 is equal to 6. This contrasts with both Atlanta ($\frac{O3}{NOy}$ = 14, above) and with the rural eastern sites from Trainer et al. shown in Figure 4-1 ($\frac{O3}{NO_Z}$ = 15). If the $O3/NO_Z$ ratio is interpreted as a photochemical indicator, the low $\frac{O3}{NO_Z}$ in Los Angeles would suggest ROG-sensitive chemistry, in contrast with the higher $\frac{O3}{NO_Z}$ and NO_X-sensitive chemistry in Atlanta and the rural eastern sites. Measured $\frac{O3}{NO_Z}$ in Los Angeles is also comparable with measured values for $\frac{O3}{NO_Z+2H_2O_2}$ over the Atlantic Ocean from Daum et al. (1996), presented above (Figure 4-5). The latter ratio represents a likely limiting value for $\frac{O3}{NO_Z}$ under ROG-sensitive conditions.

Figure 5-4 shows O3 and NO_Z from simulations for Los Angeles by Wagner et al. (1992) including scenarios with anthropogenic emissions equal to the base case and with anthropogenic ROG increased by factors of two and three. The simulated values represent the same time period (1-5 pm) and the same locations as the measurements. A comparison between Figures 5-3 and 5-4 is used to evaluate the performance of model scenarios. It is apparent that the base case represents a significant underestimate of peak O3, although the $\frac{O3}{NO_Z}$ ratio associated with peak O3 ($\frac{O3}{NO_Z}$=5) is reasonable in comparison with measurements. The scenario with doubled anthropogenic ROG shows good agreement both with measured O3 and with $\frac{O3}{NO_Z}$ (average $\frac{O3}{NO_Z}$=6, $\frac{O3}{NO_Z}$=5 concurrent with peak O3). The simulation with tripled anthropogenic ROG significantly overestimates $\frac{O3}{NO_Z}$ (average $O3/NO_Z$= 7, $\frac{O3}{NO_Z}$=9 concurrent with peak O3). This scenario shows greater sensitivity to NO_X (see Wheeler et al., 1992),which is consistent with the higher $\frac{O3}{NO_Z}$.

In contrast with the Atlanta event, evaluation of the three model scenarios for Los Angeles are consistent with evaluations based solely on measured O3. The model evaluation shown in Figures 5-3 and 5-4 suggest that the scenario with doubled ROG is more accurate than either the base case or the scenario with tripled ROG. This conclusion is consistent with the original analysis by Wheeler et al. (1992) and also with the analysis of emission rates in southern California by Fujita et al. (1992). Fujita et al. found that measured ROG/NO_X ratios during the morning lower than ROG/NO_X ratios in the UAM base case by approximately a factor of two.

Results from this case study were constrained by the limited geographical extent of the measurements. Milford et al. (1989) has shown that model NO_X-ROG sensitivity in

Los Angeles shows great geographical variation with ROG-sensitive chemistry downtown and NO_X-sensitive chemistry at downwind sites. The measurement sites included in this analysis were almost all located in the region identified as ROG-sensitive in Milford et al. A more complete analysis would require measurements that would identify the region of transition between ROG-sensitive and NO_X-sensitive chemistry.

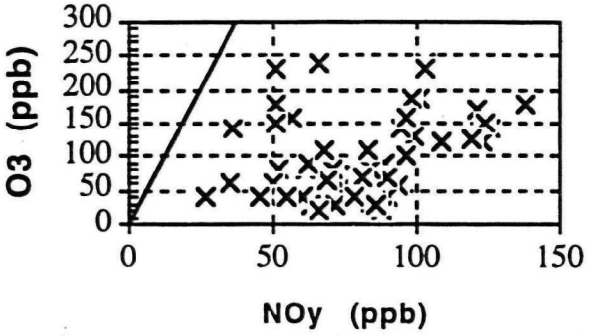

(a)

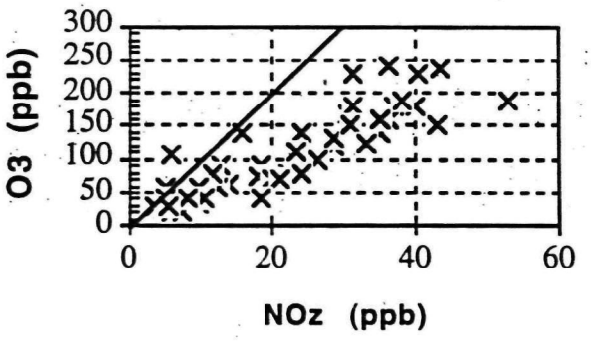

(b)

Figure 5-3: Measured O_3 and concurrent NO_y (ppb) and O_3 versus NO_z at 1-5 pm August 27, 1987 at eight sites in the Los Angeles basin. The line represents the transition between NO_x- and ROG-sensitive chemistry based on O_3/NO_y and O_3/NO_z as photochemical indicators

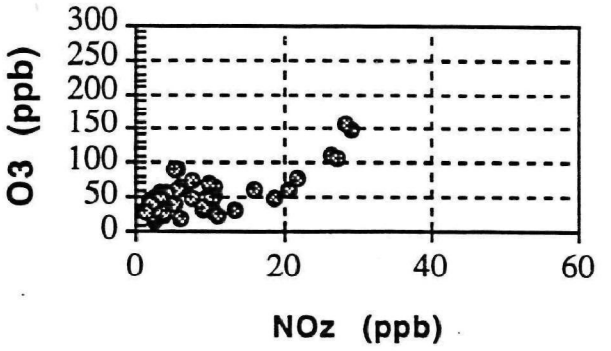

(a)

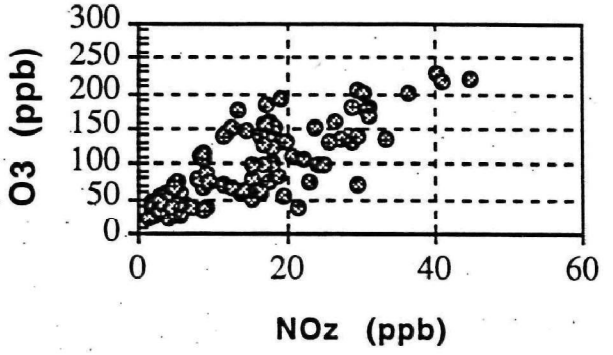

(b)

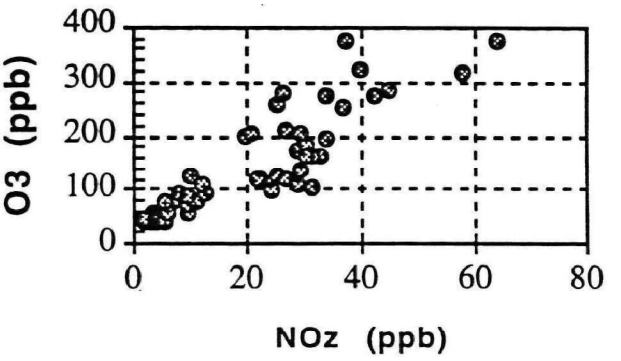

(c)

Figure 5-4: Simulated O_3 versus NO_Z during the afternoon of August 27, 1987 for locations corresponding to measurements shown in Figure 6, from simulations by Wagner et al. (1992) using (a) base case emissions, (b) doubled ROG emissions and (c) tripled ROG emissions.

SECTION 6
SUMMARY AND CONCLUSIONS

This report has presented a series of results associated with the use of photochemical indicators as a basis for investigating O3-NO_X-ROG sensitivity. The method of photochemical indicators seeks to identify species or species ratios that are closely associated with NO_X-ROG predictions in models. A successful correlation between model NO_X-ROG predictions and indicator values has been found for six species ratios: $\frac{O3}{NO_y}$, $\frac{O3}{NO_Z}$, $\frac{O3}{HNO3}$, $\frac{H_2O_2}{HNO3}$, $\frac{H_2O_2}{NO_Z}$, and $\frac{H_2O_2}{NO_y}$. In each case, high values are associated with NO_X-sensitive model predictions for ozone and low values are associated with ROG-sensitive predictions. The close correlation between NO_X-ROG predictions and indicator values suggests that measured indicator values can be used as a basis for evaluating the accuracy of model NO_X-ROG predictions.

Indicator-NO_X-ROG correlations have been examined for a wide variety of model applications, including two different model types (UAM-IV and a regional model developed at the University of Michigan) with different photochemical mechanisms. They have been examined for several locations (Lake Michigan, northeast corridor, Atlanta and Los Angeles). They have been examined in model scenarios with a range of assumptions about emission rates, including scenarios with anthropogenic ROG emissions doubled or reduced by half in comparison with inventory values and scenarios with radically different emission rates for biogenic ROG. They have been examined in scenarios with changed wind speeds and vertical mixing heights. They have been examined in scenarios with strongly ROG-sensitive chemistry and in scenarios in strongly NO_X-sensitive chemistry. In all these cases, the correlation between model NO_X-ROG predictions and indicator values remains largely unchanged, even though the model NO_X-ROG predictions vary.

It is especially noteworthy that changes in model assumptions that affect NO_X-ROG predictions also cause a corresponding change in the model values for photochemical indicators. This feature is especially striking in the Atlanta case study (Table 5-1 and Figure 5-2). In this case, model predictions for $O3/NO_y$ concurrent with peak O3 varied

from 13 in the strongly NO_X-sensitive model scenarios to 6 in the ROG-sensitive scenario. The Atlanta case study is especially important because the NO_X-sensitive and ROG-sensitive scenarios each give similar predictions for peak O_3, suggesting that an evaluation vs. measured O_3 does not provide a basis for confidence in model NO_X-ROG predictions. A similar contrast between NO_X-sensitive and ROG-sensitive scenarios is apparent in the scenarios for Lake Michigan with different ROG emission rates (Figures 3-1a and b) and in the simulations for New York /northeast corridor for events with different meteorology (Figures 3-1c and 3-1d). The predicted contrast in indicator values between NO_X-sensitive and ROG-sensitive locations is partially confirmed by measurements in Atlanta and Los Angeles. Model results (Figures 3-1e and 3-1f) predict high values for O_3/NO_Z in Atlanta and low values in Los Angeles. This prediction is consistent with measurements (Figures 5-1, 5-2 and 5-3).

This study has identified a several factors that might be sources of error in the indicator method. A list of caveats is given in Section 1. The most important uncertainties are associated with the removal rate for the indicator species (especially through wet and dry deposition); the possible role of particulate nitrate as a sink for NO_Y; and uncertainties associated with the chemistry of organic peroxides, which are not represented in some of the chemical mechanisms that are frequently used for air quality analysis (e.g. CB-IV). It is especially imporant to identify uncertainties that might lead to bias in the NO_X-ROG interpretation of indicator values.

A more general problem associated with the method of photochemical indicators is that, as with all methods designed to predict the sensitivity of O_3 to NO_X and ROG, it is very difficult to find direct confirmation that the predictions are accurate. This report has recommended investigation of model and measured correlations between O_3, NO_Z and H_2O_2 as a basis for evaluating model assumptions that represent uncertainties in the indicator method. The models that were used to derive indicator-NO_X-ROG correlations also predict a linear correlation between O_3 and the sum: $NO_Z+2H_2O_2$. This prediction should be verified vs. measurements. In addition, model results predict that the ratio \f(O_3, $NO_Z+2H_2O_2$) should have similar values in NO_X-sensitive and ROG-sensitive locations (although it may show diurnal variations and day-to-day variation in responses to changing cloud cover and the effect of wet deposition). Because this ratio is closely associated with the proposed indicators (especially with O_3/NO_Z), it might also be used as a basis for evaluating the accuracy of the proposed NO_X-ROG transition values associated with the indicators.

REFERENCES

Benjamin S. G., K. J. Brundage and L. L. Morone, Implementation of the Rapid Update Cycle, Part I: Analysis/Model Description, NOAA/NWS Technical Procedures Bulletin, Series No. 416, 1994.

Blanchard, C. L., P. M. Roth and G. Z. Whitten. The influence of NOx and VOC emissions on ozone concentrations in rural environments. Electric Power Research Institute, Palo Alto, CA, May, 1991.

Blanchard, C. L., P. M. Roth and H. E. Jeffries. Spatial mapping of preferred strategies for reducing ambient ozone concentrations nationwide. Paper #93-TA-37A.04, presented at the Air and Waste Management Association 86th Annual Meeting and Exposition, Denver, CO, June 13-18, 1993.

Bollinger, M. J., R. E. Sievers, D. W. Fahey, and F. C. Fehsenfeld, Conversion of nitrogen dioxide, nitric acid and n-propyl nitrate to nitric oxide by gold-catalyzed reduction with carbon monoxide. *Ana. Chem.*, 55, 1980-1986, 1983.

Bott, A., A positive definite advection scheme obtained by nonlinear renormalization of the advective fluxes. *Mon. Wea. Rev.*, 117, 1006-1015, 1989.

Buhr, M., D Parrish, J. Elliot, J. Holloway, J. Carpenter, P. Goldan, W. Kuster, M. Trainer, S. Montzka, S. McKeen, and F. C. Fehsenfeld, Evaluation of ozone precursor source types using principal component analysis of ambient air measurements in rural Alabama. *J. Geophys. Res.*, 100, 22853-22860, 1995.

Cardelino, C., W-L. Chang and M. E. Chang, 1994: Comparison of emissions inventory estimates and ambient concentrations of ozone precursors in Atlanta, Georgia. Presented at the Air and Waste Management Association International Conference on the Emission Inventory: Applications and Improvement, Raleigh, N.C., November 1-3, 1994.

Cardelino, C. and W. L. Chameides. An observation-based model for analyzing ozone-precursor relationships in the urban atmosphere. *J. Air Waste Manage. Assoc.*, 45, 161-180, 1995

Carter, W. P. L. Development of ozone reactivity scales for volatile organic compounds, *J. Air Waste Manage. Assoc.*, 44, 881-899, 1994.

Carter, W. P. L., Computer modeling of environmental chamber studies of maximum incremental reactivities of volatile organic compounds, Atmos. Environ., 29-18, p. 2513, 1995.

Chameides, W. L., F. Fehsenfeld, M. O. Rodgers, C. Cardellino, J. Martinez, D. Parrish, W. Lonneman, D. R. Lawson, R. A. Rasmussen, P. Zimmerman, J. Greenberg, P. Middleton, and T. Wang, Ozone precursor relationships in the ambient atmosphere. *J. Geophys. Res.*, 97, 6037-6056, 1992.

Chameides, W. L., D. D. Davis, J. Bradshaw, S. Sandholm, M. Rodgers, B. Baum, B. Ridley, S. Madronich, M. A. Carroll, G. Gregory, H. I. Schiff, D. R. Hastie, A. Torres, E. Condon, Observed and model-calculated NO2/NO ratios in tropospheric air sampled during the NASA GTE/CITE2 field study. *J. Geophys. Res.*, 95, 10235-10247, 1990.

Chameides, W. L., R. W. Lindsay, J. Richardson, C. S. Kiang, The role of biogenic hydrocarbons in urban photochemical smog: Atlanta as a case study, *Science*, 241, 1473-1474, 1988.

Chang, M. E., D. Hartley, C. Cardelino, and W.-L. Chang, Temporal and spatial distribution of biogenic emissions of isoprene based on an inverse method using ambient isoprene observations from the 1992 Southern Oxidants Study, Atlanta Intensive, *Atmos. Environ.*, in press, 1996.

Chock, D.P. A comparison of numerical methods for solving the advection equation - III. *Atmos. Environ.*, 25A, 853-871, 1991.

Daum, P. H., L. I. Kleinman, L. Newman, W. T. Luke, J. Weinstein-Lloyd, C. M. Berkowitz and K. M. Busness, Chemical and physical properties of anthropogenic pollutants transported over the North Atlantic during NARE, *J. Geophys. Res.*, 101, 29029-29042, 1996.

DeMore, W. B., S. P. Sander, D. M. Golden, R. F. Hampson, M. J. Kurylo, C. J. Howard, A. R. Ravishankara, C. E. Kolb, and M. J. Molina. Chemical kinetics and photochemical data for use in stratospheric modeling. JPL 92-20, Jet Propulsion Laboratory, NASA, 1992.

Drummond, J., H. Schiff, D. Karecki, G. Mackay. Measurements of NO_2, O_3, PAN, HNO_3, H_2O_2 an H_2CO during the Southern California Air Quality Study. Presented at the 82nd annual meeting of the Air and Waste Management Association, Anaheim, CA, 1989; Paper 89-139.4.

Ellestad, T. G., L. Stockburger, and K. T. Knapp. Measurements of nitric acid and particulate nitrate by transition-flow reactor during the 1987 Southern California Air Quality Study. Presented at the 82nd annual meeting of the Air and Waste Management Association, Anaheim, CA, 1989; Paper 89-152.2.

Environmental Protection Agency (EPA) Development of the 1980 NAPAP emissions inventory, *EPA-600/7-86-057a*, Environmental Protection Agency, Research Triangle Park, N.C. 1986.

Environmental Protection Agency (EPA). The 1985 NAPAP emissions inventory (version 2): development of the annual data and modelers' tapes, *EPA-600/7-89-012a*, Environmental Protection Agency, Research Triangle Park, NC, 1989.

Environmental Protection Agency (EPA), Regional Interim Emission Inventories (1987-1991), Volume I and II, EPA-454/R93-021a and b, Environmental Protection Agency, Research Triangle Park, N.C., 1993.

Fujita, E. M., B. E. Croes, C. L. Bennett, D. R. Lawson, F. W. Lurmann and H. H. Main, Comparison of emission and ambient concentration ratios of CO, NO_X, and NMOG in California's south coast air basin. *J. Air Waste Mgmt. Assoc.*, 42:264-276 1992.

Georgia Department of Natural Resources, 1987: Georgia's State Implementation Plan for Ozone in the Atlanta Area, Air Protection Branch.

Geron, C. D., A. B. Guenther, and T. E. Pierce, An improved model for estimating emissions of volatile organic compounds from forests in the eastern United States. *J. Geophys. Res.*, 99, 12773-12791, 1994.

Geron, C. D., T.E. Pierce and A.B. Guenther, Reassessment of biogenic volatile organic compound emissions in the Atlanta area, *Atmos. Environ.*, 29, 1569-1578, 1995

Gery, M. W. G. Z. Whitten, J. P. Killus and M. C. Dodge. A photochemical kinetics mechanism for urban and regional computer modeling. *J. Geophys. Res.*, 94, 12925-12956, 1989.

Godowitch, J. M. and J. M. Vukovich, 1994: Photochemical urban airshed modeling using diagnostic and dynamic meteorological fields. Presented at the 87th Air and Waste Management Association Meeting and Exhibition, Cincinnati, OH, June 19-24, 1994.

Hall, B. D. and C. S. Claiborn, Measurements of the dry deposition of peroxides to a Canadian boreal forest, *J. Geophys. Res.*, in press, 1997.

Hanna, S. R., G. E. Moore and M. E. Fernau. Evaluation of photochemical grid models (UAM-IV, UAM-V, and the ROM/UAM-IV couple) using data from the Lake Michigan Ozone Study (LMOS). Atmos. Environ., 30, 3265-3279, 1996.

Harley, R. A., A. G. Russell, G. J. McRae, G. R. Cass, and J. H. Seinfeld. Photochemical modeling of the Southern California Air Quality Study. *Environ. Sci. Technol.*, 27, 378-388, 1993.

Hillery, J. F. Spatial and temporal distribution of aloft ozone and oxides of nitrogen in a mesoscale lakeshore environment. In Ranzieri, A. J. and P. A. Solomon, eds., Regional Photochemical Measurement and Modeling Studies: The Proceedings of an International Specialty Conference, San Diego, CA, November 8-12, 1993. Air and Waste Management Association, 1995.

Imhoff, R. E., R. J. Valente, J. F. Meagher and M. Luria, 1995: The production of O_3 in and urban plume: airborne sampling of the Atlanta urban plume. *Atmos. Environ..*, 29, 2349-2358.

Jacob, D. J., B. G. Heikes, R. R. Dickerson, R. S. Artz and W. C. Keene. Evidence for a seasonal transition from NO_x- to hydrocarbon-limited ozone production at Shenandoah National Park, Virginia. *J. Geophys. Res.*, 100, 9315-9324, 1995.

Johnson, G. M., A simple model for predicting the ozone concentration of ambient air. Proc. Eighth Inter. Clean Air Confer., Melbourne, Australia, May 2, 1984, p. 715-731.

Johnson, G. M., S. M. Quigley, and J. G. Smith. Management of photochemical smog using the AIRTRAK approach. 10th International Conference of the Clean Air Society of Australia and New Zealand, Aukland, New Zealand, March, 1990, p. 209-214.

Kirchner, F., and W. R. Stockwell, The effect o peroxy radical reactions on the predicted concentrations of ozone, nitrogenous compounds and radicals. J. Geophys. Res., 101, 21007-21023, 1996.

Kleinman, L. I., Photochemical formation of peroxides in the boundary layer. *J. Geophys. Res.*, *91*,10889-10904, 1986.

Kleinman, L. I., Seasonal dependence of boundary layer peroxide concentration: the low and high NO_X regimes. *J. Geophys. Res.*, 96, 20721-20734, 1991.

Kleinman, L. I., Low and high NO_X tropospheric photochemistry. *J. Geophys. Res.*, 99, 16831-16838, 1994.

Kumar, N., M. T. Odman, and A. G. Russell. Multiscale air quality modeling: Application to southern California. *J. Geophys. Res.*, 99, 5385-5397, 1994.

Lake Michigan Air Directors Consortium (LADCO). Lake Michigan Ozone Study: Evaluation of the UAM-V Photochemical Grid Model in the Lake Michigan Region. Version 2.0. Submitted to U.S. Environmental Protection Agency by Lake Michigan Air Directors Consortium, Des Plaines, IL, September, 1994.

Lamb, B., Westberg, H., Allwine, G. and Quarles, T. (1985) Biogenic hydrocarbon emissions from deciduous and coniferous trees in the United States, *J. Geophys. Res.*, 90, 2380.

Lawson, D. R., The Southern California Air Quality Study. *J. Air. Waste Manage. Assoc.*, 40, 156-165, 1990.

Logan, J. A., Ozone in rural areas of the United States, *J. Geophys. Res.*, **94**, 8511-8532, 1989.

Lu, R. and R. P. Turco. Air pollution transport in a coastal environment: Part II: three-dimensional simulations over the Los Angeles basin. *Atmos. Environ.*, 29, 1499-1518, 1995.

Luke, W. T., and R. R. Dickerson, The flux of reactive nitrogen compounds from eastern North America to the western Atlantic Ocean, *Global Biogeochem. Cycles*, 1, 329-343, 1987.

Lurmann, F. W., Lloyd, A. C., and Atkinson, R. A chemical mechanism for use in long-range transport/acid deposition computer modeling. *J. Geophys. Res.* 91, 10905-10936, 1986.

Madronich, S. Photodissociation in the atmosphere: 1. Actinic flux and the effect of ground reflections and clouds, *J. Geophys. Res.* **92**, 9740-9752, 1987.

Marsik, F. M., K. Fischer, T. D. McDonald and P. J. Samson, 1993: Comparison of methods for estimating mixing height used during the 1992 Atlanta field intensive. *j. Appl. Meteo.*, 34, 1802-1814, 1995.

Matthews, E. Global vegetation and land use: new high-resolution data bases for climate studies. *J. Climate Appl. Meteorol.*, **22**, 474-487, 1983.

McKeen, S. A., E-Y. Hsie, and S. C. Liu, A study of the dependence of rural ozone on ozone precursors in the eastern United States. *J. Geophys. Res.*, **96**, 15377-15394, 1991.

Milford, J. B., Gao, D., Sillman, S., Blossey, P., and Russell, A. G., Total reactive nitrogen (NO_Y) as an indicator for the sensitivity of ozone to NO_X and hydrocarbons. *J. Geophys. Res.*, 99, 3533-3542, 1994.

Milford, J. B., A. G. Russell, and G. J. McRae. A new approach to photochemical pollution control: Implications of spatial patterns in pollutant responses to reductions in nitrogen oxides and reactive organic gas emissions. *Environ. Sci. Tech.*, 23, 1290-1301, 1989.

Morris, R. E. and Myers, T. C., 1990: User's guide for the urban airshed model, Vol. I-V. EPA-450/4-90-007A-E.

National Research Council (NRC), Committee on Tropospheric Ozone Formation and Measurement. *Rethinking the Ozone Problem in Urban and Regional Air Pollution*, National Academy Press, 1991.

Ozone Transport and Assessment Group (OTAG). Summary of Basecase A OTAG UAM-V modeling: BEIS1 and BEIS2. Presented at the OTAG Regional and Urban Scale Modeling Workgroup meeting, May 2, 1996.

Parrish, D. D., M. Trainer, M. P. Buhr, B. A. Watkins, and F. C. Fehsenfeld. Carbon Monoxide concentrations and their relation to concentrations of total reactive oxidized nitrogen at two rural U.S. sites. *J. Geophys. Res.*, 96, 9309-9320, 1991.

Parrish, D. D., M. P. Buhr, M. Trainer, R. B. Norton, J. P. Shimshock, F. C. Fehsenfeld, K. G. Anlauf, J. W. Bottenheim, Y. Z. Tang, H. A. Wiebe, J. M. Roberts, R. L. Tanner, L. Newman, V. C. Bowersox, K. J. Olszyna, E. M. Bailey, M. O. Rodgers, T. Want, H. Berresheim, U. K. Roychowdhury, and K. L. Demerjian, The total reactive oxidized nitrogen levels and the partitioning between individual species at six rural sites in eastern North America. *J. Geophys. Res.*, 98, 2927-2939, 1993.

Paulson, S. E. and J. H. Seinfeld. Development and evaluation of a photooxidation mechanism for isoprene. *J. Geophys. Res.*, 97, 20703-20715, 1992.

Pierce, T. E., B. K. Lamb and A. R. Van Meter, 1990: Development of a biogenic emissions inventory system for regional scale air pollution models. Presented at the 83rd Air and Waste Management Association Annual Meeting, Pittsburgh, PA, Paper No. 90-94.3, June 24-29, 1990.

Prather, M. J., Numerical advection by conservation of second-order moments, *J. Geophys Res.*, *91*, 6671-6681, 1986.

Rao, S. T. and G. Sistla, Efficacy of nitrogen oxides and hydrocarbon emissions controls in ozone attainment strategies as predicted by the Urban Airshed Model. *Water Air Soil Pollut.*, 67, 95-116, 1993.

Ridley, B. A., S. Madronich, R. B. Chatfield, J. G. Walega, R. E. Shetter, M. A. Carroll, and D. D. Montzka, Measurements and model simulations of the photostationary state during the Mauna Loa Observatory Photochemistry Experiment: Implications for radical concentrations and ozone production and loss rates. *J. Geophys. Res., 97*, 10375-10388, 1992.

Roberts, J. M., R. L. Tanner L.Newman, V. C. Bowersox J. W. Bottenheim, K. G. Anlauf, K. A. Brice, D. D. Parrish, F. C. Fehsenfeld, M. P. Buhr, J. F. Meagher, and E. M. Bailey, Relationships between PAN and ozone at sites in eastern North America. *J. Geophys. Res.*, 100, 22821-22830, 1995.

Roselle, S. J. and K. L. Schere. Modeled response of photochemical oxidants to systematic reductions in anthropogenic volatile organic compound and NOx emissions. *J. Geophys. Res.*, 100, 22929-22941, 1995.

Sillman, S., Logan, J. A. and Wofsy, S. C. The sensitivity of ozone to nitrogen oxides and hydrocarbons in regional ozone episodes. *J. Geophys. Res.*, 95, 1837-1851, 1990a.

Sillman, S., Logan, J. A. and Wofsy, S. C. A regional-scale model for ozone in the United States with a sub-grid representation of urban and power plant plumes, *J. Geophys. Res*, 95, 5731-5748, 1990b.

Sillman, S., P. J. Samson and J. M. Masters, Ozone production in urban plumes transported over water: photochemical model and case studies in the northeastern and midwestern U.S. *J. Geophys. Res.*, 98, 12687-12699, 1993.

Sillman, S., The use of NO_y, H_2O_2 and HNO_3 as indicators for ozone-NO_X-ROG sensitivity in urban locations. *J. Geophys. Res.*, 100, 14175-14188, 1995a.

Sillman, S. and Samson, P. J., The impact of temperature on oxidant formation in urban, polluted rural and remote environments. *J. Geophys. Res.*, 100, 11497-11508, 1995b.

Sillman, S., K. Al-Wali, F. J. Marsik, P. Nowatski, P. J. Samson, M. O. Rodgers, L. J. Garland, J. E. Martinez, C. Stoneking, R. E. Imhoff, J-H. Lee, J. B. Weinstein-Lloyd, L. Newman and V. Aneja. Photochemistry of ozone formation in Atlanta, GA: models and measurements. *Atmos. Environ.*, 29, 3055-3066, 1995c.

Sillman, S., D-Y. He, C. Cardelino and R. E. Imhoff, The use of photochemical indicators to evaluate ozone-NO_X-hydrocarbon sensitivity: case studies from Atlanta, New York and Los Angeles. *J. Air Waste Manage. Assoc.*, 47, 1030-1040, 1997a.

Sillman, S., D. He, M. Pippin, P. Daum, L. Kleinman, J. H. Lee and J. Weinstein-Lloyd. Model correlations for ozone, reactive nitrogen and peroxides for Nashville in comparison with measurements: implications for VOC-NOx sensitivity. Submitted to *J. Geophys. Res.*, upcoming special section on the Middle Tennessee Ozone Study, 1997b.

Sillman, S., Review Article: The Relation between Ozone, NO_X and Hydrocarbons in Urban and Polluted Rural Environments. Submitted to *J. Geophys. Res.*, upcoming special section on the Middle Tennessee Ozone Study, 1997c.

Smolarkiewicz, P. K. A simple positive definite advection scheme with small implicit diffusion, *Mon. Wea. Rev.*,111, 479-486, 1983.

Staffelbach, T., A. Neftel, A. Blatter, A. Gut, M. Fahrni, J. Stahelin A. Prevot, A. Hering, M. Lehning, B. Neininger, M. Baumie, G. L. Ko, J. Dommen, M. Hutterli and M. Anklin. Photochemical oxidant formation over southern Switzerland, part I: Results from summer, 1994. *J. Geophys. Res.*, in press, 1997a.

Staffelbach, T., A. Neftel and L. W. Horowitz. Photochemical oxidant formation over southern Switzerland, part II: model results. *J. Geophys. Res.*, in press, 1997b.

Trainer, M., D. D. Parrish, M. P. Buhr, R. B. Norton, F. C. Fehsenfeld, K. G. Anlauf, J. W. Bottenheim, Y.Z. Tang, H.A. Wiebe, J.M. Roberts, R.L. Tanner, L. Newman, V.C. Bowersox, J.M. Maugher, K.J. Olszyna, M.O. Rodgers, T. Wang, H. Berresheim, and K. Demerjian, 1993: Correlation of ozone with NO_y in photochemically aged air. *J. Geophys. Res.*, 98, 2917-2926.

Tuazon, E. C., A. M. Winer, and J. N. Pitts, Jr. Trace pollutant concentrations in a multiday smog episode in the California south coast air basin by long path length Fourier Transform Infrafred Spectroscoy. *Environ. Sci. Technol.*, 15, 1232-1237, 1981.

Wagner, K. W., N. J. M. Wheeler and D. L. McNerny, 1992: The effect of emission inventory uncertainty on Urban Airshed Model sensitivity to emission reductions. Presented at the Air and Waste Management Association International Specialty Conference, "Tropospheric Ozone: Nonattainment and Design Value Issues", Boston, October, 1992.

Wheeler, N. J. M., and K. K. Wagner, *SCAQS Modeling Project Documentation.* Technical Support Division Report, California Air Resources Board, Sacramento, 1992.

White, W. H., D. E. Patterson and W. E. Wilson, Jr. Urban exports to the nonurban troposphere: results from project MISTT. *J. Geophys. Res.*, 88, 10745-10752, 1983.

Ulrickson, B. L. and C. F. Mass, Numerical investigation of mesoscale circulations over the Los Angeles basin. Part I: a verification study. *Mon. Wea. Rev.*, 118, 2138-2161, 1990.

APPENDIX:
ADDITIONAL PLOTS OF NO_X-ROG SENSITIVITY vs. PHOTOCHEMICAL INDICATORS

The appendix shows correlations between NO_X-ROG sensitivity and photochemical indicators for the complete set of model results. Each figure shows the predicted reduction in O3 for the specified hour (usually 3-6 pm) resulting from a 35% reduction in anthropogenic ROG emissions (crosses) and from a 35% reduction in NO_X emissions (circles) at each location in the model domain. The simulated ozone reductions are plotted vs. the simulated value for the specified indicator ratio in the initial model scenario (without emission reductions) at the same time and location. Simulations are described in Section 3.1.

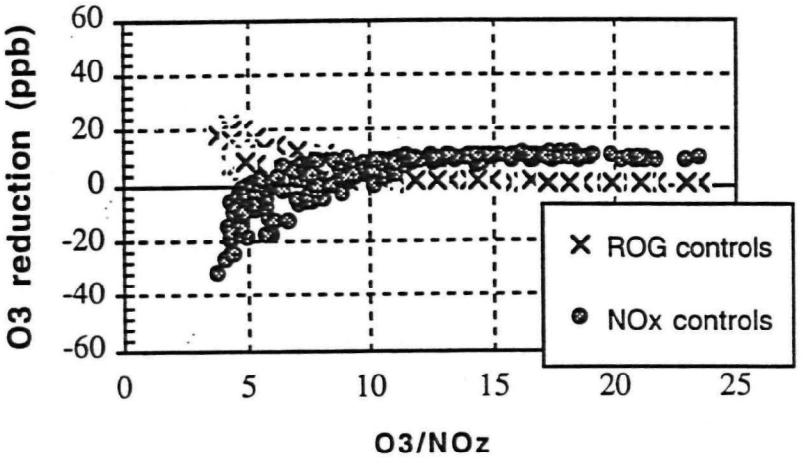

Lake Michigan, ROG reduced by half - O3/NOz

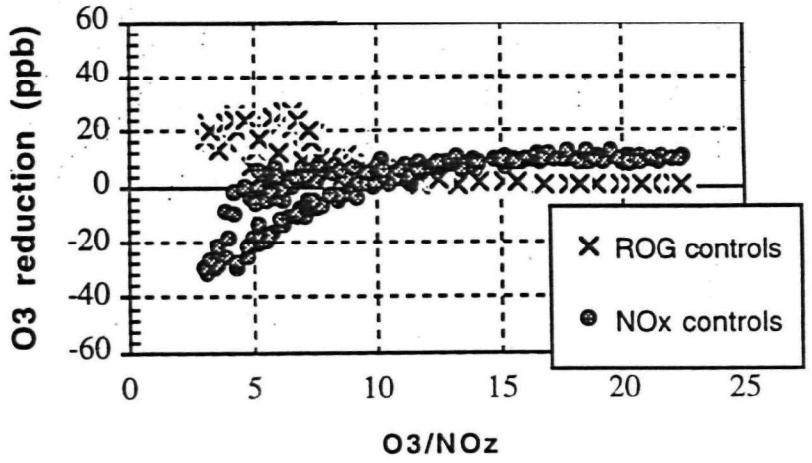

Lake Michigan, base case at noon - O3/NOz

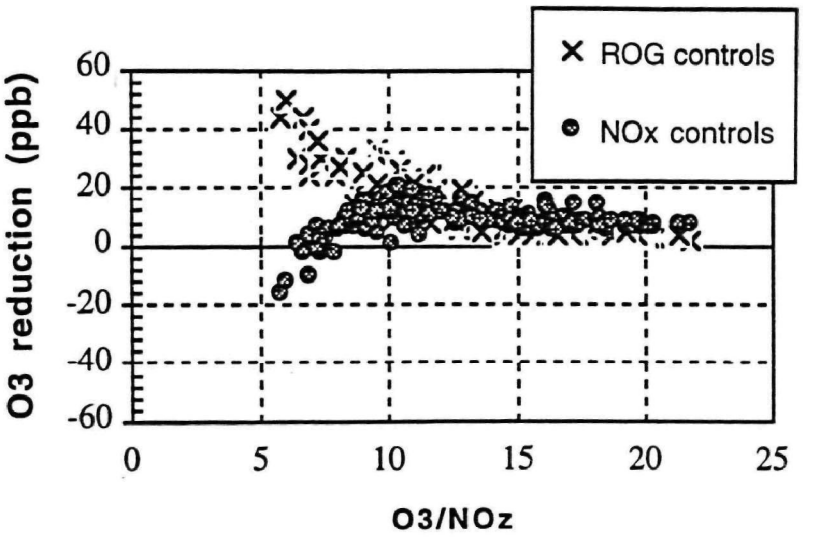

Northeast corridor, zero isoprene - O3/NOz

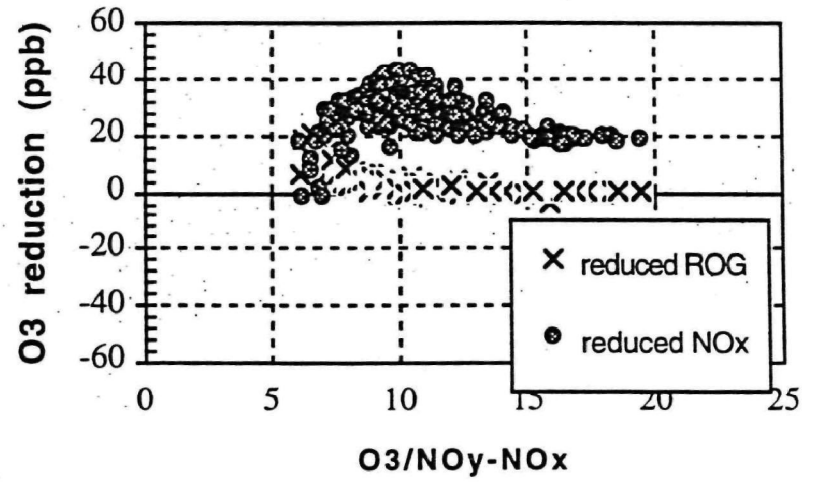

Northeast corridor, doubled isoprene: O3/NOz

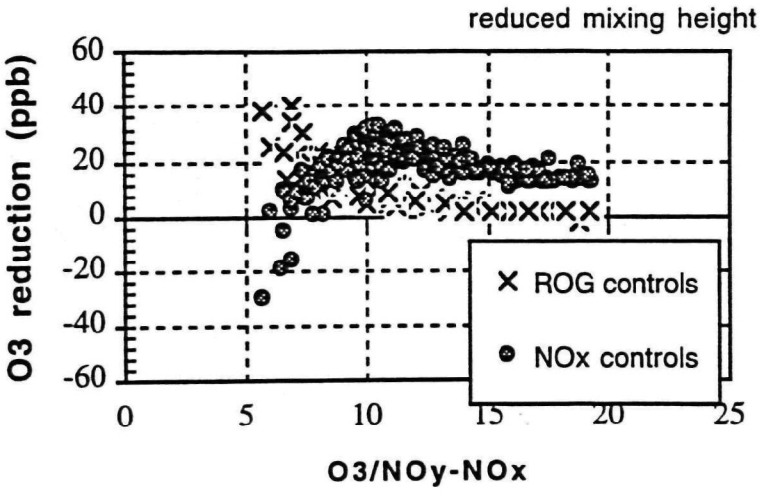

Northeast corridor, low mixing: O3/NOz

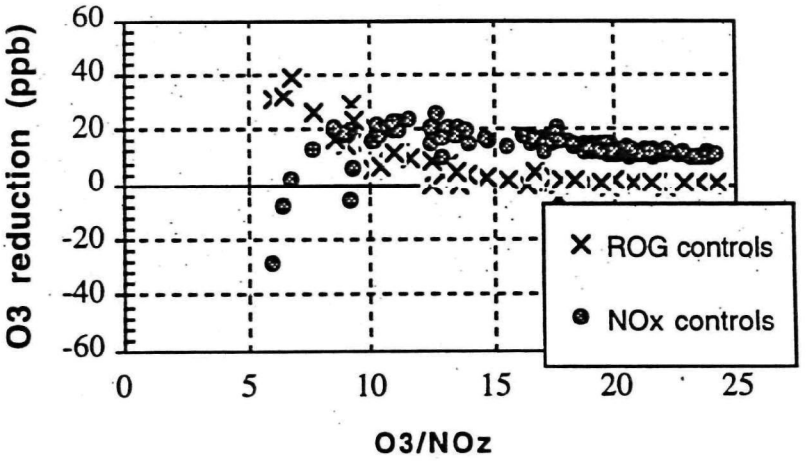

Northeast corridor, light winds and high deposition: O3/NOz

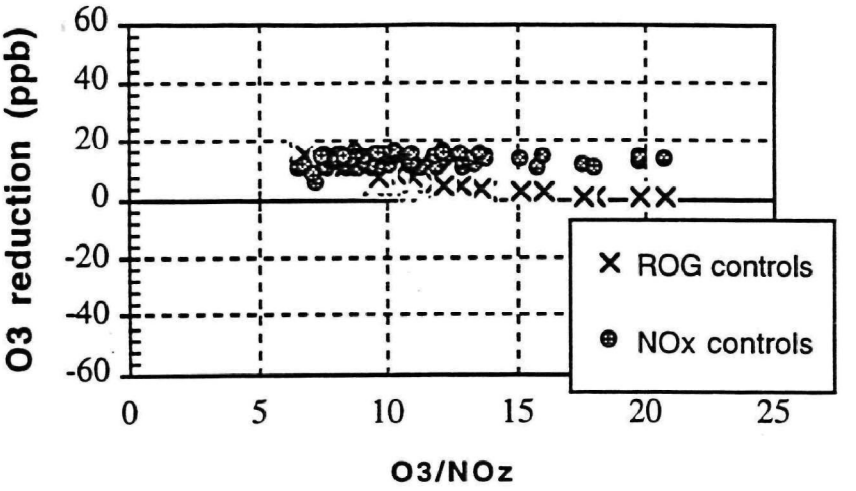

New York, DWM-5 meteorology: O3/NOz

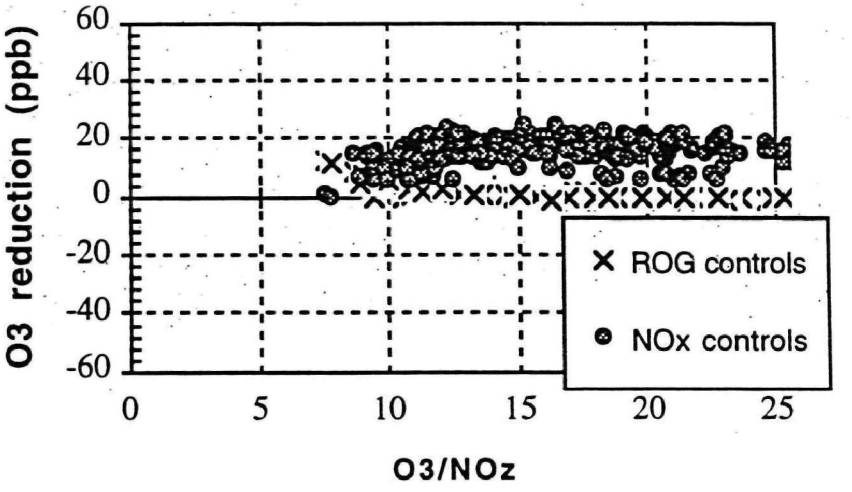

Atlanta, increased isoprene: O3/NOz

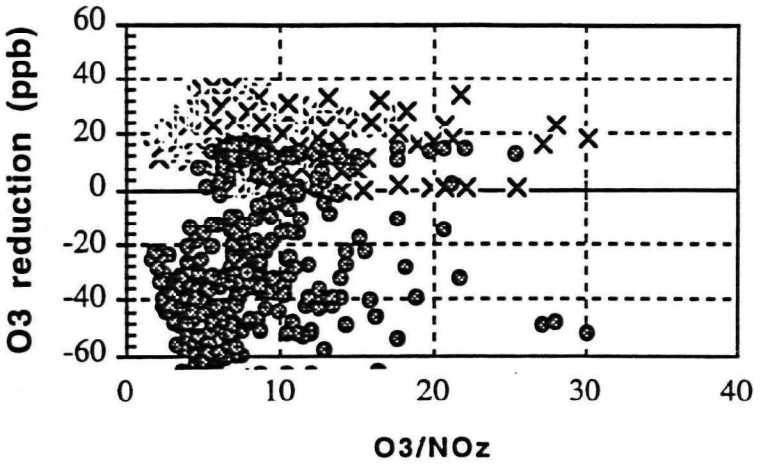

Los Angeles, Wagner base case: O3/NOz

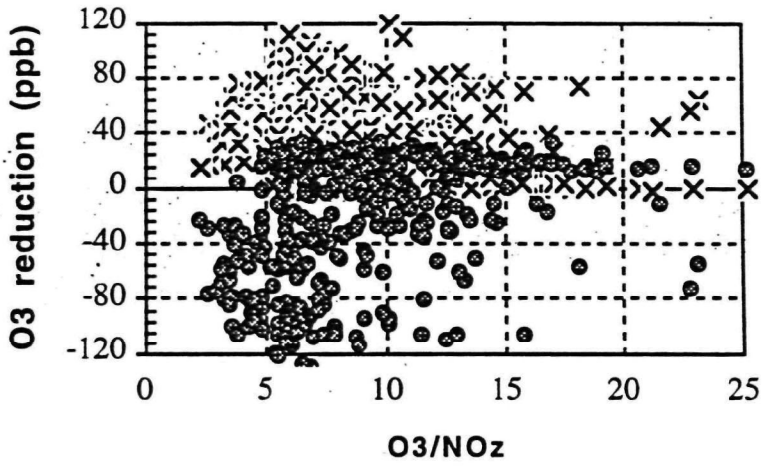

Los Angeles, Wagner with doubled ROG: O3/NOz

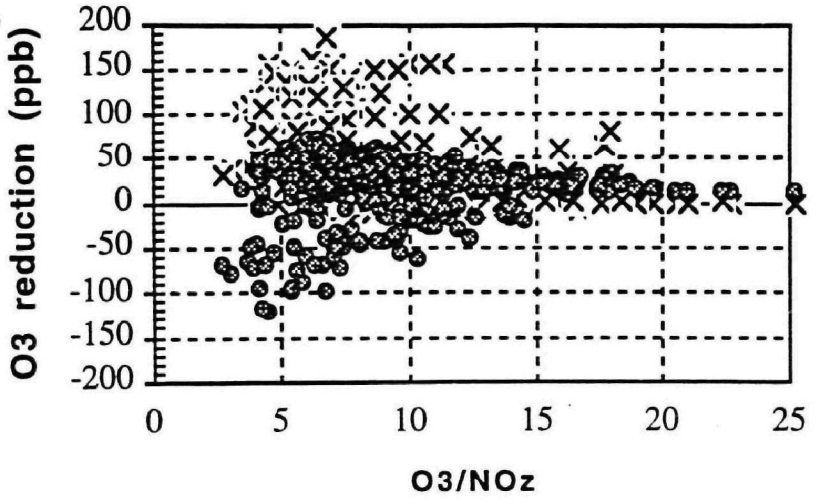

Los Angeles, Wagner with tripled ROG: O3/NOz

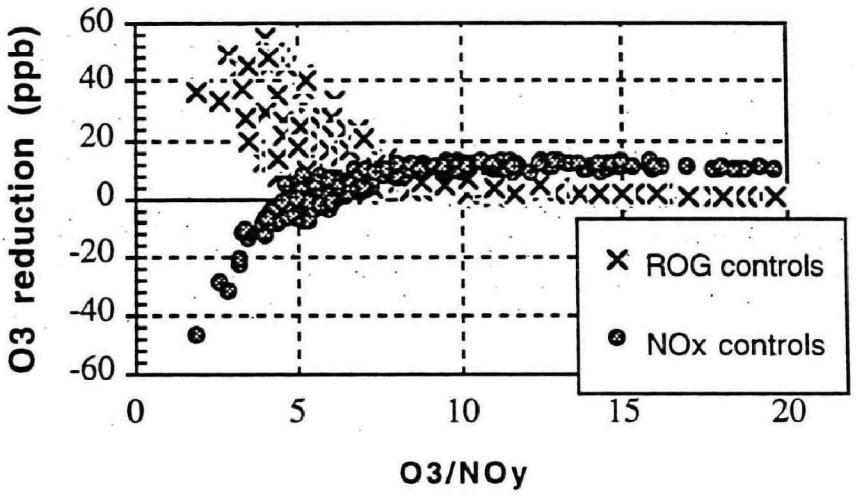

Lake Michigan base case O3/NOy

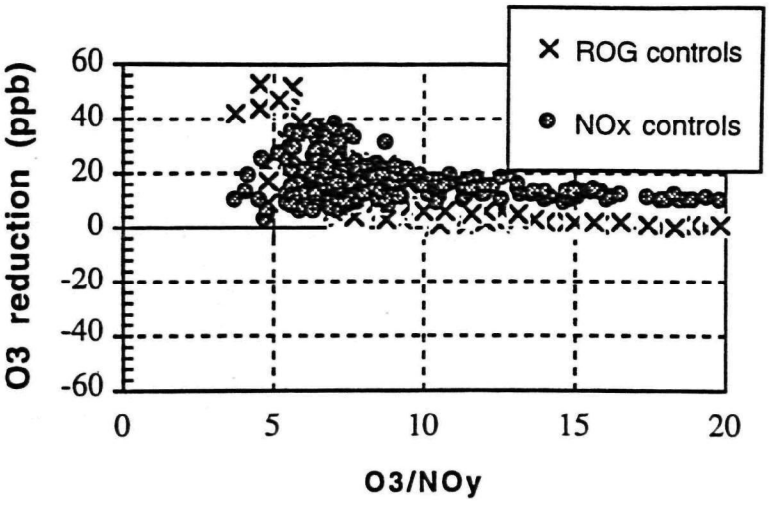

Lake Michigan, doubled ROG emissions: O3/NOy

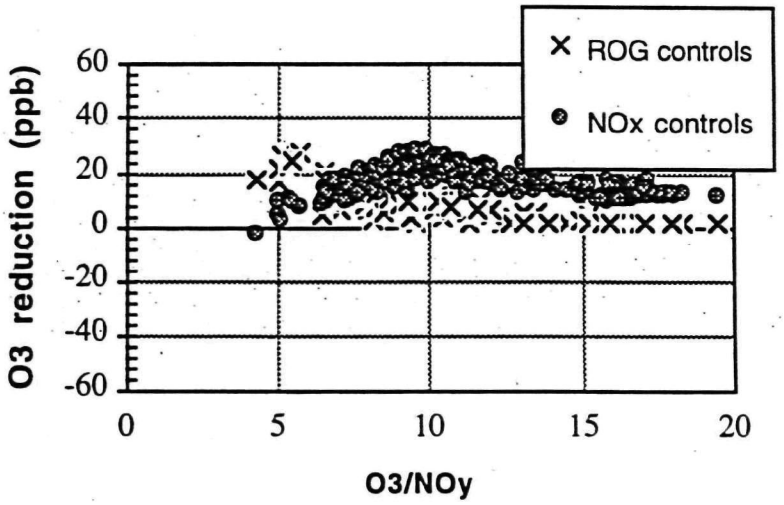

Northeast corridor base case O3/NOy

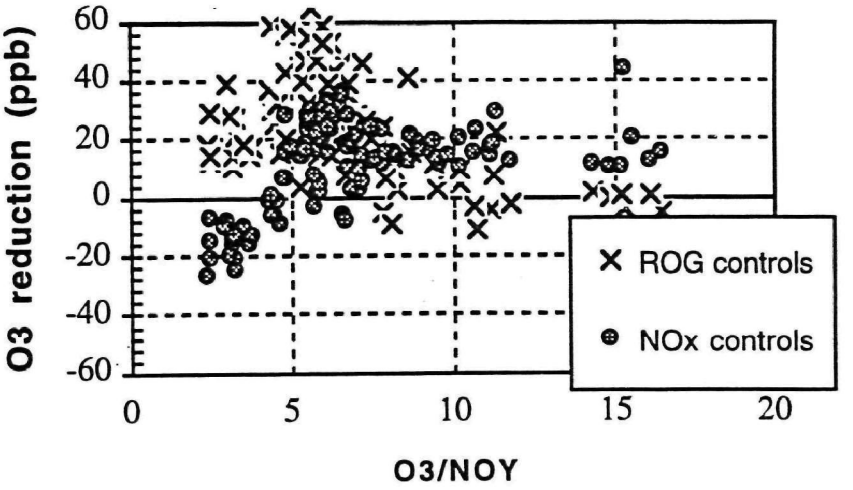

New York with MM7 meteorology: O3/NOy

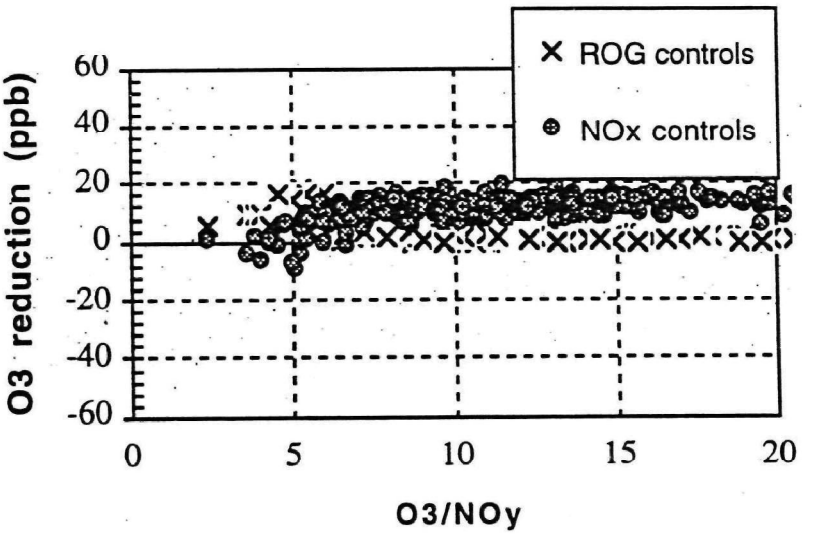

Atlanta, BEIS1 biogenics: O3/NOy

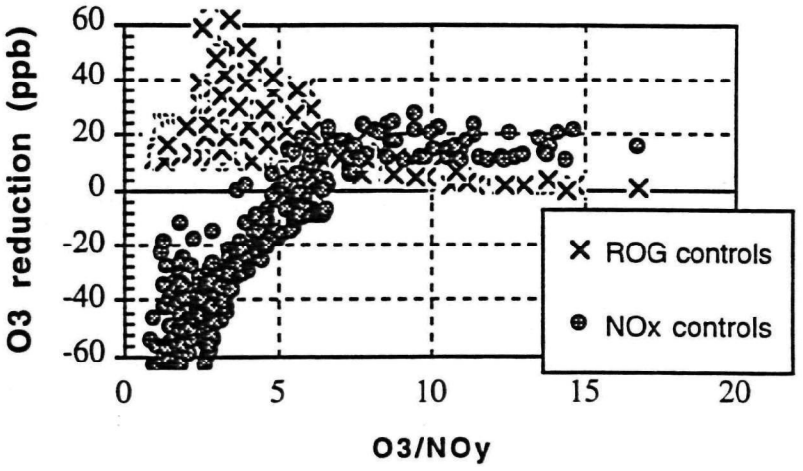

Los Angeles (Godowitch): O3/NOy

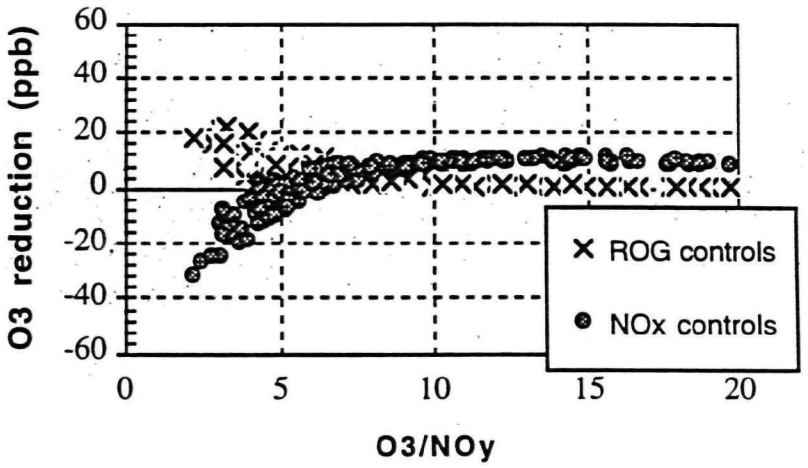

Lake Michigan, ROG reduced by half - O3/NOy

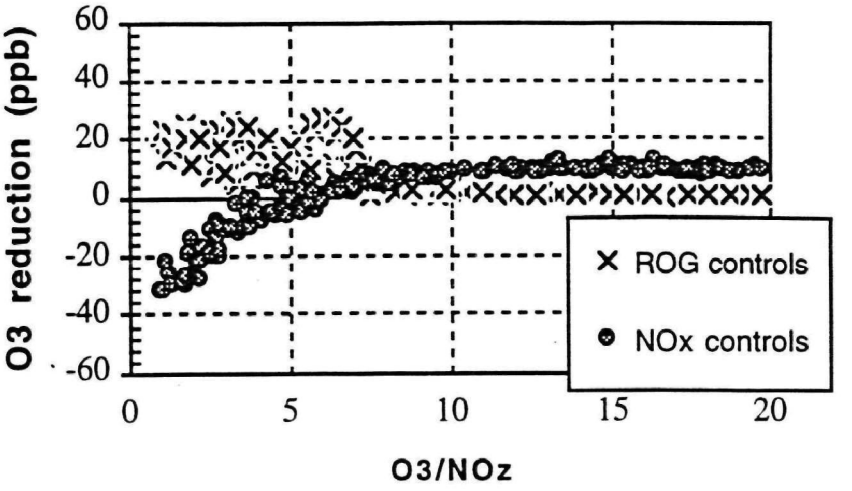

Lake Michigan, base case at noon - O3/NOy

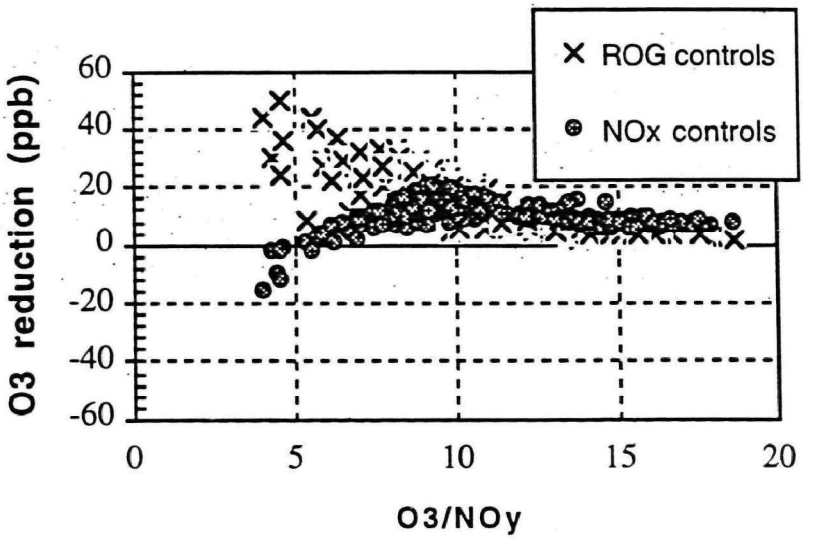

Northeast corridor with zero isoprene - O3/NOy

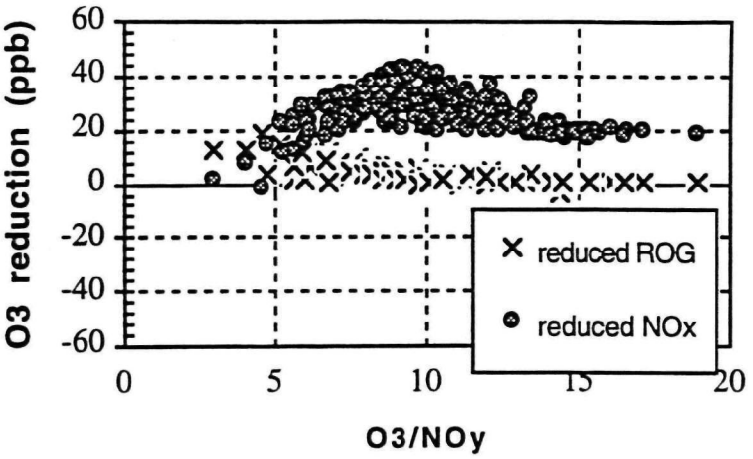

Northeast corridor, low mixing and doubled isoprene: O3/NOy

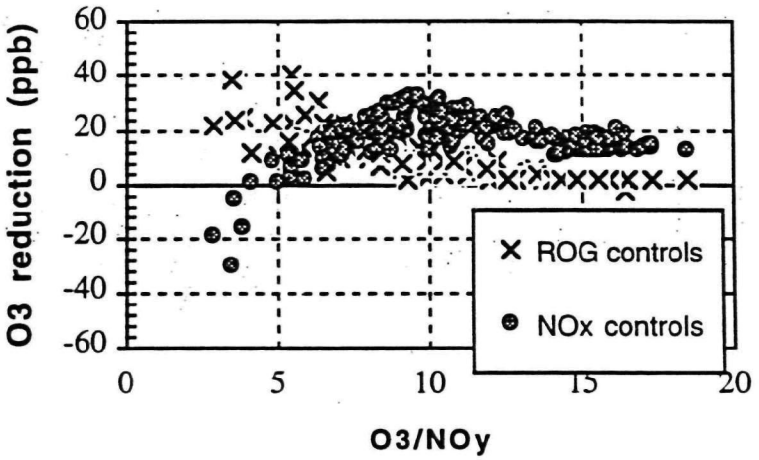

Northeast corridor, low mixing: O3/NOy

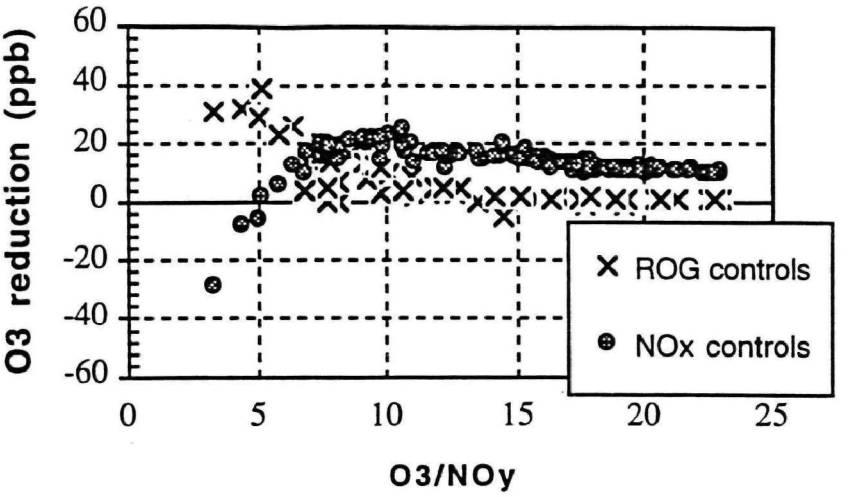

Northeast corridor, light winds and high deposition: O3/NOy

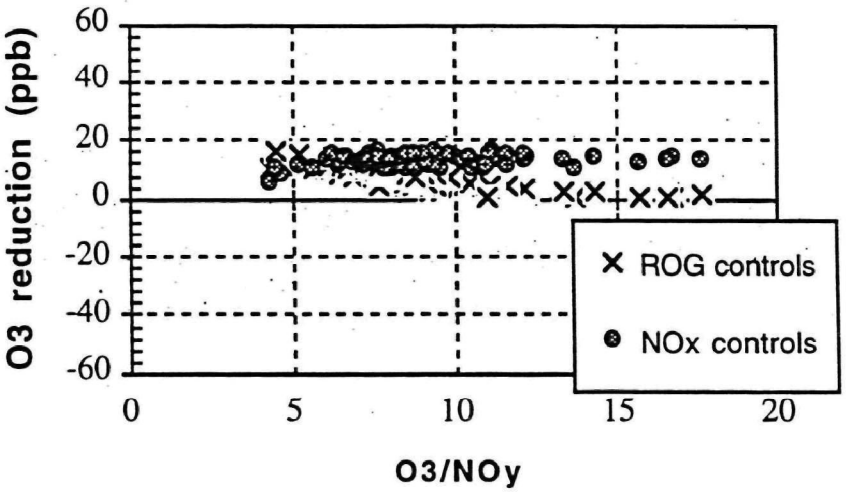

New York DWM-5 meteorology: O3/NOy

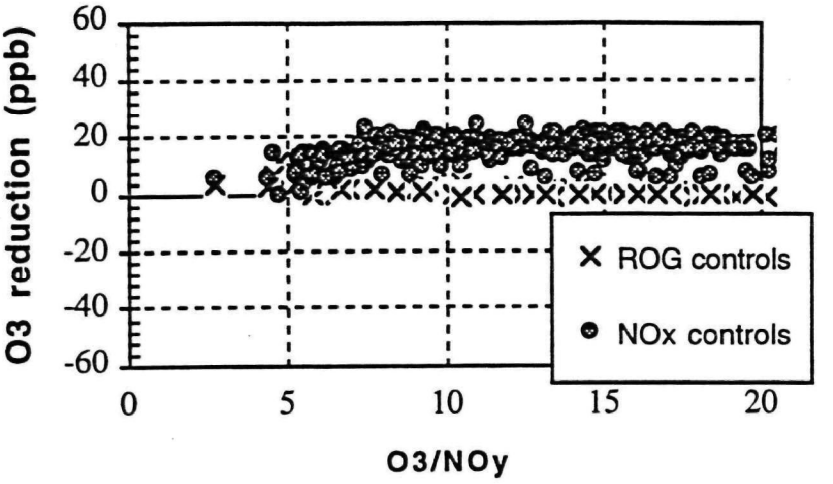

Atlanta, increased biogenis: O3/NOy

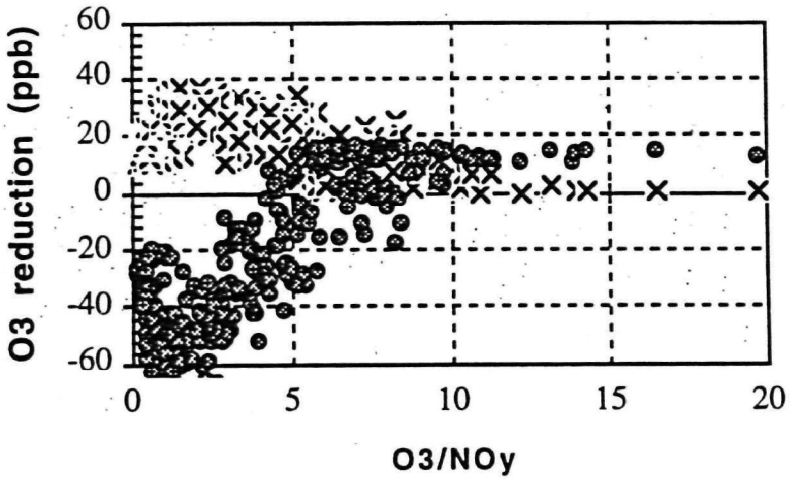

Los Angeles, Wagner base case: O3/NOy

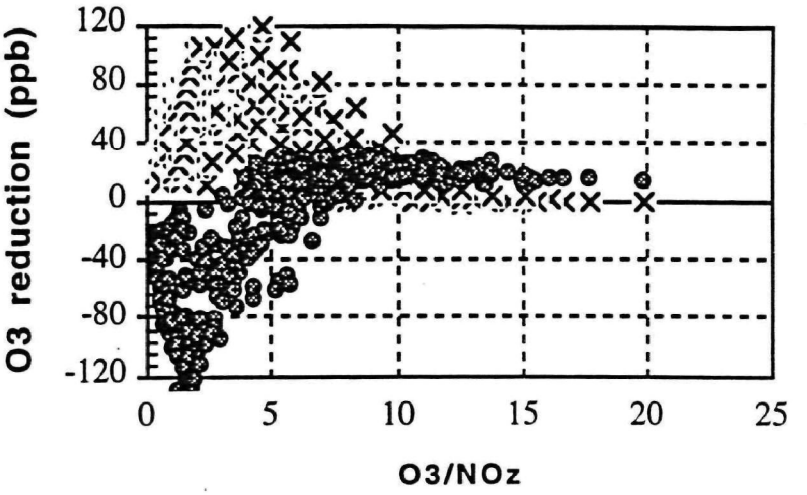

Los Angeles, Wagner with doubled ROG: O3/NOY

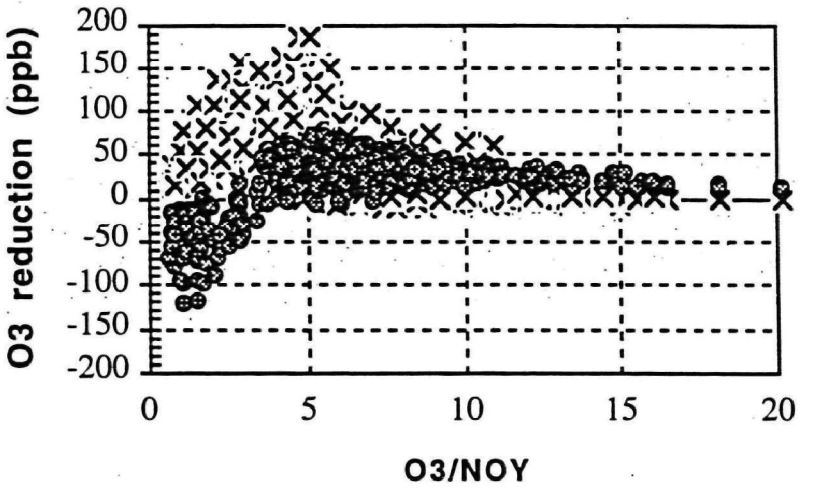

Los Angeles, Wagner with tripled ROG: O3/NOy

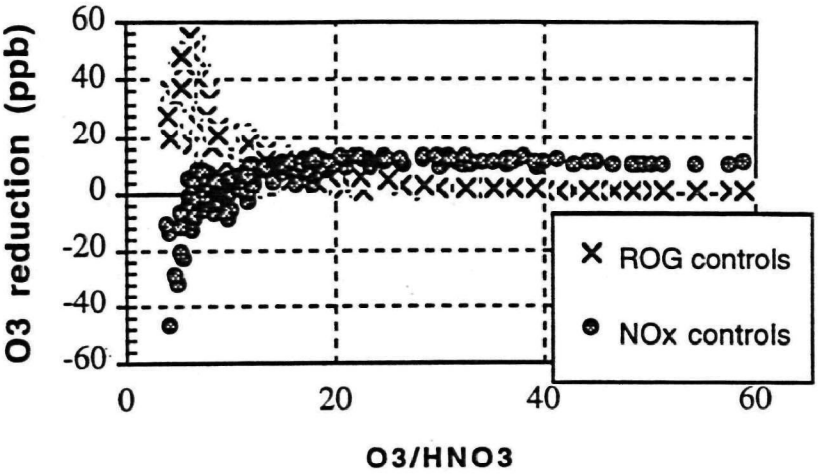

Lake Michigan base case: O3/HNO3

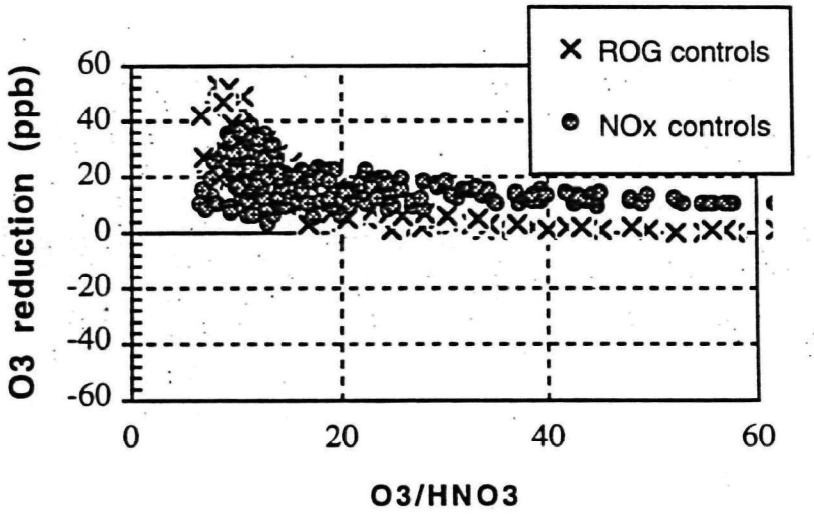

Lake Michigan, doubled ROG emissions: O3/HNO3

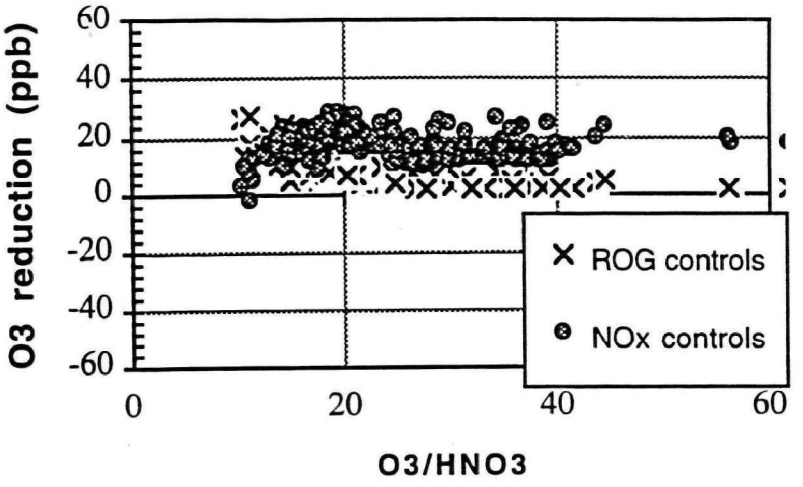

Northeast corridor base case: O3/HNO3

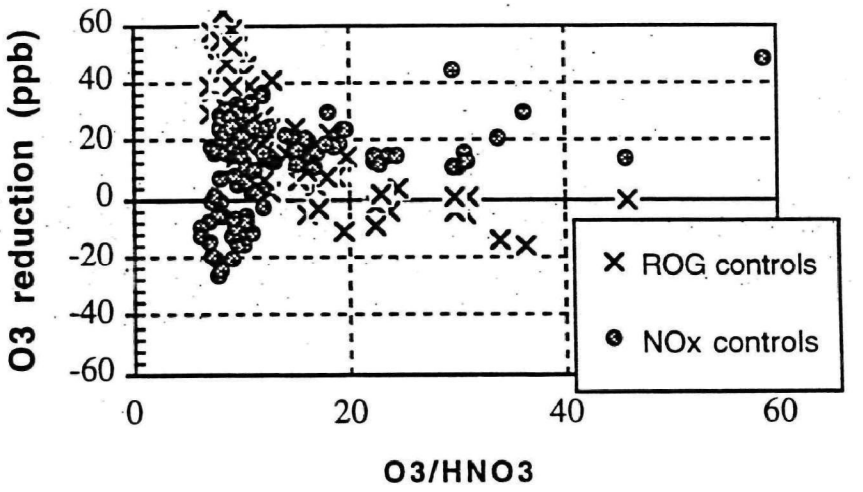

New York with MM7 meteorology: O3/HNO3

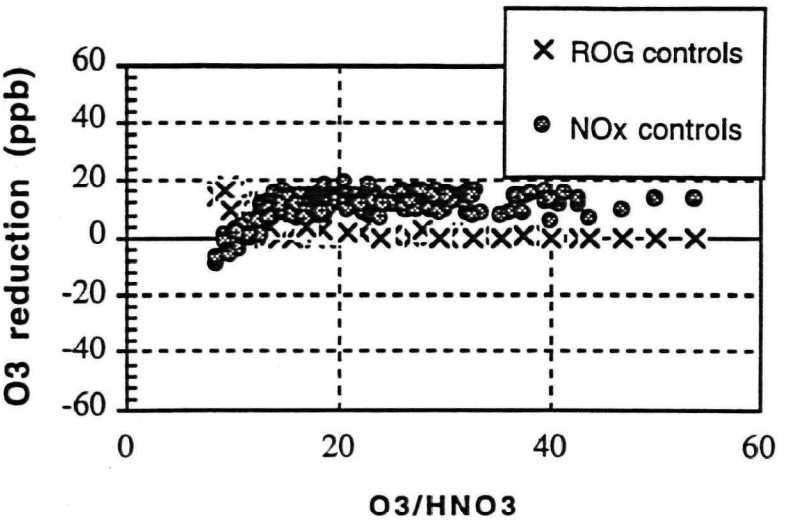

Atlanta, BEIS1 biogenics: O3/HNO3

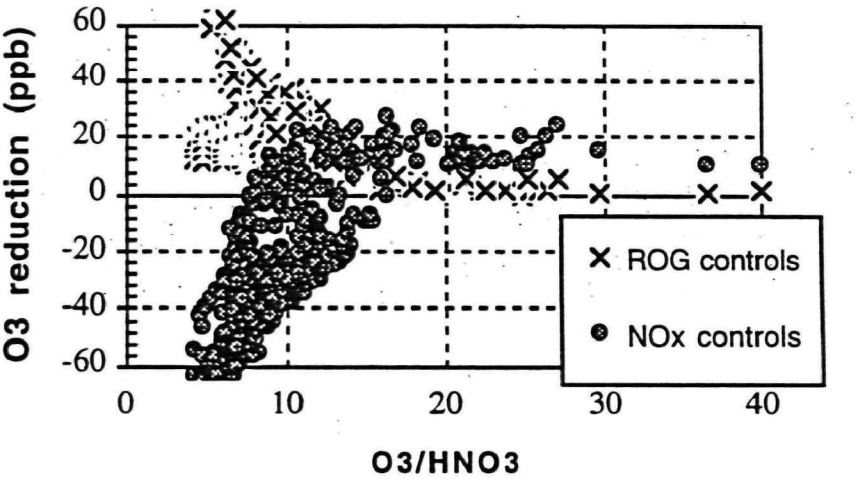

Los Angeles (Godowitch): O3/HNO3

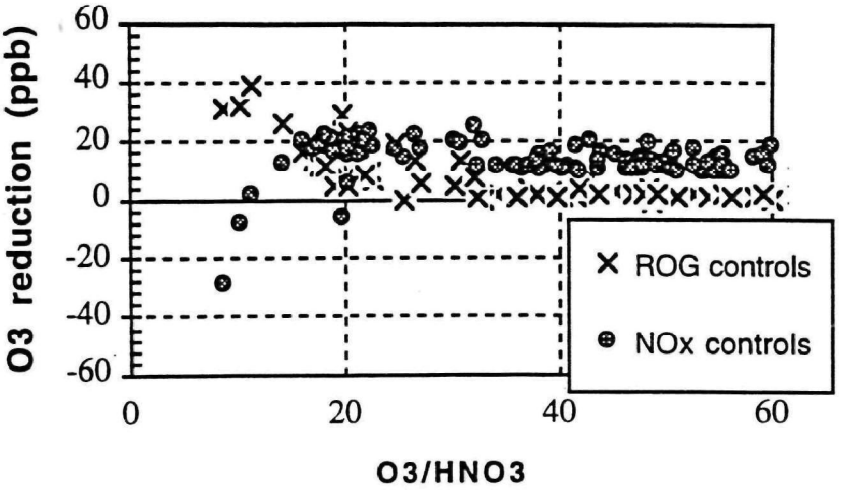

Northeast corridor, light winds and high deposition: O3/HNO3

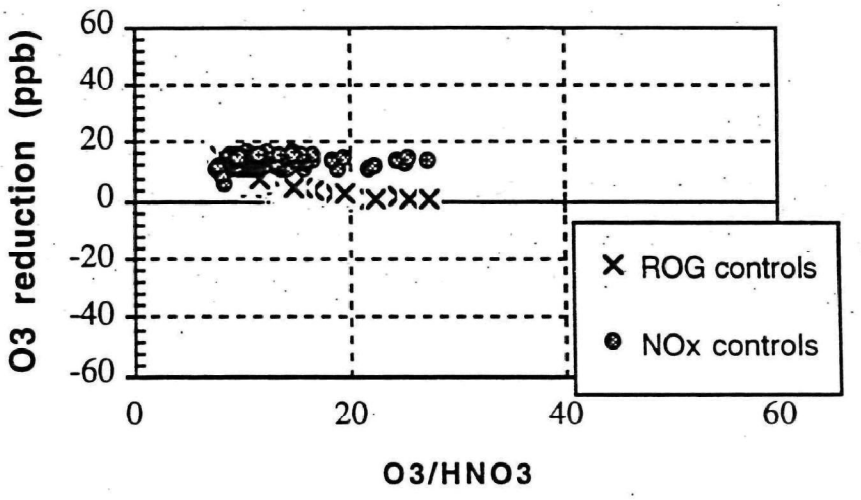

New York, DWM-5 meteorology: O3/HNO3

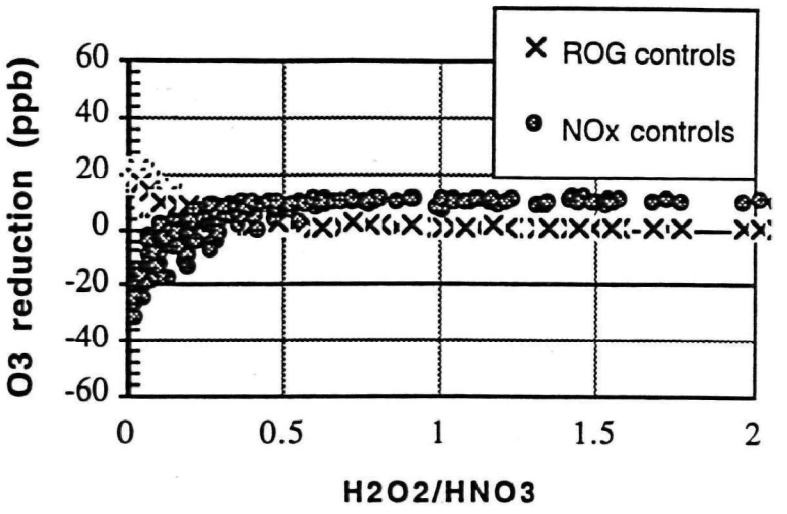

Lake Michigan, ROG reduced by half: H2O2/HNO3

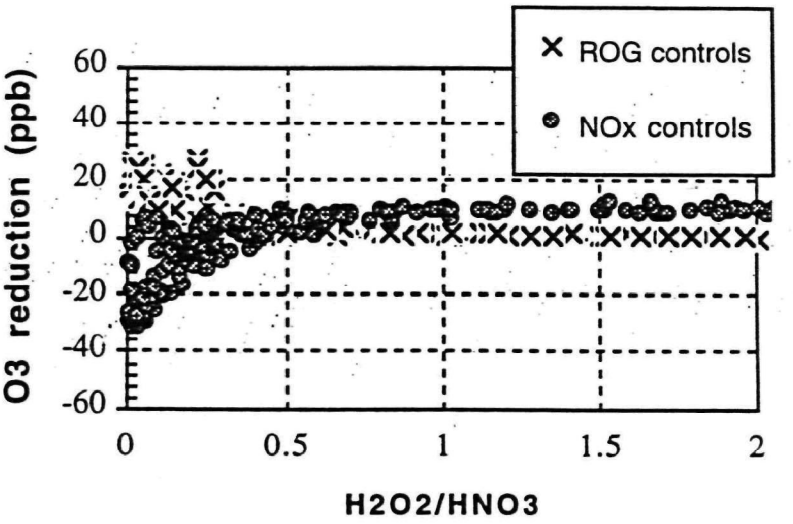

Lake Michigan, base case at noon: H2O2/HNO3

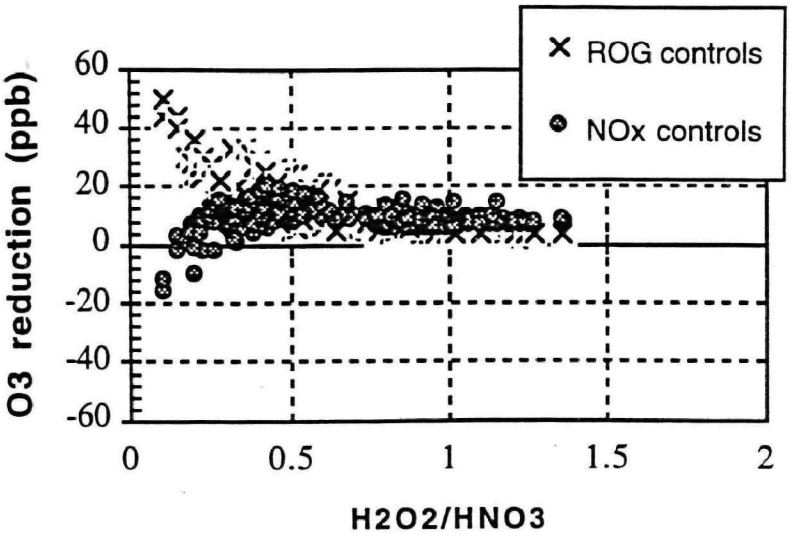

Northeast corridor with zero isoprene: H2O2/HNO3

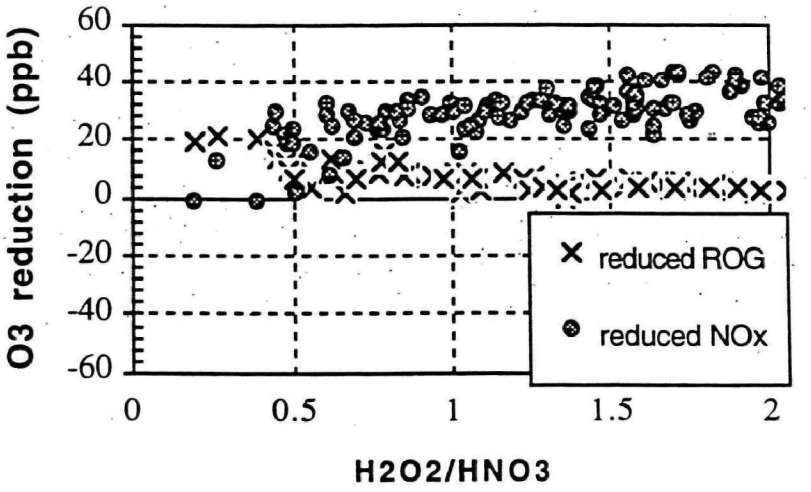

Northeast corridor, low mixing and doubled isoprene: H2O2/HNO3

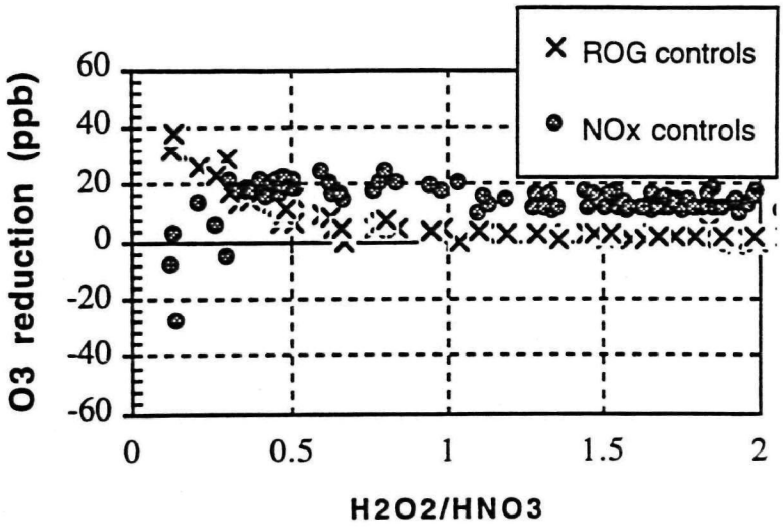

Northeast corridor, light winds: H2O2/HNO3

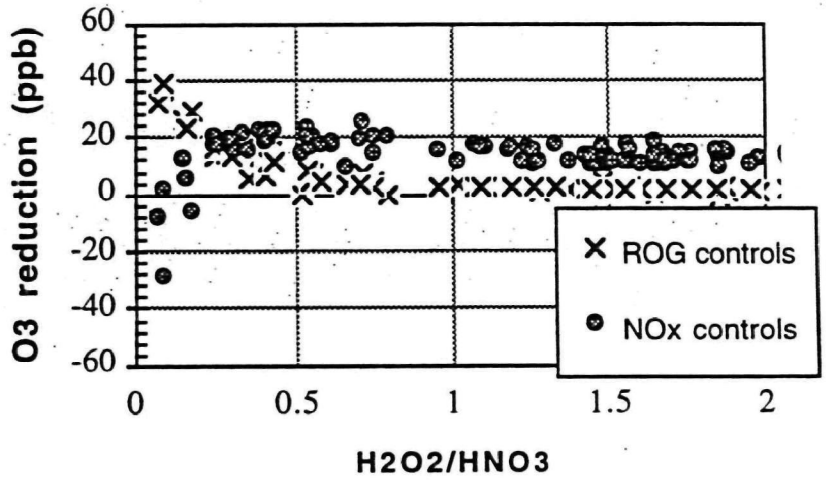

Northeast corridor, light winds and high deposition: H2O2/HNO3

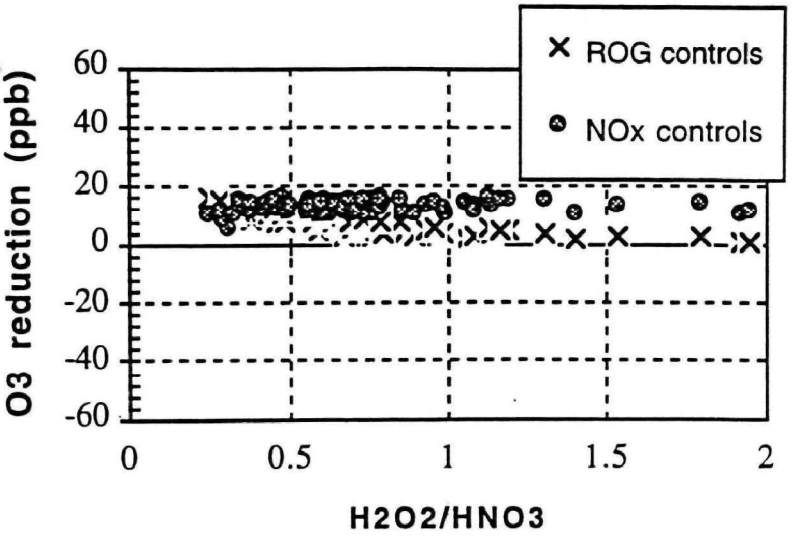

New York DWM-5 meteorology: H2O2/HNO3

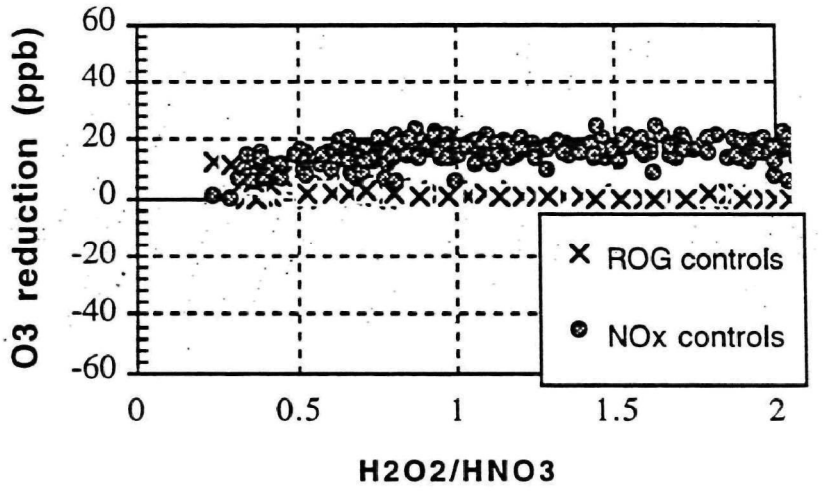

Atlanta, increased biogenics: H2O2/HNO3

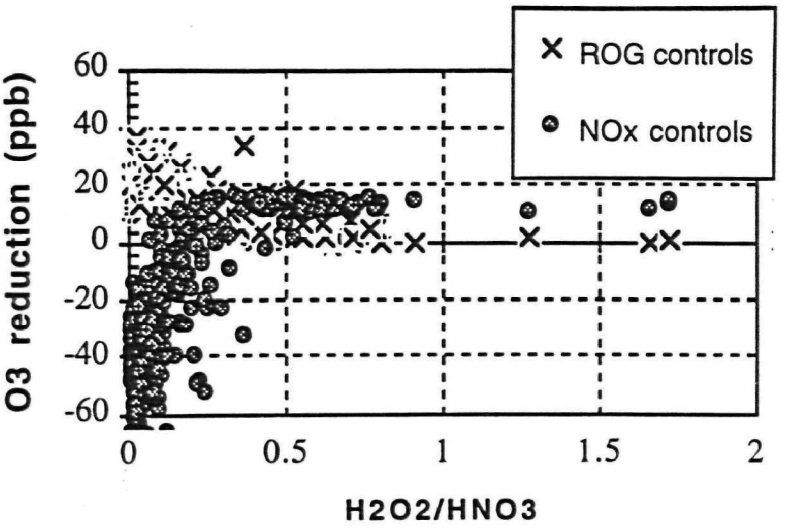

Los Angeles, Wagner base case: H2O2/HNO3

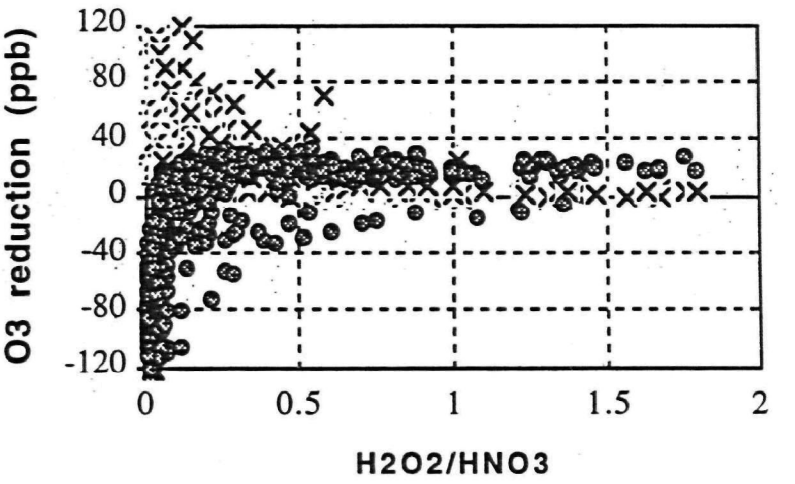

Los Angeles, Wagner with doubled ROG: H2O2/HNO3

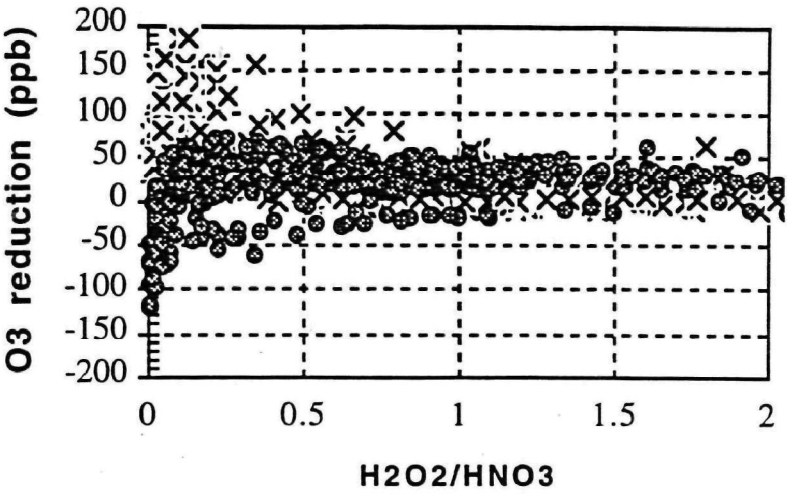

Los Angeles, Wagner with tripled ROG: H2O2/HNO3

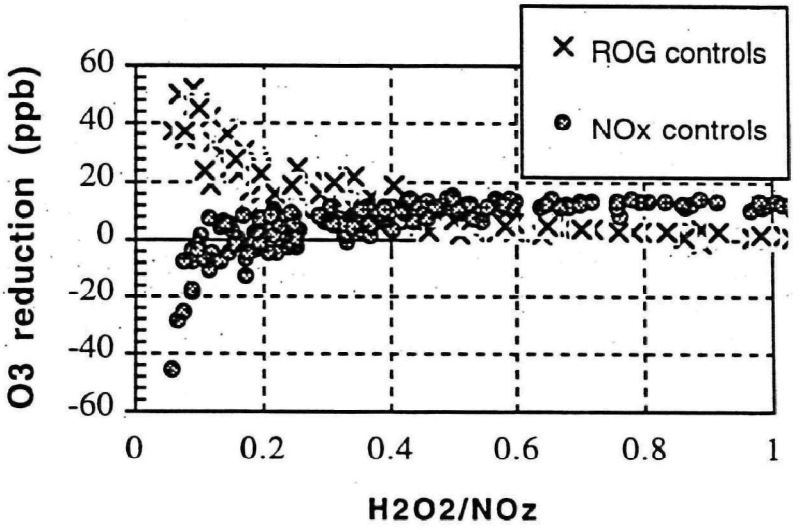

Lake Michigan base case H2O2/NOz

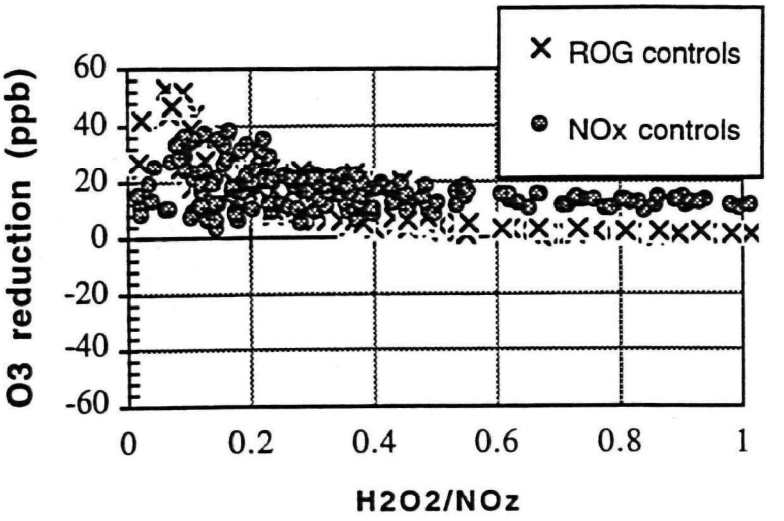

Lake Michigan, doubled ROG emissions: H2O2/NOz

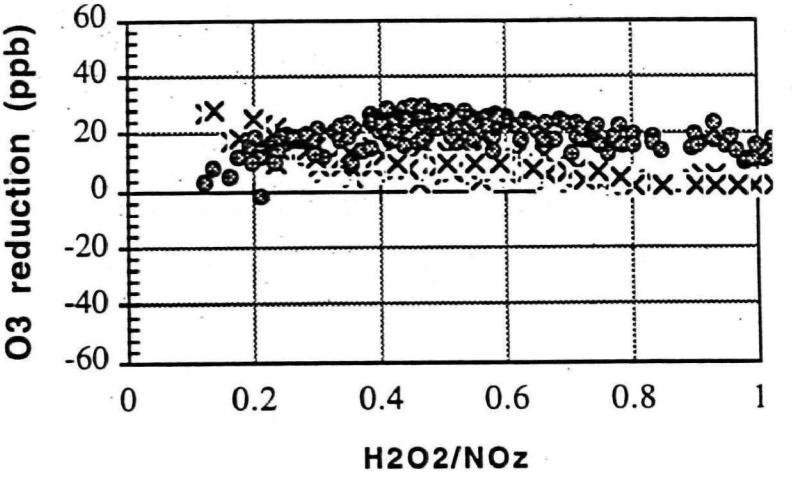

Northeast corridor base case, H2O2/NOz

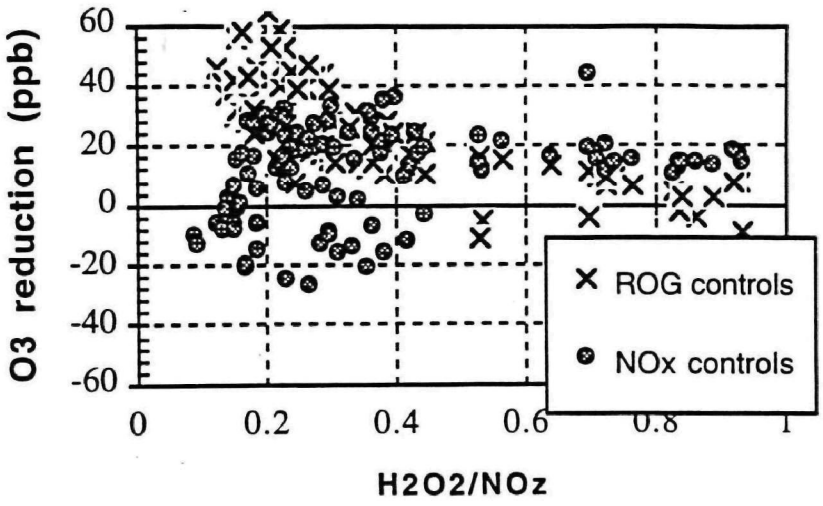

New York MM7: H2O2/NOz

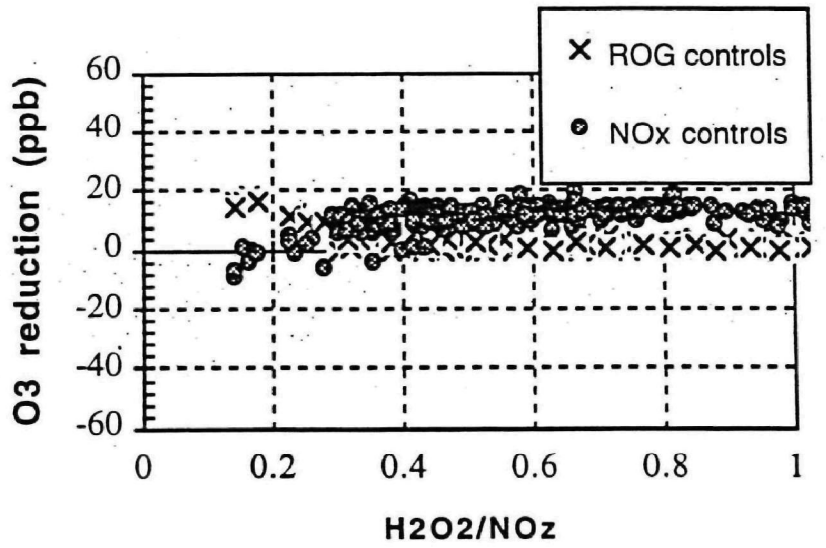

Atlanta, BEIS1 biogenics - H2O2/NOz

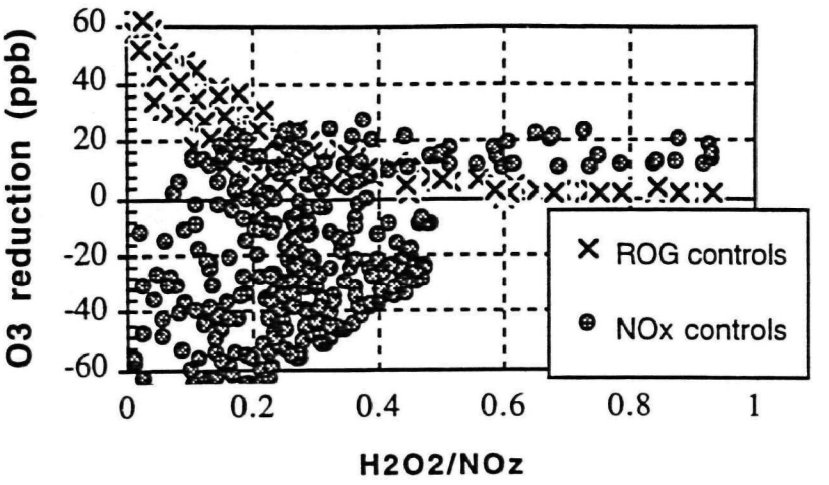

Los Angeles (Godowitch): H2O2/NOz

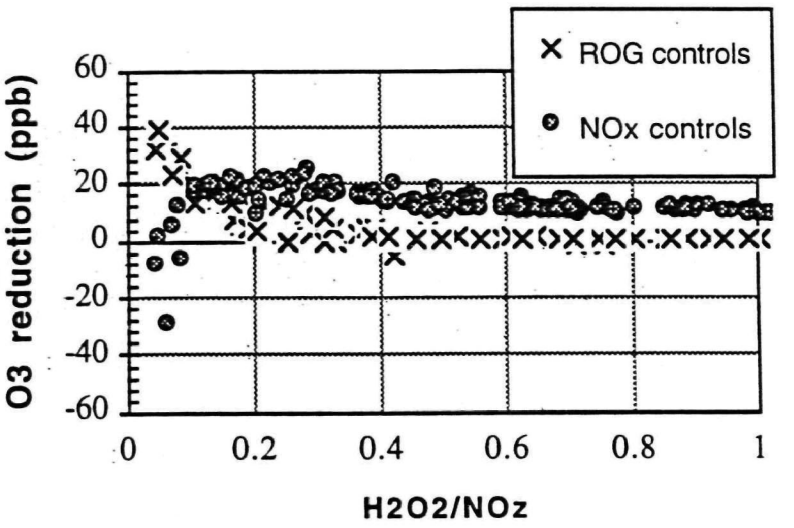

Northeast corridor, light winds and high deposition, H2O2/NOz

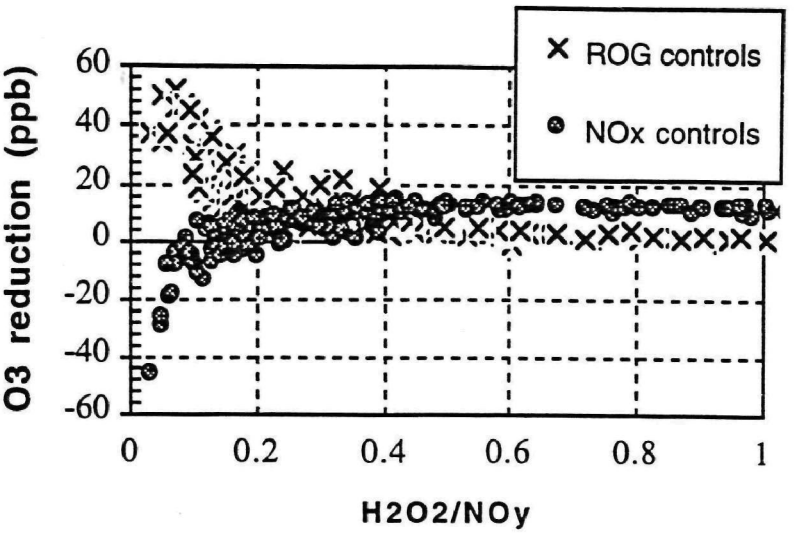

Lake Michigan base case H2O2/NOy

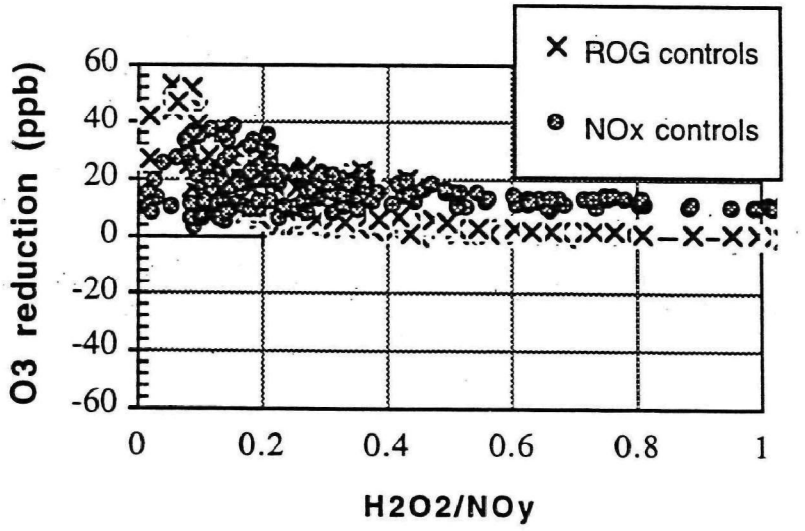

Lake Michigan, doubled ROG: H2O2/NOy

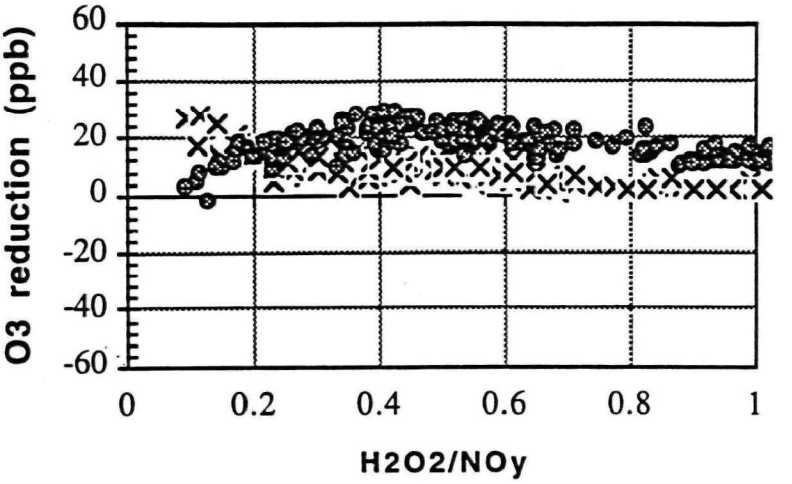

Northeast corridor base case H2O2/NOy

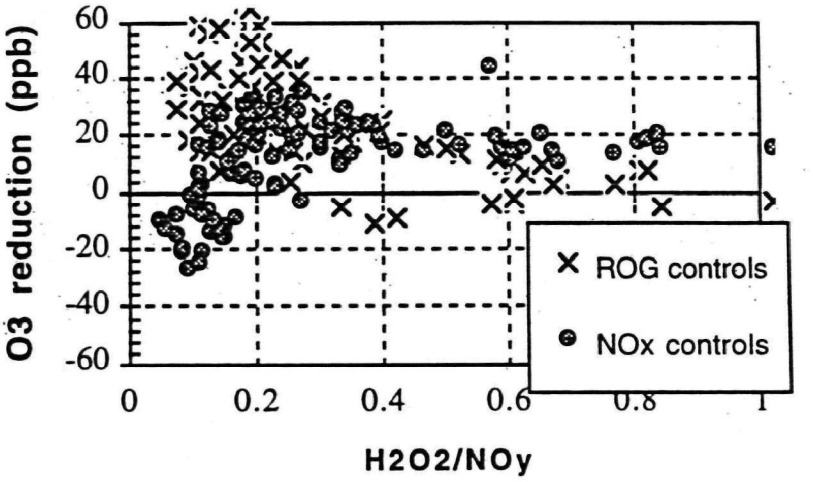

New York MM7 simulation: H2O2/NOy

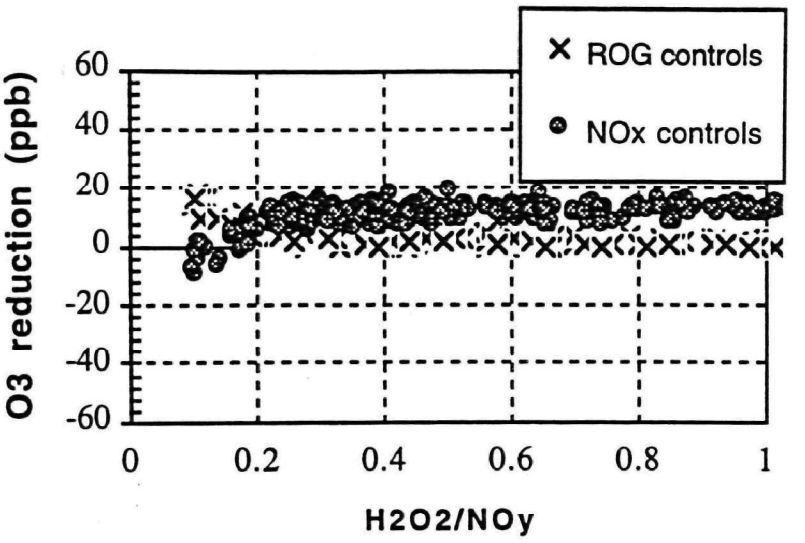

Atlanta, BEIS1 biogenics: H2O2/NOy

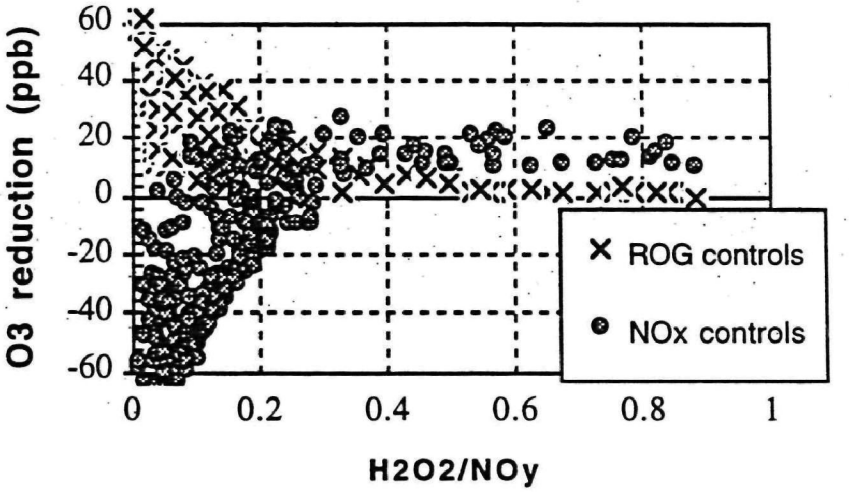

Los Angeles (Godowitch): H2O2/NOy

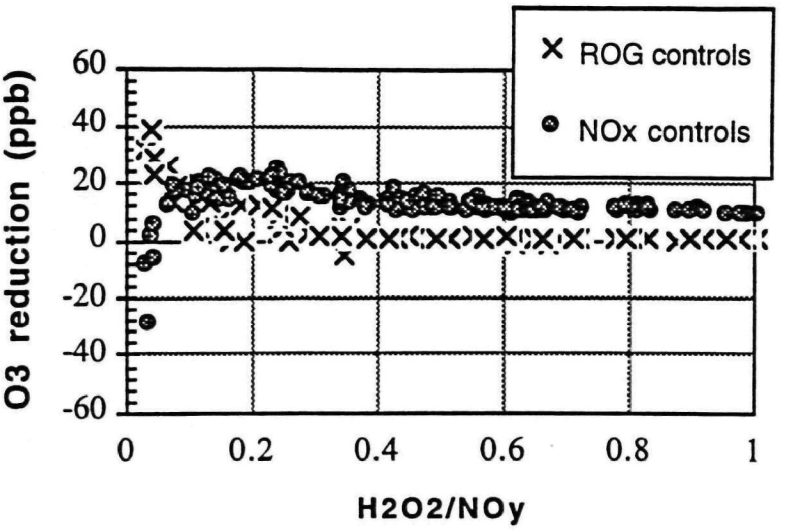

Northeast corridor, light winds and high deposition, H2O2/NOy